Spring 5-2008

Broadband Dielectric Spectroscopy Studies of Nafion

David Walter Rhoades
University of Southern Mississippi

The University of Southern Mississippi

BROADBAND DIELECTRIC SPECTROSCOPY STUDIES OF NAFION

by

David Walter Rhoades

A Dissertation
Submitted to the Graduate Studies Office
of The University of Southern Mississippi
in Partial Fulfillment of the Requirements
for the Degree of Doctor of Philosophy

Approved:

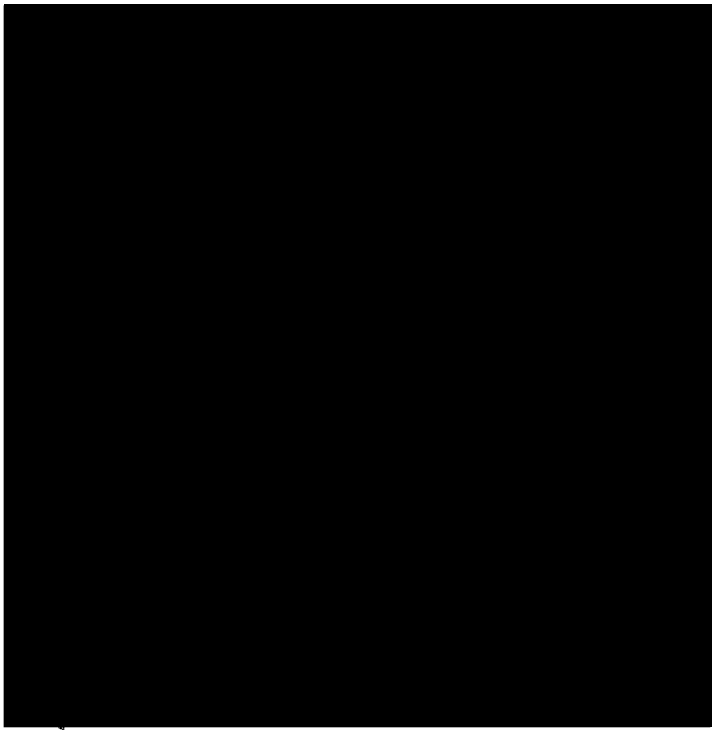

May 2008

The University of Southern Mississippi

BROADBAND DIELECTRIC SPECTROSCOPY STUDIES OF NAFION

by

David Walter Rhoades

Abstract of a Dissertation
Submitted to the Graduate Studies Office
of The University of Southern Mississippi
in Partial Fulfillment of the Requirements
for the Degree of Doctor of Philosophy

May 2008

ABSTRACT

BROADBAND DIELECTRIC SPECTROSCOPY STUDIES OF NAFION

by

David Walter Rhoades

May 2008

In light of available literature regarding Nafion® materials it is apparent that an information gap exists between the current state of understanding of Nafion® relaxations and the dielectric behavior of these materials. Although the currently available dielectric relaxation data is accurate it is very limited in its scope—specifically in-depth broadband analyses are not available. As a result very little information is available regarding the dependence of the relaxation processes on frequency and temperature. This presents an important opportunity for the exploration of the dielectric broadband relaxation behavior of Nafion® materials. The primary intent of this research is to quantify the dependence of the α and β relaxations on frequency and temperature from 10^{2}-10^{-6} Hz and -130 to 200° C by using the VFT equation in conjunction with the fragility index *m*. Four particular systems are analyzed: the non-ionic precursor form of Nafion®, a chemically crosslinked form of Nafion, the acid form of Nafion® and a chemically degraded acid of Nafion®. Specifically for the acid form special attention is paid to the impact of thermal history and film preconditioning on these relaxation processes. This later step is frequently overlooked but as we confirm it is crucial for reliable and repeatable BDS data. For all forms of Nafion® studied here $\tau_0 >> 10^{-14}$; however, τ_0 typically equals 10^{-14} for most polymers. Higher τ_0 and *m* values correlate with greater restriction imposed on the side

chains via the physical or chemical cross-link which is transferred to the segmental motions of the backbone.

DEDICATION

To the One who created the glass transition.

Thank you for science—a window into your mind!

ACKNOWLEDGEMENTS

Many thanks are in line to the numerous people who aided me in completing this work. Without their presence, provisions and guidance in my life this work would never have been completed. Thank you.

I first thank Dr. Kenneth Mauritz for his integrity and depth of scientific knowledge. His mind is more valuable than any reference book. I give him special thanks for his kindness and silent mentoring which in part redeemed my interest in science. I also give thanks to my committee: Dr. Hoyle, Dr. Jarrett, Dr. Moore, and Dr. Storey. Thank you for the guidance in this research and for providing an excellent polymer science foundation during my first year in graduate school. In addition, I thank Dr. Douglas Wicks for his candid advice and benevolence to my wife and me. I also thank the Mauritz group members, especially Mohammad Hassan, for their willingness to learn with me and the Polymer Science staff for their administrative work, in particular Laura Fosselman and Machel Haynes.

Beyond the scientific community a warm congregation of people upheld me and lifted me to higher ground. These people modeled for me how to be a scientist, husband, father, and child. Particularly the Dr. Phil Stayer family, the Dr. Ralph Davis family and the Dr. Alan Curry family are thanked for their open and sacrificial love. Particular thanks is also given to the Christian and Sunny Corral.

Additionally, I thank my parents who devoted themselves to my well being and advancement. In particular my father is thanked for his compulsory interest in science. His curiosity for earth and space science planted the science seed in me as young child which yielded this fruit.

And to my wife I give nothing but thanks, admiration and devotion without reservation. She truly is the second most remarkable gift. She not only stood beside me, but at the right time she stood behind and in front of me. Her love sanctified all my work. Without her I would be destitute.

I also thank Eli and Benjamin, my sons, who help me to realize what is important.

Finally I thank my Redeemer. For without his grace I would have none of these wonderful people to thank or anything of accomplishment.

TABLE OF CONTENTS

LIST OF FIGURES

LIST OF TABLES

CHAPTER I

INTRODUCTION TO NAFION® MATERIALS AND BROADBAND DIELECTRIC RELAXATION SPECTROSCOPY

Introduction

Despite an enormous amount of literature, generated over decades, dedicated to understanding the fundamental microstructure, behavior and processes involving Nafion® materials, much remains a mystery. While the earliest industrial application for use as a separator was in chlor-alkali electrochemical cells, the current thrust is in the arena of membranes for fuel cells that power automobiles. To be sure, every aspect of Nafion® remains under extensive investigation. The focus of this research is to better understand underlying molecular processes of Nafion® materials primarily from the use of broadband dielectric relaxation spectroscopy (BDS). Very little dielectric relaxation spectral information is available on these materials, especially deriving from modern broadband analysis. This leaves an information gap, which this research will fill, at least in part.

To provide a foundation for understanding the rationale of this research, the Introduction is divided into two sections: Nafion® Materials and Broadband Dielectric Relaxation Spectroscopy. The section on Nafion® Materials is further divided into two sections that discuss the morphology and molecular relaxations in Nafion®. The latter section discusses the current understanding of molecular relaxations in Nafion®.

Nafion® Materials

Developed in the 1960's by DuPont de Nemours, Nafion® is a statistical copolymer of tetrafluorethylene (TFE) and a perfluorinated vinyl ether comonomer. The chemical structure of the melt-processible precursor form, from which films are extruded, is shown in Figure 0-1.

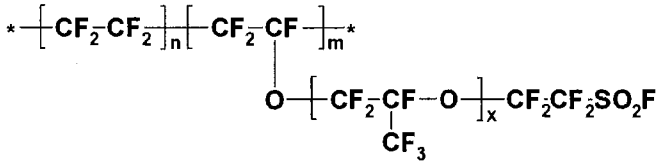

Figure 0-1. Chemical structure of the precursor form of Nafion®.

This non-ionic form is changed into an ionomer by converting this sulfonyl fluoride group into the sulfonic acid form, or counterion forms such as Na^+, Cs^+ and TBA^+. Upon conversion to the ionic form, Nafion® becomes hydroscopic. The acid form is very hydroscopic. The TFE component separates from the ionic side chain component forming distinct non-polar and polar regions. Having chemical inertness and good thermal/mechanical properties, this phase separated morphology also has exceptional proton conduction with poor electron and anion conduction—a requirement for hydrogen fuel cells. As a result, Nafion® is heavily researched as it is regarded as the benchmark membrane – against which other membranes are compared – for proton exchange membrane (PEM) applications.[1]

The degree of ionic content can be controlled and Nafion® is commonly identified by the average equivalent weight (EW), which is the ratio of number grams of dry acid form per mole of sulfonic acid groups. $EW = 100n + 446$ where n is the number of moles of TFE per mole of comonomer. The molecular weight is not usually cited, as for other

polymers, as it is difficult to accurately determine due to its resistance to dissolution and the persistence of aggregates in solution. One study, in which Nafion® was dissolved in alcohol by heating to high temperatures, estimated that the weight-average molar mass of Nafion® is approximately 2.5 x 10^5 g mol^{-1}.[2] In addition to EW, Nafion® membranes are identified by a standard thickness which is often related to performance. For example, a membrane designated 117 refers to a film having an EW of 1100 and a nominal thickness of 0.007 in.[3]

The Morphology of Nafion®

The physical and chemical properties of Nafion® are highly dependent upon its morphology. Despite the vast amount of literature dedicated to understanding morphology, the complex nature of the material makes it difficult to fully understand the relationship between structure and property. The morphology is multifaceted as it includes ionic clusters, PTFE crystals, amorphous PTFE regions and interfacial regions. In addition, this multi-component morphology is dynamic, changing with respect to temperature, hydration and processing conditions. To compound this, scattering techniques used to probe polymer morphology are limited in their ability to generate quantifiable data due to the narrow window of reciprocal space and overlap of peaks. A number of morphological models have been proposed to relate behavior to morphology.[1] However, the models are often simplified as modeling is difficult owing to the complexity of this dynamic four-component system. Several models have been proposed to better understand the nanostructures resulting from ionic side chains phase separating from the non-ionic TFE phase. To illustrate this, and to highlight some important aspects

on the structure/property relationship, three historical models and studies will be discussed.

The oversimplified, although historically significant, two-phase Gierke model, also known as the cluster-network model, has the morphology comprised of ionic and non-ionic phases to minimize unfavorable interactions.[4] In the ionic phase sulfonic acid side chains are organized as spherical inverted micelles, earlier termed clusters, with absorbed water in the center and ion exchange sites located near the water interface or imbedded in the water domain. These clusters are approximately 40Å in diameter and are theorized to be interconnected by approximately 10Å diameter channels. Going from a hydrated to a dehydrated state the clusters are thought to not simply collapse but to divide and rearrange themselves to balance the elastic energy of deformation and electrostatic interaction, as illustrated in Figure 0-2, and vice versa for going from a dehydrated state to a hydrated state.

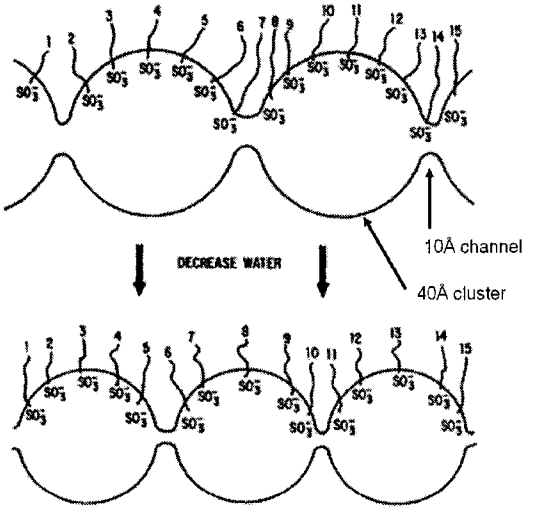

Figure 0-2. Redistribution of ion exchange sites into a different number of clusters in the cluster-network model upon dehydration (adapted from ref.[4]).

Clusters persist in the dehydrated state, yet they are smaller and greater in number than in the hydrated state. This model does not allow for isolated ion-dipole pairs imbedded in the hydrophobic PTFE matrix, which may in fact exist. The core-shell model, discussed next, accounts for isolated ion-dipole pairs and multiplets (small aggregrates of ion-dipoles) and as well, possesses other fundamental differences from the cluster-network model.

The core-shell model was originally developed to analyze hydrocarbon ionomers, although Roche adapted it to interpret Nafion® SAXS data.[5] The basic assumption of this model is that morphology is organized as ionic clusters which are phase separated as an ion-rich core surrounded by a shell rich in fluorocarbon chains, as shown in Figure 0-3. These core-shell structures are assumed to be uniformly dispersed in a PTFE matrix along with non-clustered ions and multiplets. Following Roche, Fujimura et al.[6,7] later used the core-shell model to study Bragg spacings associated with ionic and crystalline structures. Both Roche and Fujimura postulated the ionomer scattering peak to be indicative of scattering within a core-shell structure, i.e., *intra*particle scattering. This is in contrast to Gierke's cluster-network model which assumes that scattering arises from between ionic regions, i.e., *inter*particle scattering. To test the validity of the core-shell model, Fujimura compared experimental scattering data with both the core-shell and a two-phase hard sphere model. The latter model differed slightly from cluster-network model in that it allowed for lone ions and multiplets. It also assumed that ionic regions were not free to rearrange and were uniformly distributed. Fujimura found neither model to be superior as both models fit the experimental data. Despite this, Fujimura believed the core-shell model to be the better in light of the following observations: 1) the

microscopic absorption of water does not match the macroscopic absorption (macroscopic absorption was much smaller than the microscopic absorption) and 2) during uniaxial deformation the microscopic deformation does not match the macroscopic deformation.[6,7] Generally speaking, the core-shell model is not accepted as the best to describe structure-property relationships because it lacks the ability to explain long range properties such as ion-transport.[1]

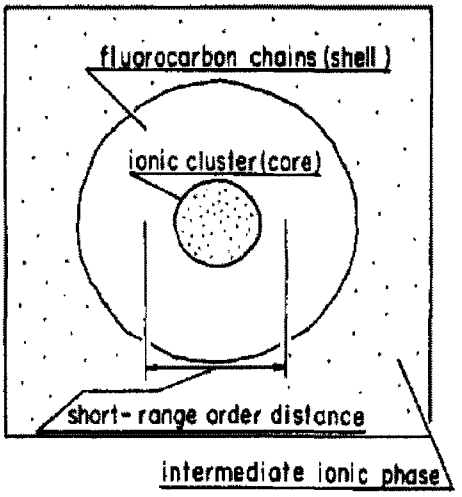

Figure 0-3. A schematic of the core-shell model as originally illustrated by Fujimura (adapted from ref.[6]).

Based on SAXS and SANS results, Gebel developed a qualitative rod-like model for the hydration process of Nafion® from the dry to the 'dissolved' state as is illustrated in Figure 0-4.[8] He based this model in part on a discrepancy with Fujimura concerning the experimental observations related to swelling. As previously stated, Fujimura's rationale for supporting the core-shell model was based on the notion that relative microscopic swelling does not equal macroscopic swelling.[6,7] Gebel purported that the discrepancy between microscopic and macroscopic swelling is reconciled by considering the area of the polymer-water interface per polar head, termed the specific surface area

term σ. He found that the specific surface was independent of water content and therefore theorized that the morphology during water content fluctuations is governed by the specific surface which is constant and equal to 55 $Å^2$. Central to Gebel's model is the assumption that ionic structures rearrange increasing the water fraction with the driving force related to the balance of interfacial energy and polymer chain elastic energy, which work to preserve the specific surface. At low water contents, the system was viewed as being in a water-in-polymer state where the ionic domains are distinct, spherical and not interconnected. Conversely, at high water contents the system was viewed as being in a polymer-in-water state where the ionic domains are an interconnected network of multi-chain rods. Gebel theorized that at approximately 0.50 volume fraction a structure inversion occurs. With increasing water content below the phase inversion point, the spherical ionic domains rearrange to preserve the specific surface so that the number of ionic groups per cluster increases and total number of clusters decreases. Furthermore, any additional water was theorized to act as a plasticizer facilitating cluster rearrangement. It was conceived that the rearrangement with increased hydration from distinct spherical particles to formation of connected cylindrical structures was the best model in light of polymer chain packing constraints and minimization of interfacial energy. However, several authors found fault with this as the scattering profiles near 0.50 volume fraction do not show any features or changes to support this claim.[1]

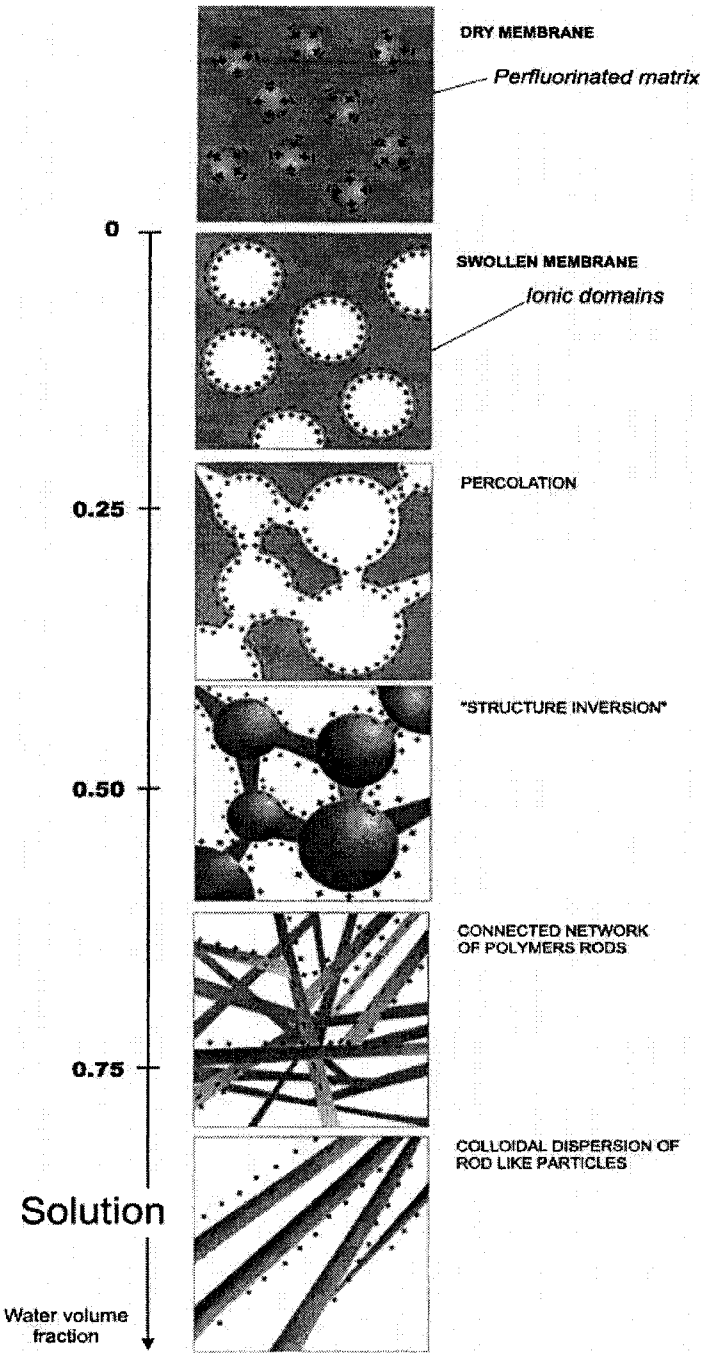

Figure 0-4. Gebel's schematic of morphological rearrangement due to the hydration Nafion® going from the dry to the dissolved state (adapted from ref.8).

While these three select examples highlight the difficulty in understanding the morphology of Nafion®, this is not an exhaustive review of the large amount of literature devoted to this topic. After almost 30 years since the introduction of the Gierke model,

no universally accepted model exists that fully describes the complex structure-property relationships.[1] Each model has attributes and shortcomings although some models are more realistic than others. Collectively speaking, it should be appreciated that all models contribute to a more comprehensive understanding of this rather ambiguous system. It must be remembered that data explained by a specific model should be analyzed in context with the model assumptions, hydration properties and processing history. Recently Mauritz and Moore published an extensive review on the current understanding of Nafion®, with more than 200 of the most important references up to 2004, and concluded that no model fully describes the morphology. The morphology of Nafion® should be regarded as three phase in nature, consisting of ionic and non-ionic phases which have a "fuzzy" interface and crystallinity in the non-ionic phase, as illustrated by Kreuer in Figure 0-9.

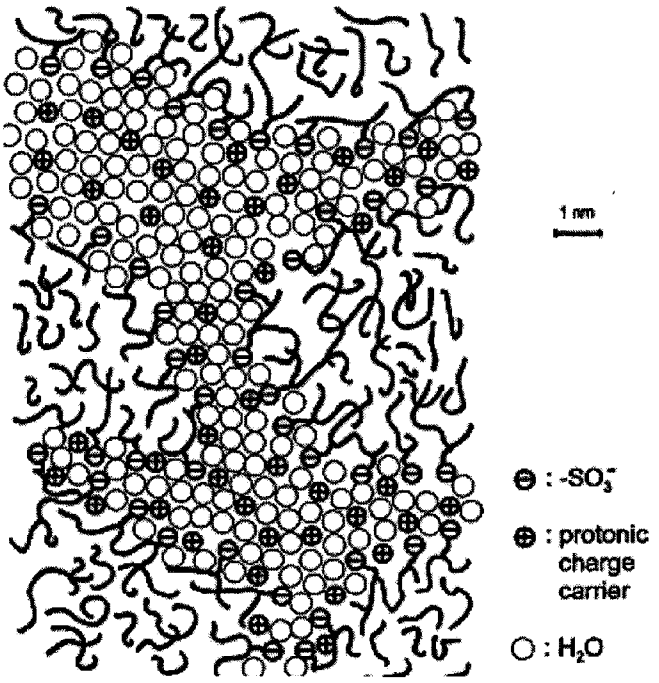

Figure 0-5. Kreuer's illustration of Nafion®'s morphology which has three phases, consisting of ionic and non-ionic phases with a "fuzzy" interface and crystallinity in the non-ionic phase.

One final note regarding the morphology of Nafion® must be mentioned. While crystallinity is not directly responsible for the ion-conductive properties, the crystallized fraction is critical as offering physical strength for a functional ion conductive network. Removing crystallinity via temperature quenching techniques (freezing in a totally amorphous state) results in reduced mechanical properties, greatly compromising the material if not rendering it useless in terms of ion conductivity and mechanical integrity, as determined by Moore, et al. [9,10] In their experimental approach they found that films cast from an ethanol-water mixtures were cracked, fragile and soluble at room temperature in polar solvents. They attributed these poor properties to the absence of crystallinity—recast films were virtually amorphous. However, when the casting temperature was raised to above 160° C, crystallinity was reinstated and mechanical integrity of the films restored. Both casting methods produced films with ionic aggregates, implying that the mechanical strength was not provided by these entities but rather the cohesiveness imparted by the semicrystallinity.

Macromolecular Relaxations in Nafion®

In both processing methods and applications, Nafion® materials are subject to a wide range of temperatures and temperature changes to which the material structure responds. It is critical that an understanding of the thermally or electrically-induced relaxations be understood. Significant research has been dedicated to understanding these relaxations from a dynamic mechanical and calorimetric standpoint, and to a much lesser extent dielectric response, and a summary of three primary areas is presented here. First the relaxations of the non-ionic precursor form of Nafion® are discussed. Molecular

motions associated with these relaxations are well understood. Second the relaxations of the ionic forms of Nafion® are discussed with special emphases on higher temperature behavior. The identities of these relaxations, namely the glass transitions in the tetrafluoroethylene matrix and order-disorder in ionic clusters, are debated. To better understand the discrepancy and misunderstanding of the two relaxation assignments a brief history of investigations in the area will be provided. Although a plethora of literature exists debating the identities of these two relaxations, only the important studies will be described to highlight the salient points. Third, in light of a recent study, the state of understanding of the higher temperature relaxations is discussed.

In the late 1970's Hodge and Eisenberg investigated the non-ionic sulfonyl fluoride melt-processible precursor form of Nafion® using dynamic mechanical and dielectric relaxation methods for samples of various equivalent weights.[11] Four peaks, labeled γ, β", β' and α in the order of increasing temperature, were seen on the dielectric ε'' vs. temperature (T) curves taken at constant frequency in the range -196 to 80° C. These same relaxations were seen on dynamic mechanical E' and tan $\delta = E''/E'$ vs. T curves for the same materials in approximately the same respective temperature ranges. The γ relaxation, seen at $T < -160°$ C, was the strongest of the three dielectric relaxations but weakest in the mechanical relaxation spectra. This short ranged relaxation was assigned to motions of the SO_2F group based in part on the fact that this is the most polar group in the entire chemical structure. This assignment is reinforced by the fact that the relaxation disappears when the SO_2F groups are converted to sulfonate or sulfonamide groups.[12] The β relaxation exists in the temperature range -100 to -20° C. For the dielectric relaxation studies this relaxation resolved into two components, β' and β", at

low frequencies. The β' peak component was said to be likely due to CF_2 backbone motions while the β" component was due to ether-containing side chain motions. Finally, the highest temperature α process, seen in the range 20 - 35° C, depended on frequency (*f*) in the usual way and the corresponding dynamic mechanical transition had the greatest decline on *E'* vs. *T* curves, thereby indicating that this is a glass transition in the usual sense. There is no confusion of this peak with a transition associated with ionic aggregates as no ionic aggregates are present in this precursor material.

Conversion of the sulfonyl fluoride form to an ionic form results in elimination of the lowest temperature γ relaxation associated with the SO_2F group. Simultaneously, with the disappearance of the SO_2F relaxation a new higher temperature relaxation emerges which is associated with the formed ionic clusters.[13] Furthermore, the glass transition of the precursor, which resembles that of pure PTFE, is shifted to higher temperatures. The identities of these two relaxations are controversial.

In 1977, using dielectric relaxation spectroscopy, Yeo and Eisenberg[14] demonstrated that the β relaxation shifts dramatically with very small changes in water contents. Adapted from their original publication, Figure 0-6 represents 1365 EW H^+Nafion® tested using dielectric relaxation spectroscopy at a frequency of 100 Hz. It not only illustrates that the β relaxation is highly susceptible to small water fluctuations but it also illustrates that the β relaxation is comprised of a major and minor peak. It must be noted that despite the profound affect of these two relaxation processes, little is known about their molecular origins. At low water contents (ca. 0.7 H_2O/SO_3H) the major peak of the glass transition relaxation is at ca. 50° C while the minor peak is at ca. 25° C. Increasing the number of water molecules per sulfonate group by only 0.4 water

molecules, e.g., 2.1 H_2O/SO_3H, reduces the temperature of both major and minor peaks to approximately -20 and -10° C, respectively. Increasing water content to 4.1 H_2O/SO_3H further reduces the temperature of the major and minor peaks to ca. -85 and -70 °C, respectively. Given this relaxation response to moisture, Yeo and Eisenberg suggested that the β relaxation is directly related to ionic domains. Part of this conclusion does appear to be accurate as this relaxation is highly susceptible to ionic forces, notably by the presence of water. However, in subsequent studies by Kyu and Eisenberg, of partially ionized and neutralized forms, this idea was revised to associate this particular relaxation as the polymer glass transition.[13]

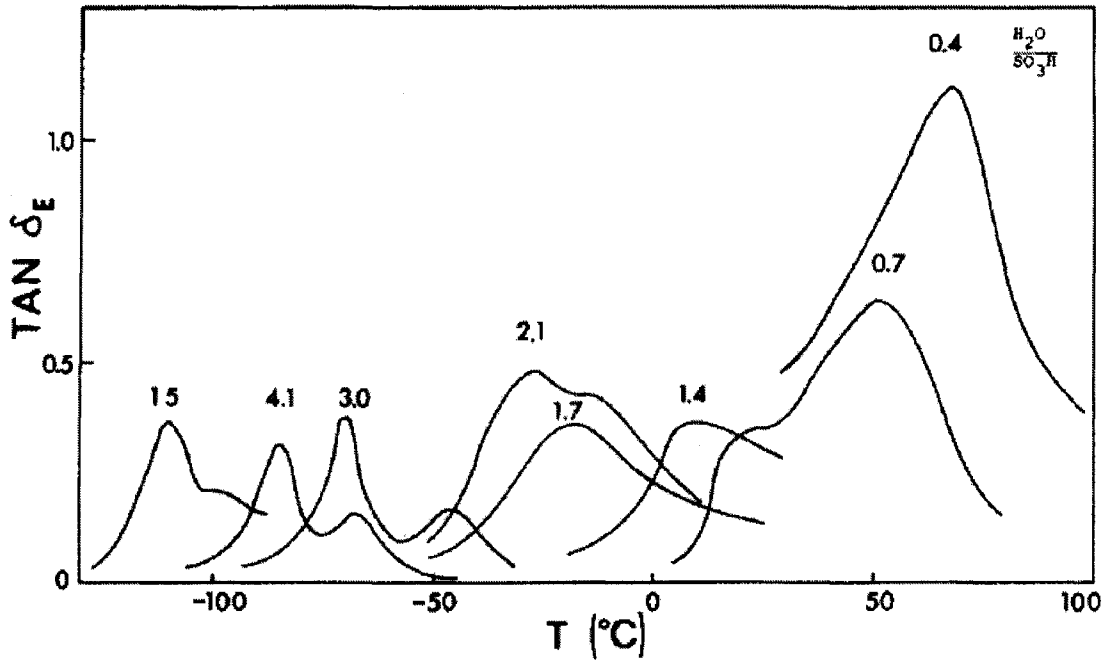

Figure 0-6. Dielectric loss tangent vs. temperature at various water contents at 100Hz for H^+Nafion® (adapted from ref.[15]). The numbers corresponding to each peak represents the average number of water molecules per sulfonate group.

Discrepancy in the results/interpretations of DSC investigations between research groups have compounded the difficulty of identifying the nature of the α and β

relaxations.[10,13,16-18] Several studies in the 1980s and 90s used DSC along with dynamic mechanical analysis (DMA) to identify the molecular motions. Most studies described two regions of endothermic behavior with one in the range 120 to 180° C and another in the range 240 to 300° C. However, many conclusions from these studies were inconsistent if not contradictory. As many DSC studies also utilized DMA to correlate mechanical relaxation with calorimetric DSC data, Page and Moore noticed a subtely between the results of the two techniques.[15] First, they noticed a commonality in the DSC studies: despite the different conclusions drawn in each, the temperatures of the endothermic peaks were somewhat similar and correlated well with corresponding DMA relaxations. However, they pointed out an overlooked discrepancy between the two techniques: after the first DSC heating scan the endothermic features typically disappeared in the second heating scan. However, this behavior did not occur with the correlated DMA processes. Page and Moore reasoned that if the two techniques were interrogating the same molecular motion then the two results should be consistent, i.e., there should be no peak disappearance with DSC when this does not happen with DMA and vice versa. To resolve this inconsistency they used the Na^+ and Cs^+ form with *in situ* annealing times of 0.5, 2, 6, 12, and 24 h. First, they confirmed the presence of the endothermic features in the first scan and the absence of these features in the second heating scan. Second, they demonstrated that the endothermic features only re-emerged with sufficient annealing time and temperature and that the rate of this re-emergence depended upon the electrostatic field (surface charge density) posed by the counterion. Third, they correlated endothermic features, or lack thereof, with variable temperature SAXS data. From this data they demonstrated that the broad shoulder on the main peak

in the scattering vector range of 0.3 - 0.7 nm-1, attributed to the crystalline lamellae, was missing for quenched samples. However, this peak returned with proper annealing temperature and time. This re-emergence of the crystallization peak for the SAXS profiles corresponded with the re-emergence of the endothermic peaks of the DSC scans. This latter point gave conclusive evidence that the DSC endothermic peaks were the result of PTFE-like crystallites melting. The missing features in the second scan results from quenching the sample, which does not give sufficient time for crystal formation from the melted state.

However, this investigation did not resolve the issue of multiple endotherms in DSC heating scans. To address this, they utilized a variable temperature annealing schedule for Cs^+ form Nafion® annealed for 2h at various temperatures. As illustrated in Figure 0-7, lower annealing temperatures generated lower temperature endotherms which resembled a step-like second order transition, commonly identified as a glass transition. However, with higher curing temperatures this feature shifted to higher temperatures eventually coinciding with the crystallization endotherm. As a result it was concluded that low annealing temperatures generate thin lamellae which have lower cohesion and therefore melt at lower temperatures. Conversely, higher annealing temperatures thicken the lamellae which increase their thermal stability and raise their melting temperature. More importantly, they concluded that the lower temperature endotherms are related to crystallization affected by processing and preconditioning and not to molecular relaxations of the matrix or the ionic regions as was previously thought. This highlights an important morphological aspect of Nafion®. Thermal treatment and history must be carefully considered as crystallization occurs at various temperatures to varying degrees.

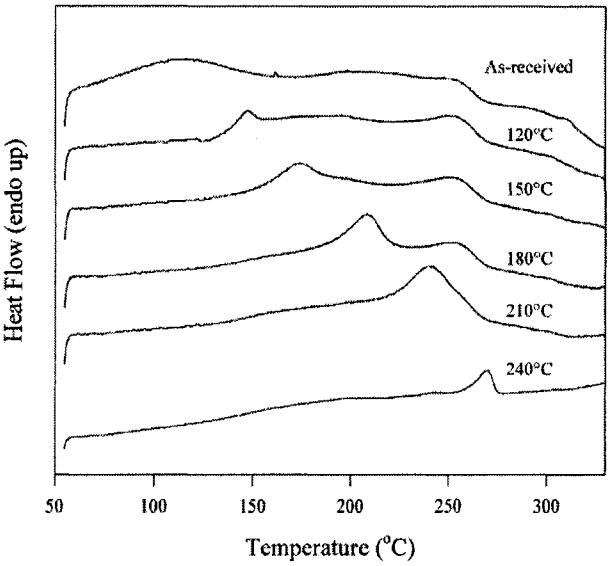

Figure 0-7. DSC thermogram of Cs^+ form 1100EW Nafion® annealed for 2h at the temperatures indicated above each trace (adapted from ref.[15]).

With melting now differentiated from macromolecular relaxation they systematically studied the effect of ionic forces on the α and β relaxations using a series of alkylammonium cation forms. By increasing the size of alkylammonium counterions they varied the surface charge density ($+e/4\pi r^2$, where r = cation radius), which is proportional to the electric field at the radius of the cation, and demonstrated that both α and the β relaxations are influenced by the strength of the counter ion. Figure 0-8 is a plot adapted from Moore and Page ref[15] demonstrating that as counterion size increases, and resultantly the ionic strength decreases, the temperatures of both the α relaxation and β relaxation decrease. This spreads the charge centers apart and weakens the electrostatic interactions. Not only does the β relaxation decrease in temperature with counterion size but it also increases in intensity. Moreover, the β relaxation temperature for the largest two alkylammonium ion forms is virtually the same as that of the glass transition of the non-ionic precursor. This latter point reinforces the notion that the β relaxation is the

glass transition. Moore and Page rationalized that larger cations have weaker electrostatic interactions with the sulfonate groups and associations of these weak anion-cation pairs are less cohesive, thereby reducing the strengths of the physical crosslinks they form. This, in effect, would increase long range chain mobility so that the β relaxation occurs at lower temperatures.

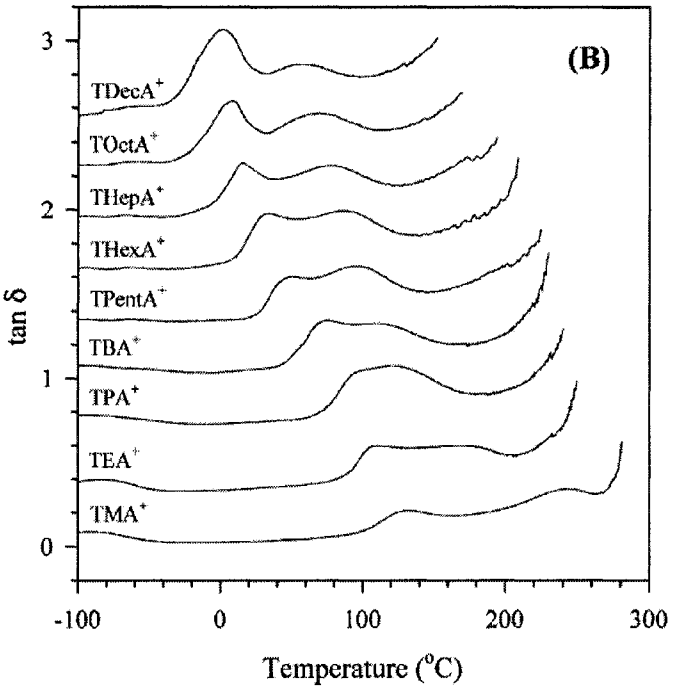

Figure 0-8. DMA plot of tanδ vs. temperature for various tetraalkylammonium counterion forms of Nafion® (adapted from ref.[15]).

Using variable temperature SAXS analysis on several alkylammonium counterion forms of Nafion® they identified the molecular motions of the α relaxation. Specifically, they discovered that the intensity of the ionomer peak was drastically reduced at high temperatures. This dramatic drop in intensity corresponded well with the α relaxation of the DMA studies. It was logically concluded that the α relaxation should be identified as a molecular relaxation related to the ionic region as there was not a corresponding

substantial reduction in the intensity of the SAXS ionomer peak at the β relaxation. Moreover, the decrease in intensity of the ionomer peak was theorized to be a result of the onset of ion hopping which occurs to relieve local stresses.[19,20] At the α relaxation the system transitions from a static network where the ions are electrostatically locked to a dynamic system where the side chains are capable of moving to relieve local stresses.

In summary, given that both α and β relaxations are highly dependent on counterion size in a homologous series, the current understanding of these macromolecular relaxations is as follows. At the α transition, the electrostatic forces that give ionic aggregates cohesion weaken, thus rendering long-range main chain and side chain motions more facile.[15] With increasing temperature, the onset of the α relaxation is thought to disrupt the physically crosslinked network from being static to a dynamic ion-hopping network. This transition allows for morphological reorganization. Conversely, the β relaxation occurs within an electrostatic network where the ion associations are frozen and the macromolecular motions resemble those of a polymer glass transition. In the work presented here, these assignments will be adopted in the analysis of macromolecular motions of Nafion® membranes using broadband dielectric spectroscopy (BDS). The bulk of the relaxation information on Nafion® pertains to studies using mechanical relaxation techniques while there is limited dielectric relaxation information.

Broadband Dielectric Relaxation Spectroscopy

Dielectric relaxation spectroscopy addresses how a material responds in a weak alternating electric field. Only some materials are said to be "dielectrics". These materials contain dipoles that orient or are induced by charge displacements in an external electric field. The general types of polarization are electronic, atomic, ionic,

dipolar and interfacial/space charge. These arise from electric charge distributions penetrating the material causing dipoles to orient or charges to separate. The electric field can be applied in a static or dynamic manner. The former uses a fixed voltage whereas the later uses a sinusoidal voltage with precisely defined frequencies of over a range. The latter is referred to as broadband dielectric spectroscopy (BDS). To better understand this technique, the fundamental mechanisms of polarization will first be explained via a discussion of static electric fields, which is the simplest and easiest to understand. Second, this concept will be correlated to a.c frequency experimental data via the reciprocal relationship of the response time to the applied frequency. Lastly, methods of data analysis pertinent to Nafion® materials will be discussed.

Static polarization

The basic interactions between point charges in a dielectric medium are governed by Coulomb's law[21]:

$$F_C = \frac{1}{4\pi\varepsilon_s}\frac{q_1 q_2}{r^2} \qquad \text{Equation 1}$$

F_C is the Coulombic force between two charges q_1 and q_2 that are separated by a distance r. ε_s is the static permittivity which is an inherent property of the material.

ε_s is determined by applying a static electric field charge to a system and measuring the resulting electric field change after equilibration, which is lower than the applied field strength. This is best understood by first studying the permittivity of a vacuum between two parallel plates separated by a distance d, as is illustrated in Figure 0-9. The permittivity of the vacuum is equal to the electric flux density, D_0, or displacement field, divided by the electric field strength F_0.

$$\varepsilon_0 = \frac{D_0}{F_0} \qquad \textbf{Equation 2}$$

Moreover, because this is a vacuum, D_0, by Gauss's law, is equal to the number of charges per unit area, σ_{s0}, termed the surface charge density.

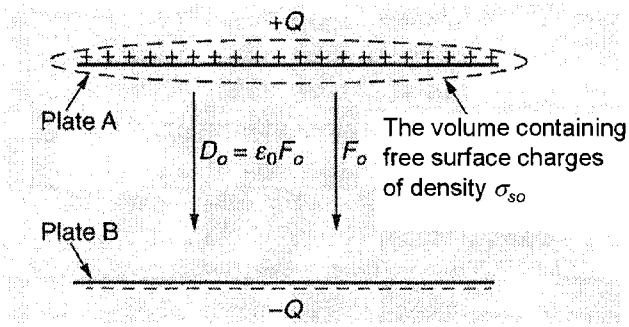

Figure 0-9. Electric field generated in a vacuum between two parallel plates of opposite charge (adapted from ref.[22]).

When a positive charge $+Q$ is on one plate and an equal and opposite charge is on the other plate, a potential difference V is generated.[22] V and Q are directly proportional and the proportionality constant C is defined as the capacitance. Q is related to the electric field strength F and it is commonly expressed in terms of the static charge density σ_s, which is the total amount of charge per area, as discussed above

$$Q = C(Fd) = \sigma_s A \qquad \textbf{Equation 3}$$

Where d is the spacing between the oppositely charged plates. From this equation the permittivity of the vacuum ε_0 is derived,

$$C_0 = \frac{Q}{V} = \frac{\sigma_s A}{Fd} = \varepsilon_0 \frac{A}{d} \qquad \textbf{Equation 4}$$

It is important to note that C_0 and ε_0 for the vacuum may be easily calculated by knowing the applied field strength, the distance between the plates, the area of the plates and

measuring the resulting electric field. When a dielectric material is placed between the two plates the system adjusts to accommodate the change in the electric field strength, as shown in Figure 0-10

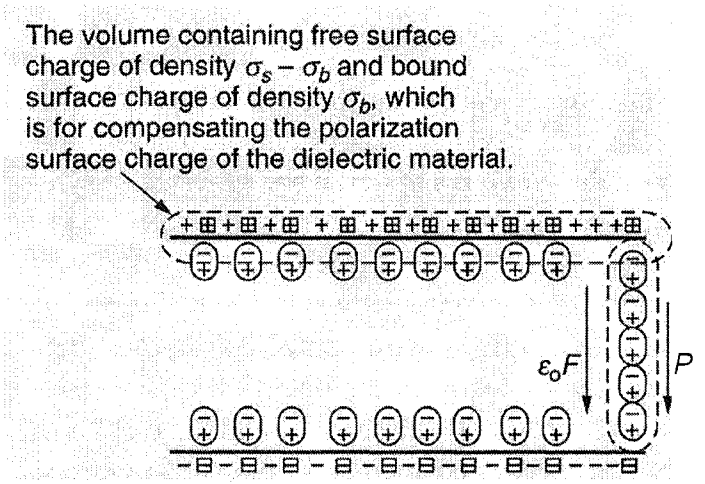

Figure 0-10. Dielectric material sandwiched between equal and opposite charged parallel plates. The + and – symbols represent free positive and negative whereas the boxed charges represent bound charges distributed on the metal electrodes. The free charges produce the electric flux density $\varepsilon_0 F$ whereas the bound charges produce the polarization P within the dielectric material (adapted from ref.[22]).

Of the original σ_s, a portion of the surface charge density σ_b is used to polarize P the dielectric material and the remainder behaves as though it were still under the prior vacuum conditions (σ_s- σ_b) creating an electric flux density D where

$$D = \varepsilon_0 F \qquad \text{Equation 5}$$

Therefore,

$$\begin{aligned} \sigma_s &= (\sigma_s - \sigma_b) + \sigma_b \\ &= D = D_0 + P \\ &= \varepsilon_s F = \varepsilon_0 F + (\varepsilon_s - \varepsilon_0) F \end{aligned} \qquad \text{Equation 6}$$

Where the polarization is expressed as

$$P = (\varepsilon_s - \varepsilon_0)F = \sigma_b = polarization \qquad \text{Equation 7}$$

As a result the static permittivity ε_s of the dielectric material can be calculated. The dielectric constant, also known as the relative static permittivity of the material can be arrived at by the ratio of

$$\varepsilon_{sr} = \frac{\varepsilon_s}{\varepsilon_0} \qquad \text{Equation 8}$$

Thus, for any dielectric material the relative dielectric constant can be experimentally derived in this manner by applying a static electric field.

Dynamic polarization

The dielectric constant ε_{sr} at low electric fields is independent of electric field strength. ε_{sr} is a function of chemical structure, material imperfections and physical parameters such as temperature and pressure. If the electric field is fluctuating, ε_{sr} depends on the frequency of the applied alternating voltage. Polarization processes do not respond instantaneously but are time dependent, which is why the frequency of the electric field oscillation is important. If the period of oscillation is faster than the natural time scale of material polarization then the polarization process will not be detected. Figure 0-11 illustrates characteristic response times for the various polarization processes. The general trend is that the larger the entities or the longer the motion the greater is the corresponding polarization time as is shown in Figure 0-11.

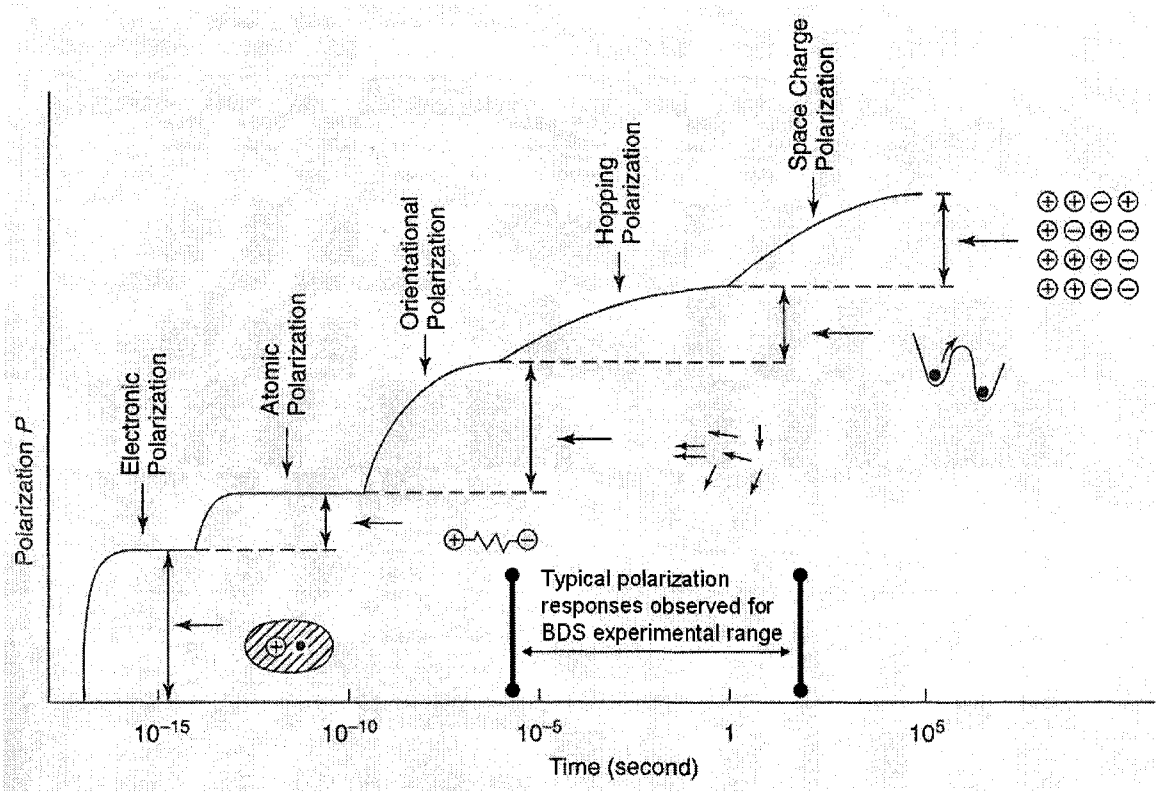

Figure 0-11. Spectrum of polarization mechanism time scales. The typical BDS frequency test window corresponds, approximately, to 10^{-6} to 10^{2} sec (adapted from ref.[22]).

Figure 0-11 depicts a multi-step function which illustrates the time scale for each type of polarization to occur. For instance, if the electric field strength is applied for 10^{-10} sec then only atomic and the electronic polarization are able to respond within the experimental time frame. The other larger polarization responses owing to more sluggish structural rearrangements, do not have sufficient time to fully respond. This concept can be correlated to the a.c. frequency experimental data via the reciprocal relationship of the polarization response time to the applied frequency. For instance if a frequency is applied at a rate of 100 Hz, which corresponds to a response time of 10^{-2} seconds, then according to Figure 0-11 electronic, atomic, orientational, and hopping polarizations

would have time to respond however space charge polarizations would not, because the latter requires cooperative rearrangements of charges over larger distances and times.

The time-dependent nature of the different relaxations must be considered when designing an experimental approach using BDS. For example, a frequency range of 10^{-2} to 10^{6} Hz corresponds to a time testing time of 100 to 10^{-6} sec. In this case, only certain polarization processes are within the frequency range. Specifically, in this frequency window the electronic and atomic polarizations occur instantly because their polarization responses ($<10^{-10}$ seconds) are much faster than the applied frequency, as indicated in Figure 0-11. As a result the sum of these two polarizations P_{∞} is analogous to an elastic material in a mechanical test, which can be described as a spring. However, the orientational, hopping and space charge polarization occur much slower in this testing regime. As a result these polarizations behave like a viscoelastic material which contains both a storage and a loss polarization component, designated here as P_1 and P_2 respectively. In other words the dipoles which cannot track the applied electric field experience some degree of energetic loss, termed dielectric loss. Thus, the polarization responses are complex, P^* as they have a storage component P' and a loss component P'',

$$P^* = P' - P'' \qquad \text{Equation 9}$$

The permittivity responses are also complex ε^*, with a storage component ε' and a loss component ε'',

$$\varepsilon^* = \varepsilon' - i\varepsilon'' \qquad \text{Equation 10}$$

with the loss tangent for both Equation 9 and 10 written as

$$\tan\delta = \frac{P''}{P'} = \frac{\varepsilon''}{\varepsilon'} \qquad \text{Equation 11}$$

Equations 9 through 11 resemble the complex modulus for dynamic mechanical studies which can have both elastic and viscous components (see appendix for more details). The storage and loss polarization responses to the applied sinusoidal electric field with increasing angular frequency are shown in Figure 0-12. In this figure P_∞ and P_1 comprise the storage polarization, which decreases stepwise with increasing angular frequency. The loss polarization, identified as P_2, is a peak. Notice the three distinct polarization responses of P_∞, P_1 and P_2. The P_∞ component of the storage polarization is identified as the instantaneous storage response of the electronic/atomic polarization. It characteristically has a flat line storage polarization, which is present at all tested frequencies but becomes more apparent at high frequencies in the absence of P_1 and P_2. Additionally, it has no detectable loss polarization in this frequency regime. The P_1 component is identified as the in phase storage response of relaxation process, i.e., either a dipolar, spontaneous, or interface/space charge polarization. And, The P_2 region is the corresponding out of phase relaxation response.

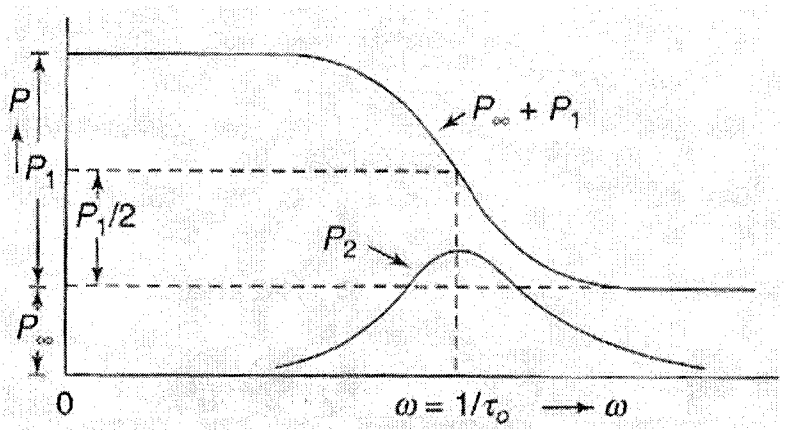

Figure 0-12. Storage and loss polarization responses vs. angular frequency = $\omega = 2\pi F$ where the complex variable $P^*(\omega)=P_\infty+P_1+P_2$. $P_\infty+P_1$ contains the storage component P_1 and the loss component is P_2 (adapted from ref.[22]).

Methods of BDS Data Analysis

The responses in Figure 0-12, of real and imaginary parts of the complex polarization P^* and corresponding complex permittivity ε^*, to frequency, are referred to as dispersion. These properties can be modeled and quantified in several ways. Most commonly, dielectric spectroscopy data is studied using ε^* therefore this quantity will be primarily used here. The simplest dipole orientation model to describe the angular frequency dependence of the complex permittivity is the Debye equation,[23]

$$\varepsilon^* = \varepsilon'_\infty + \frac{\Delta\varepsilon'}{1+i\omega\tau} = \varepsilon' - i\varepsilon'' \qquad \text{Equation 12}$$

which is for a single population of non-interacting ideal dipolar relaxations responding to a dynamic electric field, where $\Delta\varepsilon'$ is the relaxation strength which is defined as the difference between the high and low frequency permittivity limit ε'_∞. The static low frequency storage permittivity limit, as is illustrated in Figure 0-13. τ is the relaxation time which is equal to $1/2\pi f_{max}$, where $f_{max} = 2\pi\omega_{max}$.

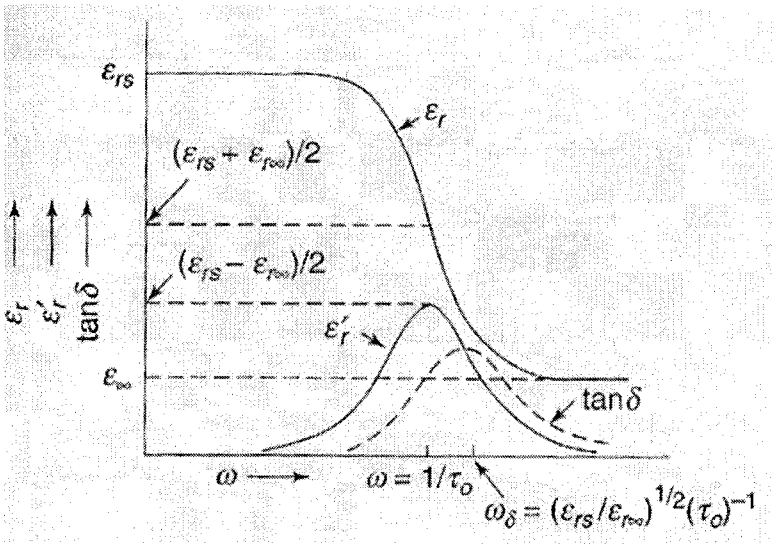

Figure 0-13. Typical relaxation response as a function of angular frequency (adapted from ref.[22]).

Equation 12 is for an ideal relaxation. Considering the Debye model as portraying an 'ideal' situation, most relaxations in real materials are not ideal in not having a single relaxation time with no asymmetric or broad distributions about an average. A distribution of relaxation times arises because each relaxing element (e.g., dipole) is in a slightly different molecular environment. Therefore, modified Debye equations, for example the Havriliak-Negami (HN) equation, are more commonly used to account for relaxation broadening and curve asymmetry. The HN equation is shown below.

$$\varepsilon^*(\omega) = \varepsilon'_\infty + \frac{\Delta\varepsilon'}{\left(1 + (i\omega\tau_{HN})^\alpha\right)^\beta} = \varepsilon' - i\varepsilon'' \qquad \text{Equation 13}$$

τ_{HN} is a time that related to the actual relaxation time, τ_{max}, which is associated with the frequency at the respective peak maximum, f_{max}. α and β are measures of the breadth and asymmetry, respectively, of the given relaxation such that $\alpha < 0 \leq 1$ and $0 < \beta \leq 1$. Figure 0-14 illustrates how breadth and asymmetry are modeled with α and β for a relaxation process. As α decreases the low and high frequency sides of the relaxation

peak open up. However, as β decreases only the high frequency side of the peak opens up.

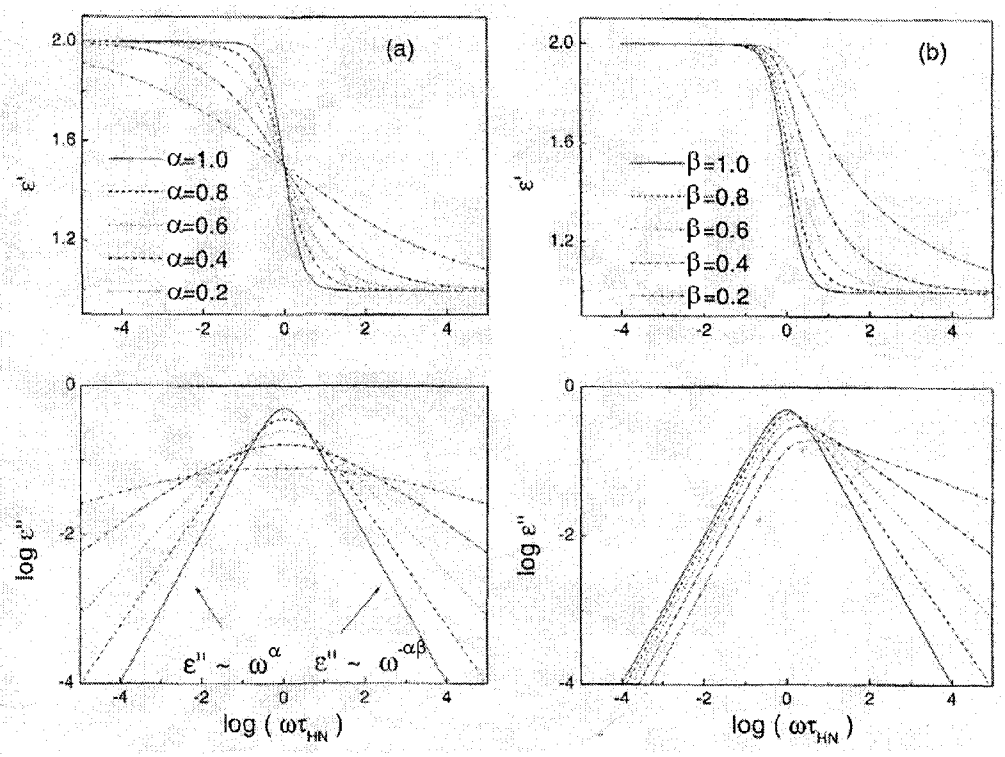

Figure 0-14. Complex permittivity vs. log $\omega\tau_{HN}$ illustrating the affect that the breadth and symmetry terms have on the relaxation (adapted from ref.[24]).

When the HN equation is fitted to data τ_{HN} does not equal τ_{max} but the relaxation time must be corrected according to the following equation[25]

$$\tau_{\max} = \tau_{HN}\left[\frac{\sin\left(\frac{\pi\alpha\beta}{2(\beta+1)}\right)}{\sin\left(\frac{\pi\alpha}{2(\beta+1)}\right)}\right]^{\frac{1}{\alpha}} \qquad \text{Equation 14}$$

Relaxation peaks are often superimposed on each other but curve resolution of the data can split the composite loss spectrum into the component peaks. The same is true for the d.c. conductivity phenomena which occurs when the frequency is so low that the period of the electrical field oscillation is long enough to sample long range charge hopping. To account for possible conduction a d.c. conductivity term is added as shown in the modified HN equation below.[26,27]

$$\varepsilon^*(\omega) = \varepsilon' - i\varepsilon'' = -i\left(\frac{\sigma_0}{\varepsilon_0 \omega}\right)^N + \sum_{k=1}^{n}\left[\varepsilon'_\infty + \frac{\Delta\varepsilon'}{\left(1+(i\omega\tau_{HN})^\alpha\right)^\beta}\right] \qquad \text{Equation 15}$$

When present, d.c. conductance can obscure weak polymer relaxations that occur at low frequencies. This obscuration is removed as follows: Once the exponent $N \leq 1$ and the d.c. conductivity σ_0 are determined by curve fitting in the low f regime, this term is subtracted point-by-point from the ε'' curves to reveal the relaxation peaks.

Conclusions

In light of available literature regarding Nafion® materials it is apparent that an information gap exists between the current state of understanding of Nafion® relaxations and the dielectric behavior of these materials. Although the currently available dielectric relaxation data is accurate, it is very limited in its scope—specifically in-depth broadband analyses are not available. As a result very little information is available regarding the dependence of the relaxation processes on frequency and temperature. This presents an important opportunity for the exploration of the dielectric broadband relaxation behavior of Nafion® materials. The primary intent of this research is to quantify the dependence of the α and β relaxations on frequency and temperature from 10^2-10^{-6} Hz and -130 to 200° C. Four particular systems are analyzed: the non-ionic precursor form of Nafion®

(sulfonyl fluoride), a chemically crosslinked form of Nafion® (diamine modified sulfonyl fluoride), the acid form of Nafion® and a chemically degraded acid of Nafion®. Specifically for the acid form special attention is paid to the impact of thermal history and film preconditioning on these relaxation processes. This later step is frequently overlooked, but as we confirm, it is crucial for reliable and repeatable BDS data.

References

(1) Mauritz, K. A.; Moore, R. B. *Chemical Reviews* **2004**, *104*, 4535-4585.

(2) Lousenberg, R. D. *Journal of Polymer Science: Part B: Polymer Physics* **2005**, *43*, 421-428.

(3) Doyle, M.; Rajendran, G., Eds. *Handbook of Fuel Cells-Fundamentals, Technology and Applications*; John Wiley & Sons, Ltd,: Chichester, 2003.

(4) Gierke, T. D.; Munn, G. E.; Wilson, F. C. *Journal of Polymer Science: Polymer Physics Edition* **1981**, *19*, 1687-1704.

(5) Roche, E.; Pineri, M.; Duplessix, R.; Levelut, A. M. *Journal of Polymer Science Polymer Physics Edition* **1981**, *19*, 1.

(6) Fujimura, M.; Hashimoto, T.; Kawai, H. *Macromolecules* **1981**, *14*, 1309-1315.

(7) Fujimura, M.; Hashimoto, T.; Kawai, H. *Macromolecules* **1982**, *15*, 136-144.

(8) Gebel, G. *Polymer* **2000**, *41*, 5829-5838.

(9) Moore, R. B.; Martin, C. R. *Analytical Chemistry* **1986**, *58*, 2569.

(10) Moore, R. B.; Martin, C. R. *Macromolecules* **1988**, *21*, 1334-1339.

(11) Hodge, I. M.; Eisenberg, A. *Macromolecules* **1978**, *11*, 289-293.

(12) Rhoades, D. W.; Mauritz, K.; Peusch, D. *Polymeric Materials: Science & Engineering* **2006**, *94*, 675.

(13) Kyu, T.; Hashiyama, M.; Eisenberg, A. *Canadian Journal of Chemistry* **1983**, *61*, 680-687.

(14) Yeo, S. C.; Eisenberg, A. *Journal of Applied Polymer Science* **1977**, *21*, 875-898.

(15) Page, K. A.; Cable, K. M.; Moore, R. B. *Macromolecules* **2005**, *38*, 6472-6484.

(16) Su, S.; Mauritz, K. A. *Macromolecules* **1994**, *27*, 2079-2086.

(17) de Almeida, S. D.; Kawano, Y. *Journal of Thermal Analysis and Calorimetry* **1999**, *58*, 569-577.

(18) Moore, R. B.; Cable, K. M.; Croley, T. L. *Journal of Membrane Science* **1992**, *75*, 7-14.

(19) Hird, B.; Eisenberg, A. *Macromolecules* **1992**, *37*, 5995-6003.

(20) Kim, J. S.; Eisenberg, A. *Macromolecules* **1992**, *27*, 2719-2734.

(21) Neelakanta, P. S. *Handbook of Electromagnetic Materials: Monolithic and Composite Versions and their Applications*; CRC Press, 1995.

(22) Kao, K. C. *Dielectric Phenomena in Solids*; Elsevier Academic Press: New York, 2004.

(23) Schonhals, A.; Kremer, F. *Broadband Dielectric Spectroscopy*, 1 ed.; Springer, 2003.

(24) Kremer, F.; Schonhals, A. *Broadband Dielectric Spectroscopy*; Springer: Heidelberg, Germany, 2003.

(25) Diaz-Calleja, R. *Macromolecules* **2000**, *33*, 8924.

(26) Havriliak, S.; Negami, S. *Journal of Polymer Science, Polymer Symposia* **1966**, *14*, 99-103.

(27) Havriliak, S.; Negami, S. *Polymer* **1967**, *8*, 161-205, appendix 206-110.

CHAPTER II

DIELECTRIC RELAXATION STUDIES OF THE NAFION® SULFONYL FLUORIDE PRECURSOR

Abstract

While there have been numerous efforts toward elucidating the structure and properties of the acid and ion forms of Nafion®,[1] little has been reported on its non-ionic sulfonyl fluoride form. Of particular interest here is establishing baseline relaxation behavior of these materials so as to better assign the molecular motions in acid form materials that are more complex owing to the presence of very hydrophilic domains. This work outlined here is similar to that reported in a paper by Hodge and Eisenberg in the late 1970's on the dynamic mechanical and dielectric relaxation behaviors of the DuPont sulfonyl fluoride materials of various equivalent weights.[2] Five distinct features appear in the broadband dielectric relaxation spectra for the Nafion® membrane sulfonyl fluoride precursor. In order from high to low temperature, they are due to membrane | electrode interfacial polarization, dc conductivity, and the α, β and γ relaxations. Contrary to previous reports by Hodge and Eisenberg, the α relaxation should be fit using the VFT equation because of its non-Arrhenius behavior.

Introduction

Nafion® membranes have for some time been used as ion-permselective separators in chlor-alkali cells and recently as a fuel cell membrane. Despite diminished fuel cell performance near and above 100° C and high methanol permeation, it remains the benchmark proton exchange membrane in hydrogen-oxygen and hydrogen-air fuel cells, against which other membranes are compared. The chemical structure of the non-

ionic precursor form of Nafion® is a perfluorocarbon backbone with perfluoroalkylether side chains terminated with SO_2F functional groups, as shown below.

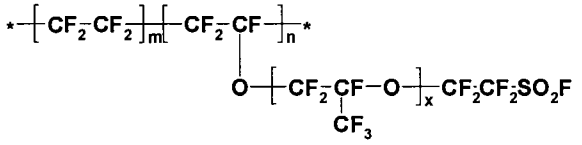

In this work, n = x = 1. The polymer is converted to the ionic form by reacting it with KOH, water and DMSO solvent. Then, after conversion to the sulfonic acid form, the equivalent weight (EW), which is the number of moles of acid groups per gram of polymer, is determined by titration.

The sulfonyl fluoride form, being non-ionic and not possessing nanophase separation, can be melt processed and extruded into films for membranes. While numerous efforts in elucidating the structure and properties of the acid and ion forms of Nafion® exist,[3] little has been reported on the precursor material. Of particular interest here is establishing the baseline relaxation behavior of these materials so as to better assign the molecular motions in acid form materials that are more complex owing to the presence of very hydrophilic domains.

This work outlined here is similar to studies by Hodge and Eisenberg on the dynamic mechanical and dielectric relaxation behaviors of the DuPont sulfonyl fluoride materials of various equivalent weights, as they existed in the late 1970's time frame.[4] In this early work, four peaks, labeled α, β", β' and γ (in order of decreasing temperature), were seen on ε'' vs. temperature (T) curves taken at constant frequency in the range of -196 to 80° C. These same relaxations were seen on dynamic mechanical E' and tan $\delta = E''/E'$ vs. T curves for the same materials in approximately the same respective temperature ranges. The dielectric α process, seen in the 20 - 35° C range, depended on frequency (f) in the

usual way and the corresponding dynamic mechanical transition had the greatest decline on E' vs. T curves, thereby indicating that this is a glass transition in the usual sense. There is no confusion of this peak with a transition associated with ionic aggregates which are not present in this precursor material. The β relaxation occured in the temperature range -100 to -20° C and at low frequencies it resolved into two components, β' and β". The β' component was said to be likely due to CF_2 backbone motions while the β'' component was due to side chain motions. The γ relaxation, seen at $T < -160°$ C was the strongest of the three in dielectric relaxation spectra but the weakest in mechanical relaxation spectra. This relaxation must be rather local and was assigned to motions of the SO_2F group based in part on the fact that this is the most polar group in the entire chemical structure. This assignment is reinforced by the fact that the relaxation disappears when the SO_2F are converted to sulfonate or sulfonamide groups.[5,6]

Broadband dielectric spectroscopy has the great advantage of interrogating molecular motions over a very wide range of time and distance scales.[7] The complex dielectric permittivity is given by the following equation in which ω, the angular frequency, is $2\pi f$ and $i = \sqrt{1}$.

$$\varepsilon^*(\omega) = \varepsilon'(\omega) - i\varepsilon''(\omega) \qquad \text{Equation 1}$$

ε' reflects material polarizability, usually due to orientation of dipoles in polymers but can also reflect interfacial polarization. ε'' is proportional to the energy dissipated per cycle during these molecular motions.

The Havriliak-Negami (HN) equation, often used to represent dielectric relaxation spectra, is shown below with an additional term to account for possible dc conductivity at low f.[8,9]

$$\varepsilon^*(\omega) = \varepsilon' - i\varepsilon'' = -i\left(\frac{\sigma_0}{\varepsilon_0 \omega}\right)^N + \sum_{k=1}^{n}\left[\frac{\Delta\varepsilon}{\left(1+(i\omega\tau_{HN})^{\alpha_{HN}}\right)^{\beta_{HN}}}\right] \qquad \textbf{Equation 2}$$

Each term in the sum represents a different relaxation such as glass and sub-glass transitions in polymers. The values of the parameters result from a fit of equation 2 to experimental data. $\Delta\varepsilon = \varepsilon_o - \varepsilon_\infty$ is the difference between the low and high frequency limits of ε' for the given process. τ_{HN} is a time that is related to the actual relaxation time, τ_{max}, which is associated with the frequency at the respective peak maximum, f_{max}. α_{HN} and β_{HN} are parameters related to the breadth and symmetry, respectively, of the given relaxation such that $\alpha_{HN} < 0 \leq 1$ and $0 < \beta_{HN} \leq 1$. Data-fitted α_{HN}, β_{HN} and τ_{HN} parameters are then used to determine τ_{max} using the following equation.[10]

$$\tau_{max} = \tau_{HN}\left[\frac{\sin\left(\frac{\pi\alpha_{HN}\beta_{HN}}{2(\beta_{HN}+1)}\right)}{\sin\left(\frac{\pi\alpha_{HN}}{2(\beta_{HN}+1)}\right)}\right]^{\frac{1}{\alpha_{HN}}} \qquad \textbf{Equation 3}$$

When present, dc conductivity can obscure weak polymer relaxations that occur at low frequencies. This obscuration is removed as follows: Once the exponent $N \leq 1$ and the dc conductivity σ_0 are determined by curve fitting in the low f regime, this term is subtracted point-by-point from ε'' curves to reveal the relaxation peaks.

Experimental

Materials

Extruded Nafion® sulfonyl fluoride precursor films having equivalent weights (EW) of 1000 and 1200 g/equivalent of resin were supplied by E.I. Dupont Co. In addition, another 1000EW sample whose end groups were chemically stabilized was used.

To ensure that samples did not contain any moisture they were heated at 100° C under vacuum for 4d before testing. These vacuum prepared samples were compared to ones that were not dried and no differences were detected.

Instrumentation

A Novocontrol GmbH Concept 40 broadband dielectric spectrometer was used over the frequency range 0.1Hz - 3MHz at temperatures ranging from -130 to 190° C and the temperature was controlled to within +/- 0.2° C. Samples were tightly pressed between two 20mm diameter brass electrodes. Frequency sweeps over this range were performed at consecutive 10° C increments. Samples were heated to 200° C for 20 min before testing to provide a consistent thermal history and good contact with the electrode.

Equation 2 was fitted to isothermal dielectric permittivity data.[8,9] The dc loss contribution was not problematic for studying the molecular relaxations as it only arose at temperatures higher than T_g and does not overlap with the α-relaxation.

Results and Discussion

Figure 0-1 and Figure 0-2 are 3-dimensional plots of ε'' vs. f and T for 1000 and 1200 EW films, respectively. The locus of all points on such plots will be referred to as a 'response surface'. Close inspection shows five distinct spectral features, in order from high to low temperature, that are assigned to (1) membrane | electrode interfacial polarization, (2) dc conductivity, and (3) the α, β and γ relaxations noted by Eisenberg and Hodge.

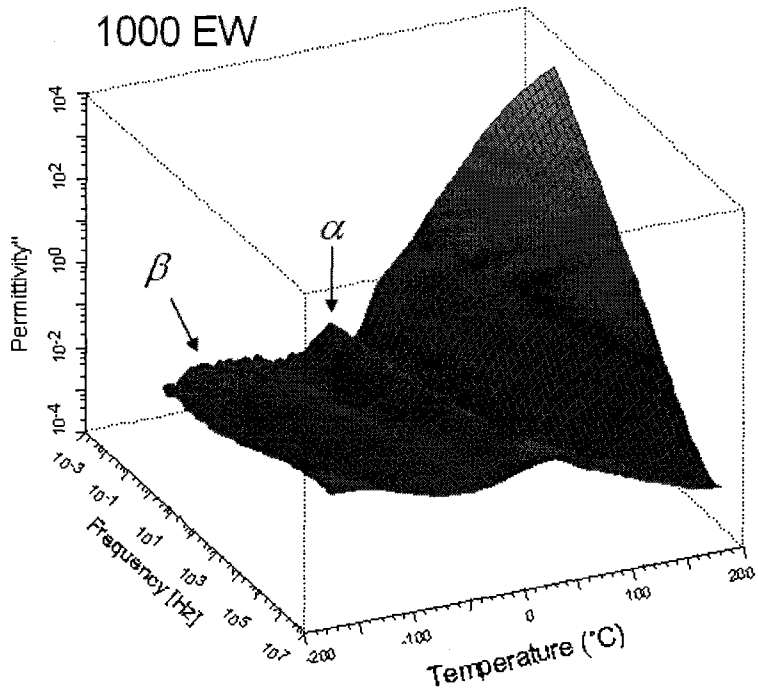

Figure 0-1 $\varepsilon'' - f - T$ response surface for a 1000 EW Nafion® sulfonyl fluoride precursor film.

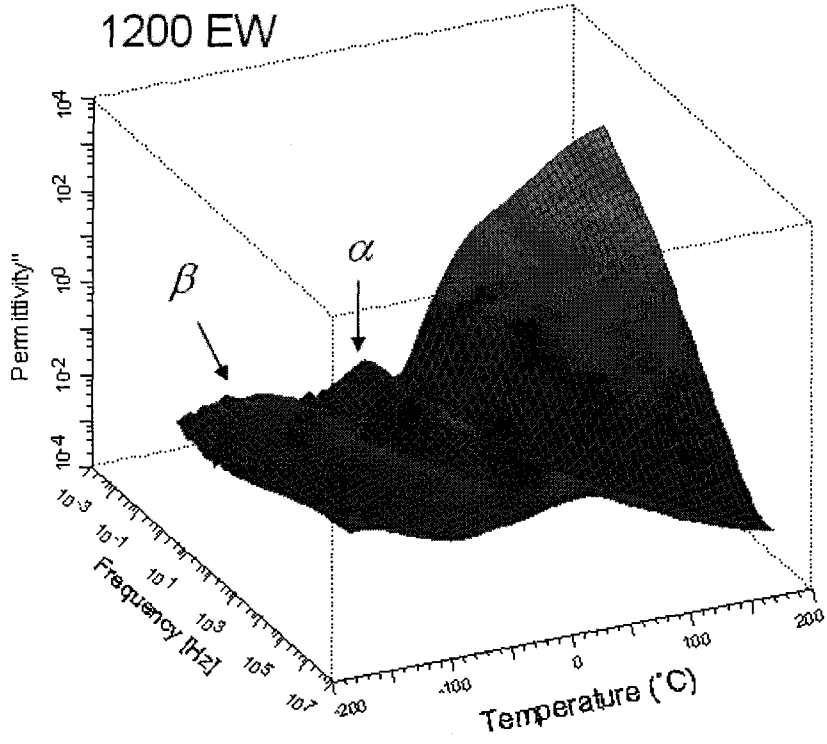

Figure 0-2. ε'' - f - T response surface for a 1200EW Nafion® sulfonyl fluoride precursor film.

Low f - high T spectral features.

The spectral manifestations of dc conductivity and membrane | electrode interfacial polarization appear on this region of the surface. dc conductivity in polymers arises from the motion of intended charges but also often as unintended, ubiquitous charge impurities in non-ionic polymers. As f becomes lower, a greater number of consecutive charge hopping events, akin to charge drift, can be sampled within a half-cycle of electric field oscillation. The spectral signature for this phenomenon is a linear segment having a slope, of ~ 1.00 for good conduction, on $\log_{10}\varepsilon''$ vs. $\log_{10}\omega$ plots.

Membrane|electrode interfacial polarization relaxation results from induced opposite charge layers adjacent to the two blocking electrodes that alternate in polarity with a characteristic relaxation time, that, in a simple electrical double layer model, is inversely proportional to σ_0.[11,12] The signature of this process is a Debye-like peak, usually at frequencies beneath the range for dc conduction. When such a low frequency peak is off-scale to the left on the $\log_{10}\varepsilon''$ vs. $\log_{10} f$ plot, it may still be seen as a slight downturn in the dc line segment at the lowest frequencies. Another signature of membrane|electrode interfacial polarization, which can be considered as a capacitive effect, is very large low frequency ε' values that cannot be accounted for in terms of molecular dipole orientation in the bulk.

Figure 0-3 and Figure 0-4 are 2-D plots of $\log_{10}\varepsilon'$ and $\log_{10}\varepsilon''$ vs. $\log_{10} f$ for the 1000 EW film at increasing constant temperatures where the curves are separated by 20° C increments. The monotonically increasing ε' vs. f curves at each temperature undergo

a uniform upward displacement with increasing temperature which reflects increased polarizability. An inflection gradually appears on each ε'' curve with increase in T. The increase in ε' in Figure 0-3 corresponds to the ε'' inflection point in Figure 0-4 at each respective temperature. Before the inflection points the slopes of the ε'' curves are close to unity as indicated in Table 0-1, which is characteristic for dc conductivity. However, after the inflection point the slope decreases, which is more pronounced for the 1200EW sample, which is indicative of a membrane|electrode interfacial polarization relaxation. These exponent values are listed in Table 0-1. The curve for 200° C in Figure 0-3 back-extrapolates to the rather high value of $\varepsilon' \sim 1000$, suggesting membrane|electrode interfacial polarization relaxation. On the ε'' vs. f curves, this appears as a relaxation which develops at low frequencies and shifts to the right with increasing temperature. Linear curve sections develop on-scale and shift upward with increasing temperature. Despite the presence of dc conductance, its origin is not clear since this is not a strongly polar polymer nor does it contain any known mobile charge carriers. Furthermore, it was dried at 100° C under vacuum for 4d before testing. This should leave the polymer without any small molecule mobile species.

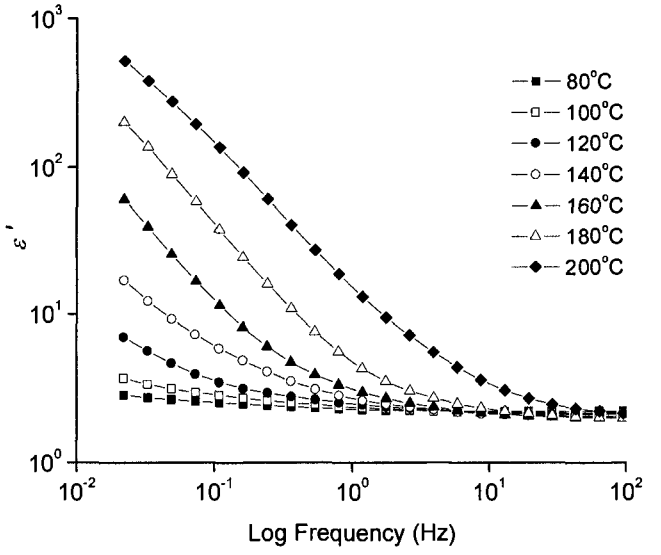

Figure 0-3. 2-D plots of $\log_{10}\varepsilon'$ vs. $\log_{10}f$ for the 1000 EW film at indicated temperatures.

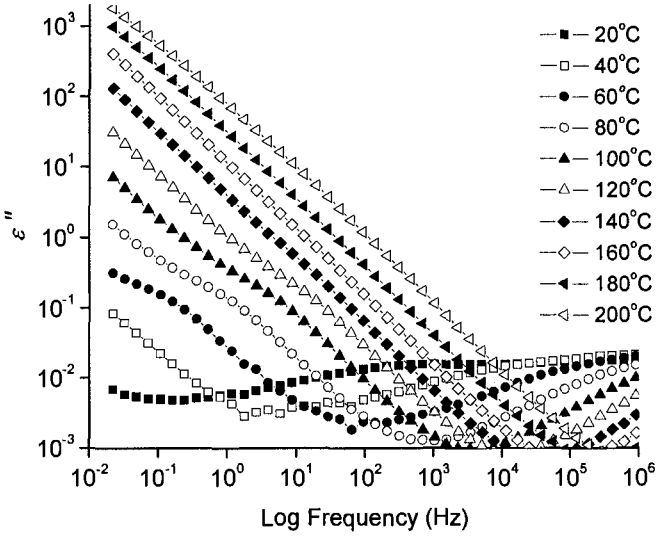

Figure 0-4. 2-D plots of $\log_{10}\varepsilon''$ vs. $\log_{10}f$ for the 1000 EW film at indicated temperatures.

Table 0-1. The N values from low frequency fitting with the conductivity term of the ε" upswing. The dc conductivity corresponds to the region fit before the inflection point and interfacial polarization corresponds to the region fit after the inflection point.

	1000EW		1200EW	
°C	N for dc conductivity	N for interfacial polarization	N for dc conductivity	N for interfacial polarization
90	0.828	-	0.828	-
100	0.929	-	0.929	-
110	0.95	-	0.950	-
120	0.948	-	0.948	-
130	0.966	0.914	0.966	0.451
140	0.972	0.925	0.972	0.504
150	0.974	0.940	0.974	0.549
160	0.974	0.933	0.974	0.587
170	0.977	0.917	0.977	0.603
180	0.98	0.890	0.980	0.614
190	0.979	0.849	0.979	0.625
200	0.977	0.803	0.977	0.638

Figure 0-5 and Figure 0-6 for the 1200EW sample are, respectively, similar to Figure 0-3 and Figure 0-4 for the 1000EW sample, but with some differences. For example, ε' vs. f curves for 1200EW do not attain values as high as those for the 1000 EW sample, but are nonetheless higher than what would be expected on the basis of simple dipole rotation. The explanation for the disparity between results for the two equivalent weights may reside in the fact that the 1000EW sample has 1.2 times as many polar side chains per gram of material. Perhaps, as side chain dipoles become more mobile with increasing temperature, they are able to orient toward the electrodes and give rise to unbalanced partial charges at the surface. Figure 6 also contains a downturn in ε " with decreasing f to the left of the linear dc segment of the curves that corresponds with the ε ' increase of Figure 0-5. This is most likely due to film-electrode interfacial polarization relaxation, as explained above.

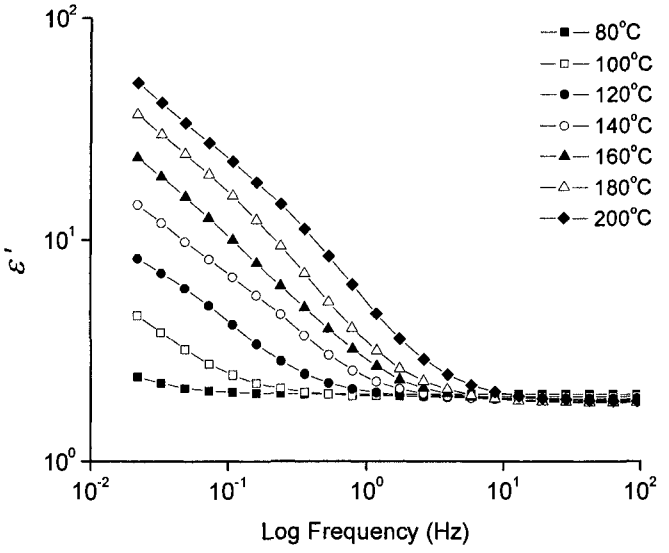

Figure 0-5. 2-D plots of $\log_{10}\varepsilon'$ vs. $\log_{10}f$ for the 1200EW film at indicated temperatures.

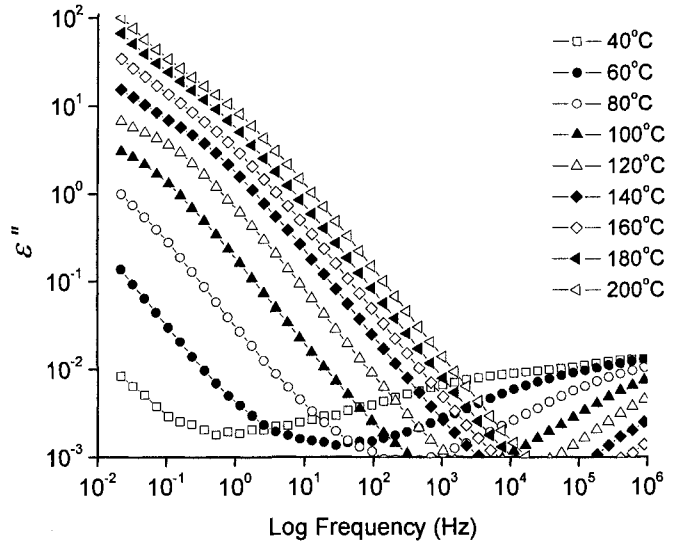

Figure 0-6. 2-D plots of $\log_{10}\varepsilon''$ vs. $\log_{10}f$ for the 1200EW film at indicated temperatures.

Macromolecular Relaxations

α relaxation. The α relaxation for polymers as observed by dielectric spectroscopy is referred to as a dynamic glass transition that corresponds to cooperative long range chain segmental motions. Poly(tetrafluoroethylene) is a polymer whose weak

dielectric activity is thought to arise from polar impurities attached to the chains. An early discussion of dielectric relaxations in PTFE is in the book by McCrum, Read and Williams.[13] For the system at hand, which has a PTFE-like backbone, the major dipoles are the SO_2F group and two C-O-C groups in the side chains. As the motions of the side chains are coupled to those of the backbone, the motions in the latter are seen indirectly through this coupling.

A relaxation signature of the glass transition is nonlinear $\log f_{max}$ or, inversely, $\log \tau_{max}$ vs. $1/T$ plots as opposed to linear Arrhenius behavior for activated processes. In this case, the empirical Vögel-Fulcher-Tammann (VFT) equation, shown below, is often well fitted to the data.[14]

$$\tau(T) = \tau_0 \exp\left(\frac{E_a}{k_B(T - T_V)}\right) \qquad \textbf{Equation 4}$$

k_B is the Boltzmann constant and τ_0, E_a, and T_V are parameters obtained by fitting this equation to experimental relaxation time vs. T data. τ_0 is a hypothetical relaxation time at infinite temperature. E_a, while having units of energy, is a ubiquitous quantity not associated with an activated process and can have values unrealistically too high. T_V, the Vögel temperature, is the temperature at which chain segments become frozen in a hypothetical situation in which a polymer is cooled at a quasi-static rate from the rubbery state and $T_V < T_g$. Systems with large deviations from linearity are described as being "fragile". E_a, is a quantitative measure of fragility but should be examined in context with τ_0 and T_V.[15]

The α relaxation peak emerges between -10 and 10° C over the frequency range 10^{-2} - 10^6 Hz depending on equivalent weight, although the high frequency tail is visible

before these temperatures are reached. With increased temperature the α peak shifts from low to high frequency, or left to right as indicated in Figure 0-9 and Figure 0-10. On increasing T to ~ 60-70° C the α relaxation begins to significantly overlap the β relaxation. Subsequently, the α relaxation merges with the β relaxation forming the α-β process. The superposition of the two relaxations compromises the accuracy of the HN and VFT fits.

Plots of log τ_{max} vs. 1/T for both the 1000 and 1200EW precursor samples are displayed in Figure 0-7 and the corresponding VFT fit parameters for these samples are listed in Table 0-2. T_V for the 1200EW sample is approximately 8° C higher than that for 1000 EW. The lower T_V values for the both 1000EW and the 1000EW CS precursor samples suggests that the 1000EW system has somewhat greater molecular mobility which might be due, in part to the greater density of side chains in this form. The closer these long motional-restrictive side chains are, and the shorter the number of CF_2 units between them, the more thermal kinetic energy is required to affect a glass transition. Also, degree of crystallinity increases with increasing EW and this would influence chain motions. This would tend to increase T_g, and therefore T_V due to an overall decrease in the tethering of amorphous chain ends that emerge from crystallites.

Starkweather reported on the suflonyl fluoride form of Nafion® that as the degree of crystallization increases both the heat of fusion (ΔH_f) and the crystalline melting temperature (T_m) decrease, indicating that the suflonyl fluoride groups are inhibiting crystallization.[16] In the present study it is believed that the higher amorphous content of the 1000EW precursor is responsible for the reduction in T_V and greater intensity of the α relaxation as observed for the normalized peaks in Figure 0-7. Interestingly, despite the

T_V differences, the high frequency relaxation times listed in Table 0-2 do not statistically differ between these two equivalent weights.

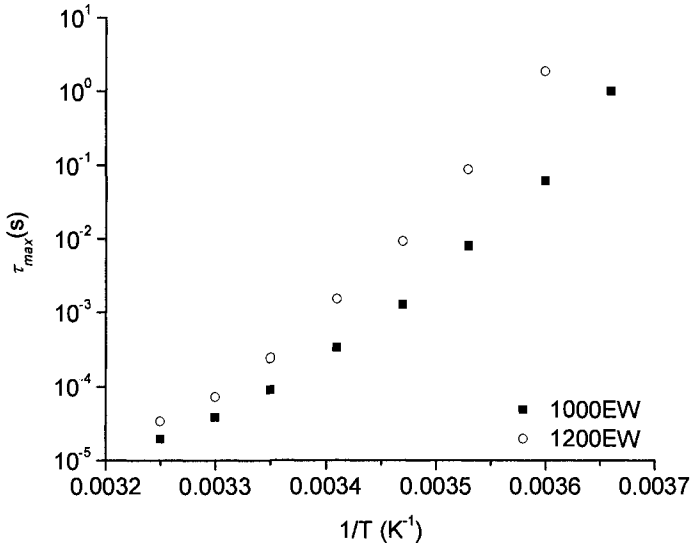

Figure 0-7. $\log_{10}\tau_{max}$ vs. $1/T$ for the α relaxation in 1000 and 1200EW precursor films.

Table 0-2: Average of three different samples values of VFT fit parameters for 1000 and 1200EW (standard deviation of the three samples).

EW	τ_0(s)	E_a (kJ/mol)	T_V (°C)	MSD
1000	2.24E-11 (2.68E-11)	9.07 (1.06)	- 42.95 (2.6)	0.030 (0.008)
1000 CS	6.19E-12 (1.03E-12)	9.46 (0.29)	- 43.25 (1.0)	0.037 (0.016)
1200	4.65E-11 (4.25E-11)	7.91 (3.67)	- 35.15 (2.5)	0.025 (0.011)

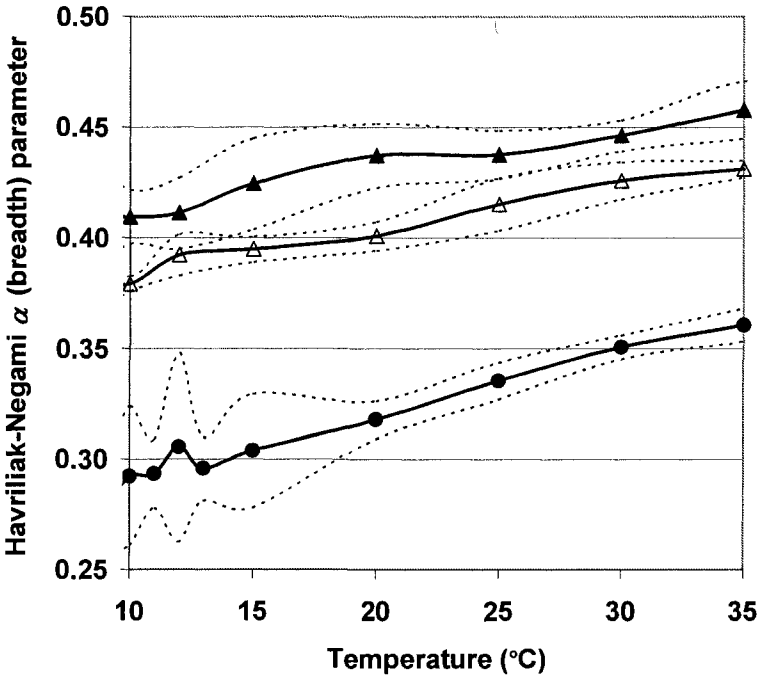

Figure 0-8. Average α values for the α relaxation obtained from H-N equation fits to ε'' vs. f data at each respective temperature. Triangles represent 1000 EW represented as solid points and 1000 EW CS represented as open points. The 1200 EW is designated by the solid circles. The dashes indicate one standard deviation from the average.

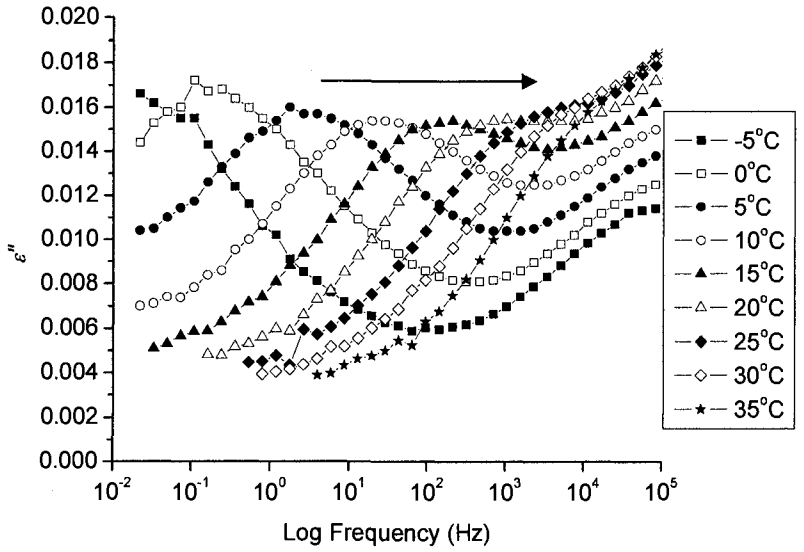

Figure 0-9. $\log_{10} \varepsilon''$ vs. $\log_{10} f$ for 1000EW films illustrating α relaxation peaks at indicated temperatures with dc conductivity subtracted. Arrow indicates direction of peak shift with increasing temperature.

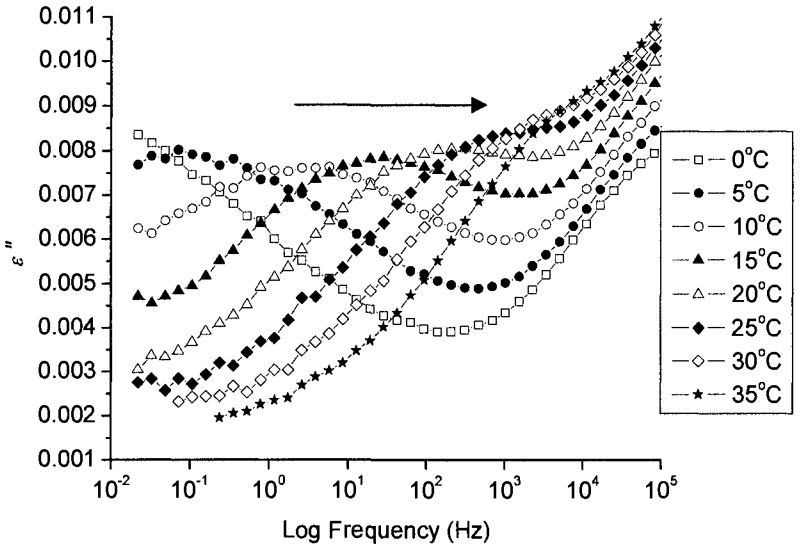

Figure 0-10. $\log_{10} \varepsilon''$ vs. $\log_{10} f$ for 1200 EW films illustrating α relaxation peaks at indicated temperatures with dc conductivity subtracted. Arrow indicates direction of peak shift with increasing temperature.

For the α relaxation, Hodge and Eisenberg reported E_a = 305 kJ/mol which is about 300 kJ/mol higher than the values we reported in Table 0-2. The discrepancy most likely lies in the use of two relaxation equations. Hodge and Eisenberg used a standard

Arrhenius equation with formal activation energy to fit the α relaxation $\log f_{max}$ vs. $1/T$ data which was logical as their data appears linear relative to the scaling used in the plot. When we use a similar scaling our data also appears linear. Fitting our points to an Arrhenius equation generates an E_a = 190 kJ/mol, which is somewhat closer to the Hodge-Eisenberg value. Furthermore, E_a increases to ~ 310 kJ/mol if only the lowest few frequency data points are used. It is believed that the α relaxation of the Nafion precursor should be fit using the VFT equation as a Figure 0-7 confirms that the data is non-linear. E_a calculated using the VFT equation is not a true activation energy rather it is regarded more as a fitting term.

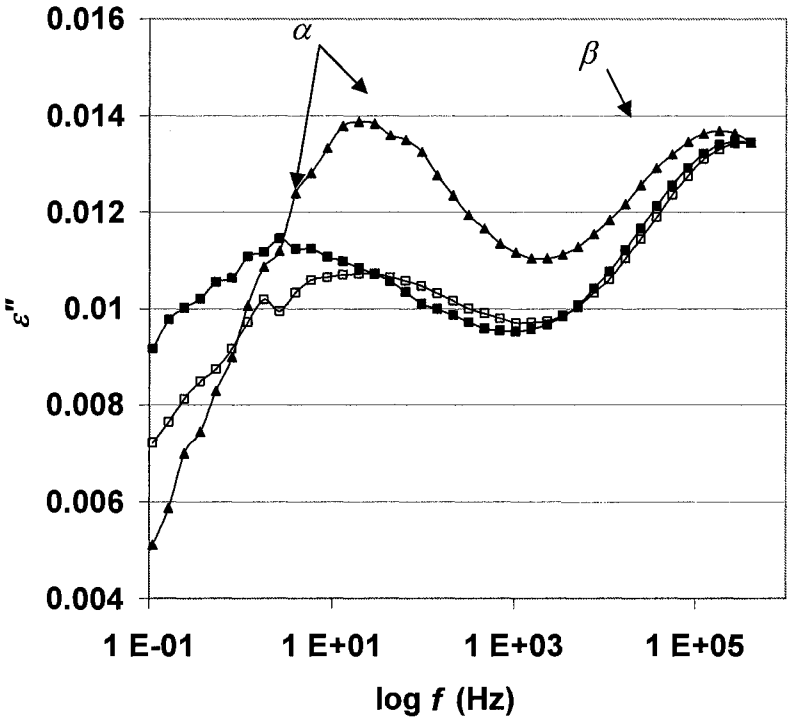

Figure 0-11. ε" vs. log *f* for 1200EW (squares) and 1000EW (triangles) films. Solid shapes are for frequency sweeps at 10° C and open shapes are for a sweep at 13° C.

As mentioned, the breadth and symmetry of the α relaxation is quantified by the α_{HN} and β_{HN} parameters of the HN function, respectively. Due to superposition of peaks

and the peaks partially moving off the scale at some temperatures, the HN fit function can be fit accurately with two methods: 1) β_{HN} is assigned to a value of 1.00 and 2) β_{HN} allowed to adjust its value with each ε" vs. f fitting. Both methods generated acceptable MSD values for each HN fit; however, the latter generated more variation with each sample. Therefore, for each fit, β_{HN} was assigned to be 1.00. As evidenced by a lower α_{HN} value, the 1200EW sample has a much broader α_{HN} relaxation than the 1000EW sample (see Figure 0-8). For both EWs, as temperature increases, α increases indicating that the distribution of relaxation times narrows.

Schönhals and Schlosser developed a model for interpreting the shape of the dielectric relaxation function at the glass transition. The model is mathematically equivalent to that of Dissado-Hill but differs in terms of the physical view upon which the model is based. The basic idea of Schönhals and Schlosser is that the glass transition is controlled by intra- and intermolecular motions. For amorphous polymeric systems, these molecular interactions correlate with the high and low frequency wings of the α relaxation, respectively. Specifically, the *high* frequency wing is controlled by local intramolecular motions of chain units whereas the *low* frequency wing is dominated by intermolecular correlated motions.[17]

Hensel et al. isolated intra and intermolecular influences using dielectric spectroscopy by studying fully amorphous and semi-crystalline poly (ethylene terephthalate) (PET). They found that the semi-crystalline relaxation spectrum is broader than the fully amorphous spectrum but only on the *low* frequency wing of the α relaxation—the high frequency wing was not affected.[18] Amorphous motions detected on the low frequency side of the α relaxation peak are more substantial such that they are

constrained by the geometrical restrictions imposed by the crystals. In other words, the crystalline regions constrain the longer range lower frequency motions from the amorphous regions. This is because longer range motions detected at the lower frequencies are of similar length scales to that of the size of the amorphous regions. The mode length of motion for these large domains is limited by the geometrical length between crystals.

For the system reported here, it is believed that the increased breadth of the low frequency wing of α relaxation peak for 1200EW, as is evidenced in Figure 0-11, is due to an increased degree of crystallinity relative to the 1000EW specimen.[16, 19] Increase in crystallinity imposes regional geometrical restrictions on the amorphous regions generating a more heterogeneous amorphous environment. The net result of this on the α relaxation is a broader distribution of long range motions. This broadening is most apparent on the low frequency wing of the α relaxation.

β relaxation. Typically the dielectric strength of the *β*-relaxation depends on the mobility of the pendent group. For many polymers with a rigidly attached dipole the dielectric strength of the β is much weaker than that of the *α*-relaxation. However, sidechain conformational flexibility may increase the dielectric strength of the β relaxation such that it is of approximately the same in intensity as the α relaxation.[15]

In the present study, the β relaxation of the Nafion® precursor is approximately equal in strength to that of the α relaxation, as illustrated in Figure 0-11, which does suggest considerable mobility of the side chain that contains two ether groups. As temperature increases, the dielectric strength of the β relaxation usually increases and the breadth of the distribution of relaxation times narrows, as shown in Figure 0-12.

Evidence for this is by the very broad low frequency tail at low temperatures. This peak narrows considerably when the temperature is increased. The broadness at low temperatures is believed to be attributed to the fact that the β relaxation separates into two peaks at low frequencies and low temperatures. These motions, as previously mentioned, are assigned to $-CF_2-$ backbone and the ether group-containing side chain motions. It is not known exactly why, but at the lowest temperatures the low frequency wing of the β relaxation has considerably more variability. The lowest temperature relaxations are difficult to fit due to this variability as well as complications due to peak breadth and superposition.

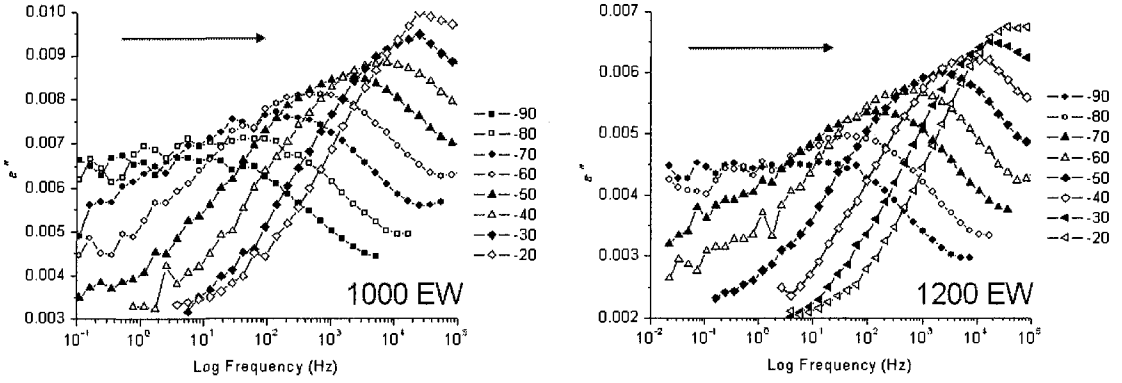

Figure 0-12. 2-D ε'' vs. f plots illustrating the β relaxation for 1000 and 1200EW samples from -90 to -20° C. dc conductivity is not present at these temperatures. Arrow indicates the peak shift direction with increasing temperature.

The β relaxation stems from both intra- and intermolecular motions arising from the dipole vector's localized rotational fluctuations. To understand the β relaxation two theoretical approaches are commonly used.[15] The first approach, developed by Heijboer, focuses on the molecular fluctuations in a glassy system. These fluctuations can either be localized parts of the main chain or rotating fluctuations of pendant groups (or parts of them). The second approach, theorized by Johari and Goldstein, takes a fundamentally

different approach in that it presupposes that the β relaxation is common to almost all glassy materials and that it is actually a "generic feature" of the glass transition.[20] This theory not only accounts for the β relaxation's presence at sub-T_g temperatures but also hypothesizes about its persistence above T_g.

The β relaxation, being associated with short range motions, is characteristically represented by the Arrhenius equation:

$$\ln \tau_{max} = \ln \tau_{\infty} - \frac{Ea}{RT} \qquad \text{Equation 5}$$

E_a is the activation energy and R is the universal gas constant. Figure 0-13 confirms that the β relaxation is linear for both the 1000 and 1200EW samples. The estimated activation energies for the 1000 and 1200 EW samples are 43.6 and 43.2 kJ/mol·K, respectively, that is, essentially equal. To estimate the variability in the data for the β relaxation, a curve was constructed from the average of five 1200EW specimens as shown in Figure 0-14. It is apparent in this figure that the most data variability is at the high and low ends of the curve. Calculated activation energy differences between the 1000 and the 1200EW samples are most likely within experimental error. From this curve, the activation energy is calculated to be 43.2 kJ/mol. Hodge and Eisenberg reported an activation energy of 46.0 kJ/mol.

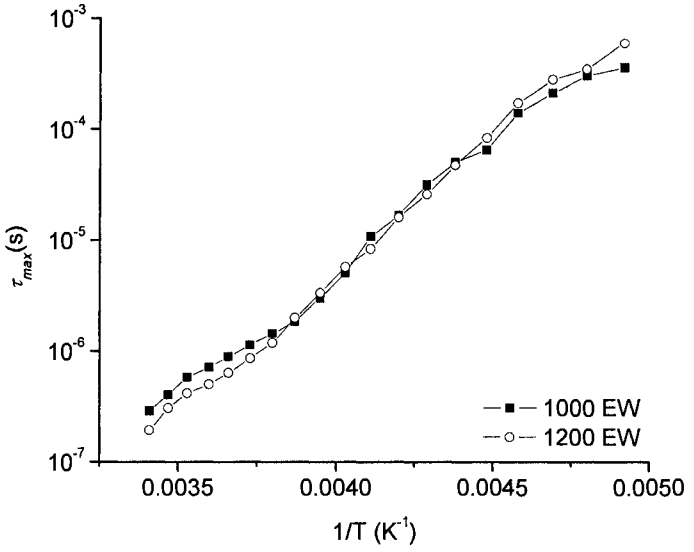

Figure 0-13: ln τ_{max} vs. T^{-1} for 1000 and 1200 EW specimens for the β-relaxation.

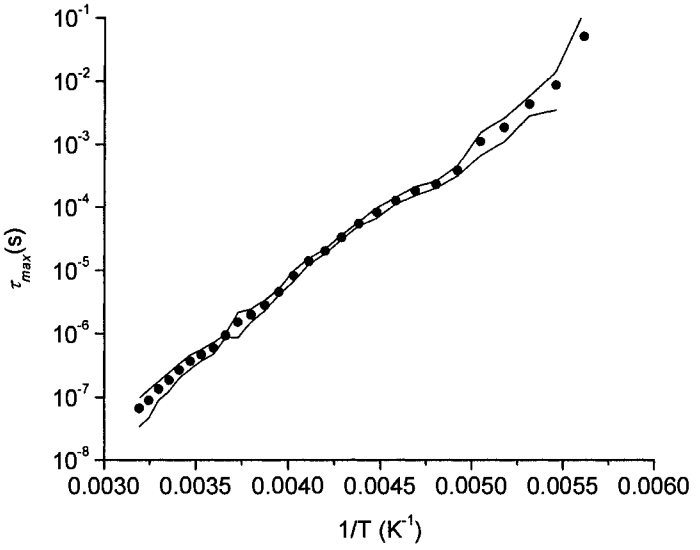

Figure 0-14. ln τ_{max} vs. T^{-1} for the β relaxation. Solid data points are the average of five 1200EW samples. The curves are one (+/-) standard deviation from the average.

As temperature increases the α-relaxation and the β-relaxation typically merge because the α-relaxation increases faster than the β-relaxation. This crossover region is termed the α–β process.[15] However, by plotting the parameters of the VFT equations for the 1000 and the 1200 EW samples as well as the Arrhenius β relaxation reveals that the

α and β relaxations do not merge as is shown in Figure 0-14.

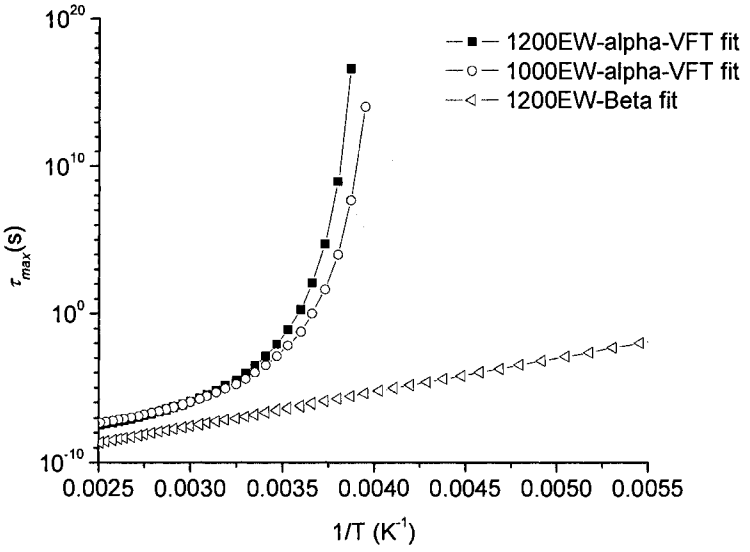

Figure 0-15. Fitted curves for the α and the β relaxations illustrating the α-β merging process.

Conclusions

Five distinct features appear in dielectric relaxation spectra for the Nafion® membrane sulfonyl fluoride precursor. In order from high to low temperature, they are due to membrane | electrode interfacial polarization, dc conductivity, and the α, β and γ relaxations.

At low frequencies the ε' values of both the 1200EW and the 1000EW specimens are relatively high. The fact that the 1000EW specimen has 1.2 times more polar side chains than the 1200 specimen may be the cause for the greater ε' values observed for the 1000EW sample. These flexible side chains may be the source for the electrode polarization that occurs at increased temperatures.

Depending on EW the α relaxation peak emerges between -10 and 10° C over the frequency range 10^{-2} to 10^{6} Hz, although the high frequency tail is visible before these temperatures are reached. With each increased temperature increment the α relaxation peak shifts from low to high frequency. On increasing the temperature to ~ 60-70° C the α-relaxation begins to significantly overlap with the β-relaxation and subsequently the two relaxations merge. The superposition of the two relaxations compromises the accuracy of the HN and VFT fits.

As typical for glassy materials, the α relaxation (glass transition) does not display Arrhenius behavior on log τ_{max} vs. $1/T$ plots. T_V for the 1200EW sample is approximately 8° C higher than that for 1000 EW. The lower T_V value for 1000EW suggests that this system has somewhat greater molecular mobility. This reduction in T_V and greater intensity of the α relaxation may be due to the higher amorphous content of the 1000 EW version, which may be related to the greater density of side chains in the 1000EW sample. Also, degree of crystallinity increases with increasing EW. This would tend to increase T_g, and therefore T_V due to an overall decrease in the tethering of amorphous chain ends that emerge from crystallites.

The previously reported E_a value of 305 kJ/mol, by Hodge and Eisenberg for the α-relaxation was mostly like determined by forcing a linear Arrhenius equation fit, whereas, it was shown here that the α relaxation is better fit using the VFT equation.

For the work reported here, it is believed that the increased breadth of the low frequency wing of α relaxation peak for the1200EW sample, is due to an increased degree of crystallinity relative to the 1000EW sample. An increase in crystallinity imposes geometrical and chain tethering restrictions on the amorphous regions generating

a more heterogeneous environment over the entire ensemble of chains. The net result is a broader distribution of long range motional time scales, i.e., distribution of relaxation times. This broadening is most apparent on the low frequency wing of the α relaxation.

The β relaxation of the Nafion® precursor is approximately equal in strength to that of the α relaxation. As temperature increases, the dielectric strength of the β relaxation usually increases and the breadth of the distribution of relaxation times narrows. The peak broadness at low temperatures is attributed to the separation of the β relaxation into two peaks at low frequencies and low temperatures. These motions are assigned to $-CF_2-$ backbone and the ether group-containing side chain motions. For the combined β relaxation, E_a = 43.2 kJ/mol with no measurable differences between 1000 and1200 EW variants.

References

[1] Mauritz, K.A.; Moore, R.B. Review: "State of Understanding of Nafion." In *Chem. Rev. Introduction: Batteries and Fuel Cells* **2004**, *Vol. 104, No. 10* (Eds. M.S. Whittingham, R.F. Savinell, T. Zawodzinski).

[2] Hodge, I. M.; Eisenberg, A. *Macromolecules* **1978**, *11*, 289.

[3] Mauritz, K.A.; Moore, R.B. Review: "State of Understanding of Nafion." In *Chem. Rev. Introduction: Batteries and Fuel Cells* **2004**, *Vol. 104, No. 10* (Eds. M.S. Whittingham, R.F. Savinell, T. Zawodzinski).

[4] Hodge, I. M.; Eisenberg, A. *Macromolecules* **1978**, *11*, 289.

[5] Rhoades, D.W.; Mauritz, K.A.; unpublished results.

[6] Kyu, T.; Hashiyama, M.; Eisenberg, A. *Canadian Journal of Chemistry* **1983**, *61*, 680-687.

[7] Kremer, F.; Schönhals, A. *Broadband Dielectric Spectroscopy* Springer: Berlin **2003**.

[8] Havriliak, S.: Negamin, S.; *J. Polym. Sci. C* **1966** 16, 99.

[9] Havriliak, S.; Negamin, S.; *Polymer* **1967** 8, 161.

[10] Diaz-Calleja, R.; *Macromolecules* **2000**, *33*, 8924.

[11] Klein, R. J.; Zhang, S.; Dou, S.; Jones, B. H.; Colby, R. H.; Runt, J. *J. Chem. Phys.* **2006,** *124*, 144,903.

[12] Mauritz, K.A.; *Macromolecules* **1989**, *22*, 4483.

[13] McCrum, N.G.; Read, B.E.; Williams, G. *Anelastic and Dielectric Effects in Polymeric Solids*, Dover: New York, 1991, p. 454.

[14] VFT eqn.

[15] Kremer, F.; Schonhals, A. Eds. *Broadband Dielectric Spectroscopy* Springer, Berlin, 2003, Chapter 4 & 7.

[16] Starkweather, Howard W. Jr. *Macromolecules.* **1982**, *15*, 320.

[17] Schönhals, A; Schlosser, E. *Colloid Polym Sci* **1989**, *267*, 125.

[18] Hensel, A.; Dobbertin, J.; Schawe, J.E.K.; Boller, A.; Schick, C.; *J. Therm. Anal.* **1996**, 46, 935.

[19] Gierke, T.D.; Munn, G.E.; Wilson, E; *J. Polym. Sci., Part B: Polym. Phys.* **1981**, 19, 1687.

[20] Johari, Gyan P.;Goldstein, Martin; *J. Chem. Phys.* **1979.** *53*, 2372.

CHAPTER III

DIALKYLAMINE - MODIFIED SULFONYL FLUORIDE NAFION® PRECURSOR MEMBRANE

Abstract

Melt-processable non-ionic Nafion® precursor films were chemically modified at room temperature in a layered fashion by diffusion reactions of different alkyl diamines with the SO_2F groups at the end of the pendant perfluoralkylether chains. Due to the contrast caused by differences in the index of refraction of the chemically modified and unmodified regions across the film thickness, optical microscopy was used to track and quantify the depth of penetration of the reacted regions. Here we report the shift in molecular motions due to constraints posed by these side chain links as characterized by broadband dielectric spectroscopy. In addition to the glass transition relaxation of the precursor all amine modified films have two relaxations (A1R and A2R). A1R and A2R track each other with increasing temperature and frequency which suggests that these two relaxations are closely linked to each other. Using infrared spectroscopy it was determined that heating drives the free amine which is attached to the side chain from a salt association to a covalent linkage. Correlating the disappearance of the A2R in the dielectric spectrum with the IR data could indicate that A2R stems from the reorientation of the dipole moment of the amine salt. Resultantly then, A1R would stem from the dipole reorientation of the amine covalent linkage. The shift of A1R to higher temperatures and frequencies implies restricted chain motion which further supports the idea that this relaxation is comprised of covalent linkages that are part of cross-links.

Introduction

Most electrical → mechanical energy conversion actuators and sensors are homogeneous polymer materials, at least above the nanoscale. However, controlled chemical inhomogeneity across the film thickness direction has the potential to generate mechanical responses that are more complicated than the symmetrical bending deflections observed for homogenous materials such as Nafion® perfluorosulfonate ionomers[1]. Chemical gradients not only affect mechanical properties but also the thermal and swelling responses as well as ionic conduction and dielectric properties, all of which are involved in actuator performance.

In this study, melt-processable non-ionic Nafion® precursor films were chemically modified by reactions of different alkyl diamines with the SO_2F groups at the end of the pendant perfluoralkylether chains. The goal of this work is to create gradient or chemically-layered films having sulfonyl fluoride groups on one side and sulfonamide groups on the other side. These films, when hydrolyzed with base, thereby converting the SO_2F groups to $SO_3^-Na^+$, groups, will form the active component of electrical-to-mechanical energy actuators having asymmetric bending responses. Here we report and provide evidence for successful reactions of this nature. Also, reported here is the shift in molecular motions due to constraints posed by these side chain links as characterized by broadband dielectric spectroscopy. Crosslinking in these materials is expected to modify the mechanical as well as ion transport properties, both of which are of paramount importance within the context of electrical → mechanical energy conversion actuators.

The chemical conversion to the sulfonamide form proceeds according to the following reaction:

Mechanism 1

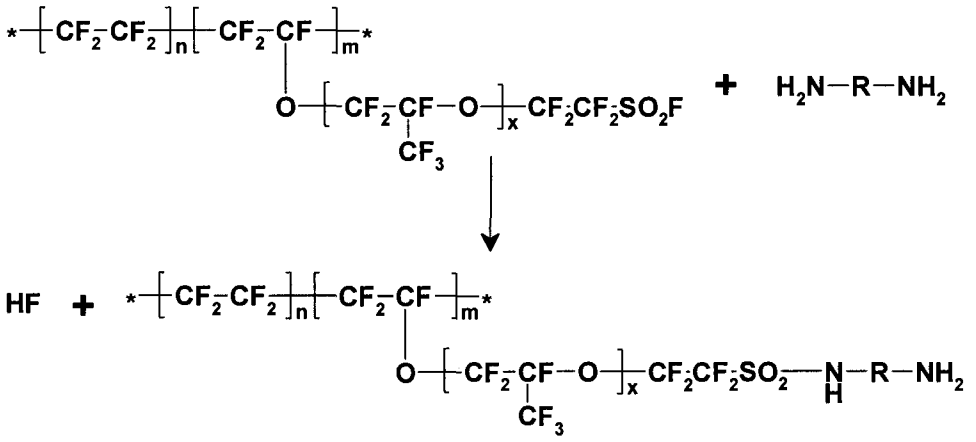

For low molecular weight alkylamines, this diffusion controlled reaction occurs readily in Nafion® sulfonyl fluoride precursor films at room temperature. Due to the contrast caused by differences in the index of refraction of the chemically modified and unmodified regions across the film thickness, optical microscopy can be used to observe and quantify the depth of penetration of the reacted regions. After this initial reaction, the films were heated to the point where both amine groups react with adjacent SO_2F groups, thereby forming cross links through the side chains. [2,3]

This Nafion® modification was originally considered within the context of membrane chlor-alkali cells for the large scale electrochemical production of NaOH and Cl_2, although the idea was abandoned due to the material's instability to the hypochlorite ion.[4]

Relaxations, i.e., molecular motions, in these chemically-layered materials were probed using the powerful technique of broadband dielectric spectroscopy. The

advantage of this method, as compared to dynamic mechanical analysis, is the ability to interrogate samples over a wider range of time scales, in this case in the frequency (*f*) range of 0.01 - 10^6 Hz, as well as being able to extract relaxation times and their distributions. Moreover, this sophisticated electrical characterization tool is quite relevant in addressing important structural-motional issues within the context of electrical-mechanical energy conversion devices An excellent text on modern broadband dielectric spectroscopy is that by Kremer and Schönhals. [5] The complex dielectric permittivity is defined by the following equation in which ω is the angular frequency ($\omega = 2\pi f$) and i = $\sqrt{1}$:

$$\varepsilon^*(\omega) = \varepsilon'(\omega) - i\varepsilon''(\omega) \qquad \text{Equation 1}$$

ε' and ε'' are the real and imaginary components that reflect polarizability via facile dipole rotation or induced charge separation, and energy dissipation that occurs during these motions, respectively.

The Havriliak-Negami (HN) equation, which is often used to represent the dielectric relaxation spectra of polymers, is shown below with an additional term to account for d.c. conductivity. The later commonly arises at low frequencies due to intended charge carriers, unwanted charge impurities, or residual water.[6,7]

$$\varepsilon^*(\omega) = \varepsilon' - i\varepsilon'' = -i\left(\frac{\sigma_0}{\varepsilon_0\omega}\right)^N + \sum_{k=1}^{n}\left[\frac{\Delta\varepsilon}{\left(1+\left(i\omega\tau_{HN}\right)^{\alpha}\right)^{\beta}}\right] \qquad \text{Equation 2}$$

Each term in the sum represents a different relaxation process depending on the number of observed peaks. In the case of polymers, these relaxations take the form of a glass and sub-glass transitions. The quantity $\Delta\varepsilon = \varepsilon_0 - \varepsilon_\infty$ is the difference between the low and high frequency limits of ε' for the given process. τ_{HN} is a fitted relaxation time parameter

that is related to the actual relaxation time, τ_{max}, which is associated with the frequency at the respective peak maximum, f_{max}. α and β are fitted parameters that are measures of the breadth and symmetry, respectively, of the given relaxation such that $\alpha < 0 \leq 1$ and $0 < \beta \leq 1$. Due to peaks being sometime asymmetric, τ_{HN} does not always equal τ_{max}, in which case α, β and τ_{HN} are used to determine τ_{max} using the following equation: [8,9]

$$\tau_{\max} = \tau_{HN}\left[\frac{\sin\left(\frac{\pi\alpha\beta}{2(\beta+1)}\right)}{\sin\left(\frac{\pi\alpha}{2(\beta+1)}\right)}\right]^{\frac{1}{\alpha}} \qquad \text{Equation 3}$$

When present, d.c. conductivity can obscure weak polymer relaxations that occur at low frequencies. Once the exponent $N \leq 1$, and the d.c. conductivity σ_0 are determined by curve fitting in the low frequency regime, this term is subtracted point-by-point from the ε'' curves to reveal the relaxation peaks.

Plots of log τ_{max} vs. $1/T$ for the relaxation associated with the glass transition are characteristically nonlinear (non-Arrhenius-like) and obey the empirical Vogel-Fulcher-Tamman (VFT) equation for glass-forming materials: [10-12 5]

$$\tau(T) = \tau_0 \exp\left(\frac{E_a}{k_B(T - T_V)}\right) \qquad \text{Equation 4}$$

τ_0 is a hypothetical relaxation time at infinite temperature, k_B is the Boltzmann constant. E_a is a fitting constant and not an activation energy. T_v, the Vögel temperature, is often considered to be related to, and typically 30 to 70 °C below, the glass transition temperature, T_g.

Experimental

Preparation of amine modified films.

Nafion® precursor sulfonyl fluoride films of 1200 equivalent weight and ~100 μm thick were reacted in two ways with four liquid amines: ethylene diamine (1,2 EDA), 1,2 propylene diamine (1,2 PDA), 1,3 propylene diamine (1,3 PDA), and 1,4 butylene diamine (1,4 BDA).

Method 1—symmetric film modification: A 4 cm x 4 cm film sample was suspended in 40 ml of each respective amine in a 50 ml Erlenmeyer flask for specified times. To ensure that the films remained in full contact with the liquid while not adhering to the sides or bottom of the flask, they were held upright with a capillary tube.

Method 2—asymmetric film modification: This method differs from method 1 only in that just one side of the film is amine modified thus leaving the opposite side unreacted. A reaction reservoir was constructed of a 2" diameter stainless steel cylinder with threaded caps on both ends. A 2" diameter section of sulfonyl fluoride film was secured onto the one end of the cylinder. Liquid diamine was then poured into the reaction reservoir from the other end and the cylinder was capped.

After reacting for the specified time, both types of samples (symmetric and asymmetric) were rinsed in DI water, placed in the vacuum oven for 12h to remove any volatile amines, and cured for various times, typically 1h or 12h at 200 °C; time and temperature were varied as specified. To determine reaction depth, a small portion of each specimen was embedded in epoxy and polished allowing for examination of the cross-section using a Nikon optical microscope with a DXM digital camera at a magnification of 20X.

ATR/FTIR spectroscopy.

FTIR-ATR spectroscopic analyses were conducted using a Bruker Equinox 55 to verify the reaction conversion and identify the mechanism of reaction. Films were clamped on top of a germanium crystal and spectra were collected in 9-bounce reflectance mode. All of the samples that were acquired are the result of at least 32 scans with the background subtracted from the spectra to enhance peaks for bonds generated by the reaction.

Dielectric spectroscopic analysis.

A Novocontrol GmbH Concept 40 broadband dielectric spectrometer was used over the frequency range of 0.1Hz - 3MHz at temperatures ranging from -130 to 200° C and the temperature (T) was controlled to within +/- 0.2 °C. Samples were then tightly pressed between two 20mm diameter brass electrodes. To protect the electrodes the samples were first sandwiched between two 20mm diameter aluminum foil sheets. Frequency sweep tests were performed at 10° C increments and iteratively at constant temperatures. This later method is beneficial in tracking the reaction progress.

Isothermal dielectric permittivity data were fitted to equation 3 to obtain τ_{HN}. Some of the data presented here is uncorrected for d.c. conductivity to illustrate its presence.

Dynamic mechanical analysis (DMA).

A TA Instruments Q800 Series was used in the tension mode at a frequency of 1Hz and a heating rate of 5 °C/min.

Results

Optical microscopy.

Figure 0-1 consists of representative optical micrographs of a film asymmetrically (one side) reacted with 1,4 BDA to a depth of 25μm, and a film symmetrically (both sides) reacted with EDA to a depth of 10μm on both sides. Without the aid of staining, it can be seen that there are two distinct regions separated by boundaries that appear clear at this level of resolution.

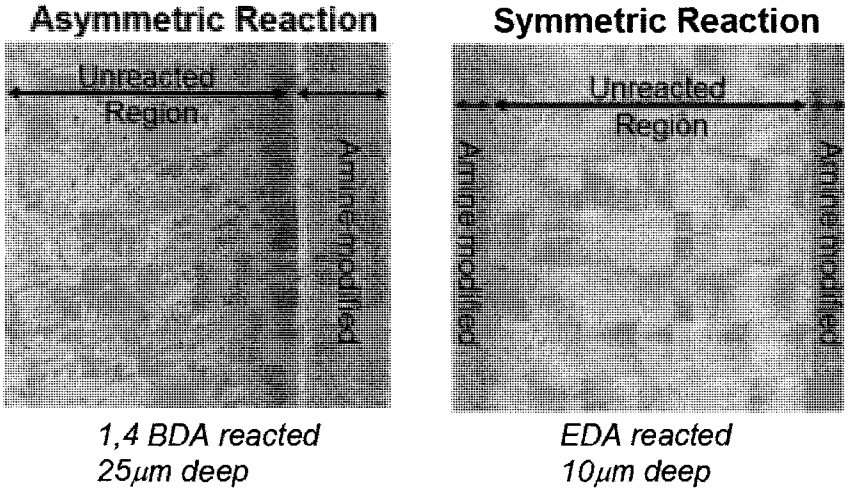

Figure 0-1. Optical micrographs of a Nafion® sulfonyl fluoride precursor film asymmetrically (one side) reacted with 1,4 BDA to a depth of 25μm (left), and film symmetrically (both sides) reacted with EDA to a depth of 10μm on both sides (right).

FTIR/ATR spectroscopy.

The postulated reaction mechanism 1 was verified by comparing FTIR/ATR spectra of the unreacted with reacted films. The reaction of mechanism 1 occurs at room temperature. While the results for only 1,2 EDA and 1,4 BDA (symmetric reactions) are shown in the region 1600-600 cm^{-1} in Figure 0-2, all four amines were seen to react in similar manner. Within the first 5 min of exposure to amine liquid, the SO_2F peak at 1470 cm^{-1} and S-F peaks at approximately 820 and 795 cm^{-1} disappear indicating that this

chemical group had undergone a reaction. Simultaneously, the sulfonamide peak appears at 1380 cm^{-1} indicating the establishment of covalent chemical bonds between sulfur and nitrogen atoms.[3]

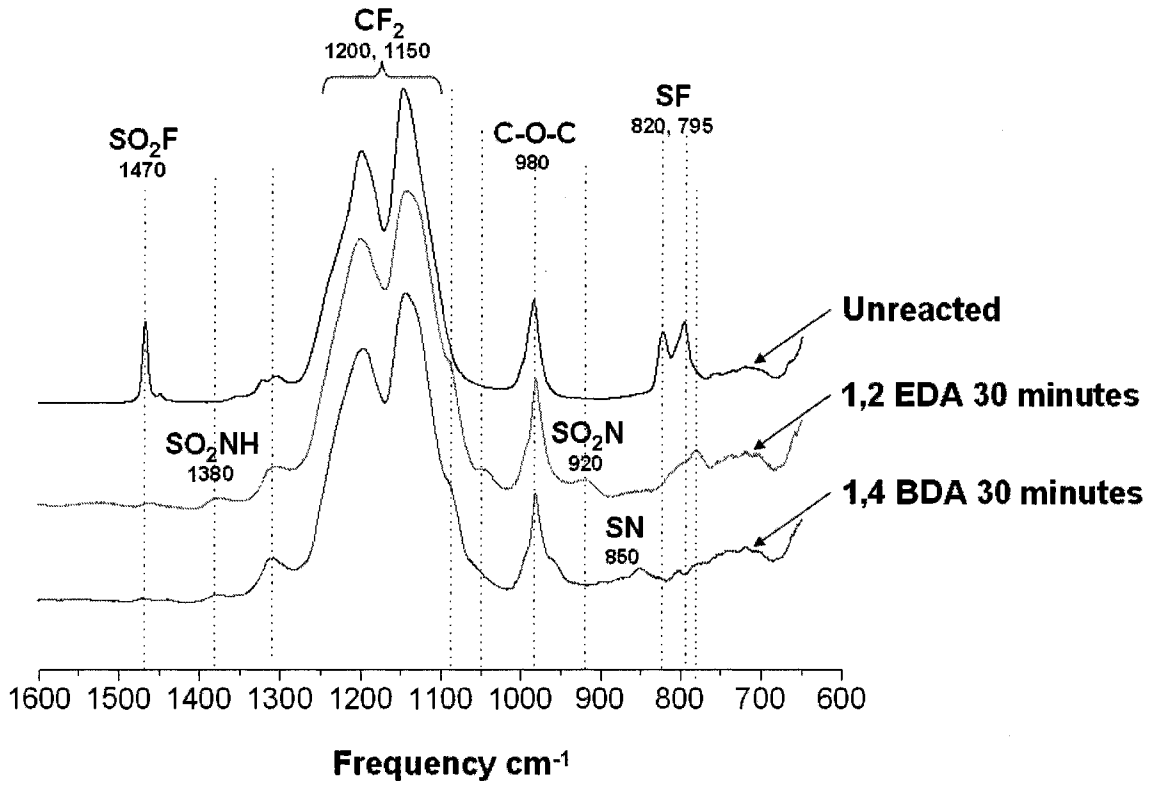

Figure 0-2. FTIR/ATR spectra for an unmodified Nafion® sulfonyl fluoride film and 1,2 films symmetrically reacted with EDA and 1,4 BDA for 30 min, but with no curing. Both film sides have the same spectra in each case

Covitch et al. demonstrated that, for EDA, only one amine group of the diamine molecule reacts with the sulfonyl fluoride group as it diffuses into the film at room temperature, thus leaving a free amine.[2] However, upon heating the amine modified films to 200° C, the free amine of the diamine appendage covalently reacts with an amine end of another NH_2 – ended sidechain forming a crosslink and releasing ammonium. These investigators suggested that the crosslinking reaction for the diamine modified

films involves two free amines reacting to form a triamine crosslink as indicated in mechanism 2 shown below.[4]

Mechanism 2

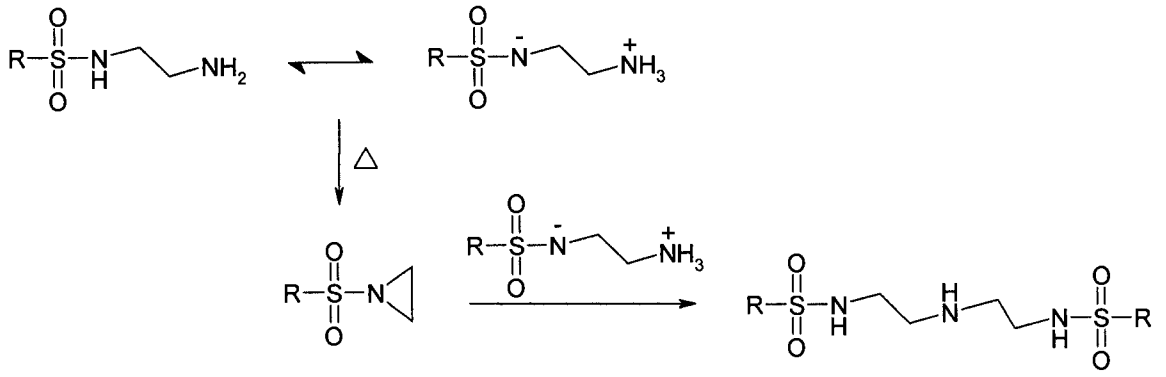

This mechanism is supported by the spectra in the region 3600-2600 cm^{-1} in Figure 0-3 when the spectrum of a model salt compound, 1,4 diaminobutane-dihydrochloride is compared with BDA modified films that were symmetrically reacted to a depth of 10μm. The model salt compound shows a very strong broad peak absorbance from approximately 3100 cm^{-1} to 2700 cm^{-1} which is characteristic of the symmetric and asymmetric stretching vibrations in the NH_3^+ group.[13] Upon heating the amine modified sulfonyl fluoride films, the intensity of this strong broad peak decreases. This suggests that at room temperature the free amines are ionic salts that convert to covalent linkages with heating. This is further indicated by weak peaks at 3500 and 3400 cm^{-1} disappearing and the appearance of the single weak band at approximately 3315 cm^{-1}. The weak absorptions at 3500 and 3400 cm^{-1} are characteristic of the free symmetric and asymmetric N-H stretching modes of *primary* amines, whereas, the single peak at 3315 cm^{-1} is characteristic of *secondary* amines (i.e., crosslinked). It appears that with the longest cure time of 720 min all amines are covalent as there are no strong broad

peaks. The peaks at 2925 and 2853 cm^{-1} are identified as CH_2 stretching associated with the diamines.

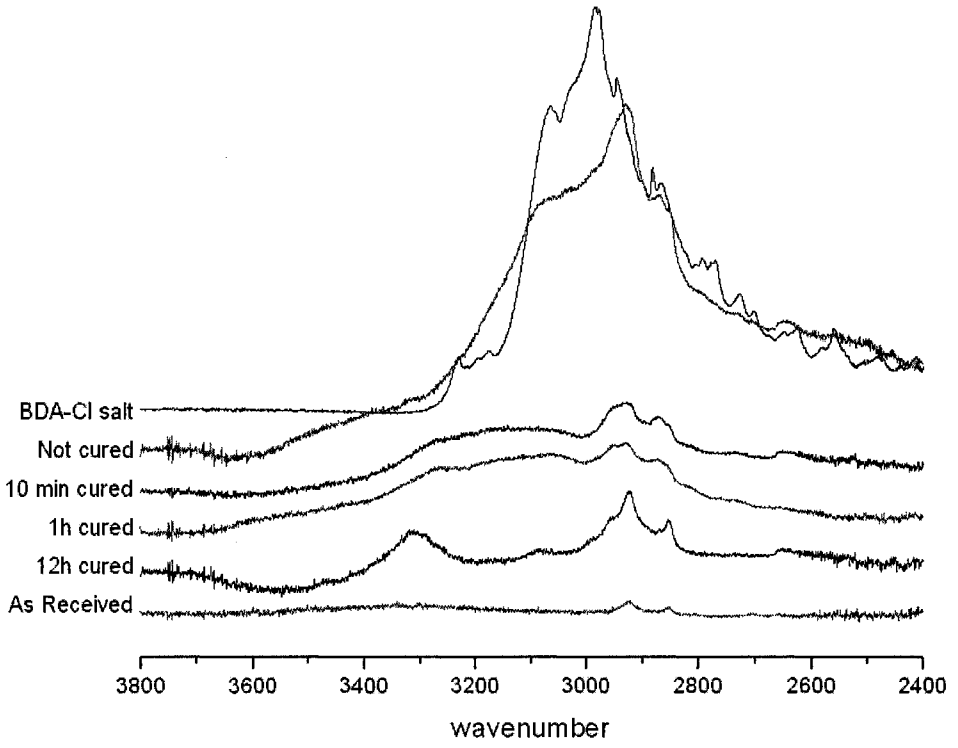

Figure 0-3. FTIR/ATR spectra in the region 3600-2600 cm^{-1} for unmodified Nafion® sulfonyl fluoride, a small molecule model salt (1,4 diaminobutane-dihydrochloride) and films symmetrically reacted with 1,4 BDA and cured for 0, 10, 60 and 720 min.

Reaction speed.

A 'reaction front' can be roughly defined as the optical interface between the unreacted and reacted regions, an example of which is in Figure 0-1. On a finer level, this interface is not expected to be extremely sharp owing to the influence of diffusion on this reaction. The progress of the reaction front, i.e., quantified by the distance from the surface into the film for all four amine types, is linear in time. The rate of advance, or speed, depends on amine type as shown in Table 0-1. Here, 'speed' does not refer to the actual reaction kinetics but to the forward progress of the chemical conversion of the film. For symmetrically reacted films the reaction depths are approximately the same from

each side. As expected, 1,2 EDA, being the smallest molecule, displays the greatest penetration depth at a given time. 1,3 PDA penetration has the second greatest rate, which is followed by that of 1,4 BDA. 1,2 PDA penetrates less than 1,3 PDA at a given time and almost the same as 1,4 BDA. Perhaps this is because 1,2 PDA is a more rigid molecule resulting from the close proximity of the two amine groups and the pendant methyl group whereas the linear 1,3 PDA and 1,4 BDA molecules have more conformational flexibility which might promote faster diffusion in the polymer medium.

Table 0-1. Reaction depth rates for tested alkyldiamine species.

Molecule	1,2 EDA	1,2 PDA	1,3 PDA	1,4 BDA
μm/min	0.48	0.25	0.43	0.22

Dielectric spectroscopic analysis of unmodified sulfonyl fluoride film.

While there is considerable literature dealing with dielectric relaxation studies of acid and cation-neutralized forms of Nafion®, including work performed in this laboratory,[14] the only dedicated study of the sulfonyl fluoride precursor form was by Hodge and Eisenberg over the temperature range -196 to +80° C.[15] Unfortunately, the equivalent weight of this early version was not reported although it was likely in the range 1050-1200. Nonetheless, the results of this important study are significant for comparative purposes because the same dielectric relaxations should be present in more recent materials and not shifted to a great degree. In the work of these authors, three peaks, which were labeled α, β and γ in the order of decreasing temperature, were seen on ε'' vs. T curves taken at constant frequency. In this same report, these same relaxations were seen in dynamic mechanical E' and tan δ vs. T curves in approximately the same respective temperature ranges. The α process, seen on dielectric relaxation spectra in the

range of 20-35° C depended on frequency in the usual way and the corresponding dynamic mechanical transition had the greatest decline on E' vs. T curves, thereby indicating that this is a glass transition in the usual sense. There is no confusion of this peak with a transition associated with ionic aggregates, which are not present in this precursor material. A two-component β relaxation seen in the temperature range -100 to -20° C was assigned to backbone and side chain motions. The γ relaxation, seen at $T <$ -160° C appeared to be the strongest of the three in the dielectric relaxation spectra but the weakest in mechanical relaxation spectra. Thus, it was concluded that this relaxation must be rather local and was assigned to motions of the SO_2F group based in part on the fact that it is the most polar group in the chemical structure.

A complete and detailed report of the dielectric relaxation characteristics of the unmodified sulfonyl fluoride films used in the present studies will be given in the future. Here, only the fundamental features are presented to provide baseline data against which the data for amine-modified films can be compared.

Figure 0-4 is a ε''–f–T response surface for an unmodified sulfonyl fluoride film. There are two distinct ridges on this surface, each of which corresponds to a molecular motion with a characteristic relaxation time that depends on temperature. Figure 0-5 are plots of ε'' vs. $\log_{10} f$ which are cuts through the surface in Figure 0-4 at different temperatures. The peak at higher temperatures is the most distinct and shifts to higher frequencies (f_{max}) with increase in temperature. This peak is associated with the glass transition as observed by Hodge and Eisenberg and is likewise ascribed here as the α-relaxation. The lower temperature peak, that reflects shorter ranged motions, is comparatively broader and can be associated with the β peak noted by these authors. The

progression of the β peak with increasing temperature is qualitatively the same as that for the α peak with which it seems to merge on the surface in Figure 0-4 as the temperature is increased. This peak merging is reminiscent of the αβ process discussed by Kremer and Schönhals who cite various examples (p. 251),[5] including the convergence of $\log f_{max}$ vs. $1/T$ plots for poly(methyl methacrylate) in which the α peak obeys VFT behavior and the β peak(s) are linear such that there is a defined activation energy.[16]

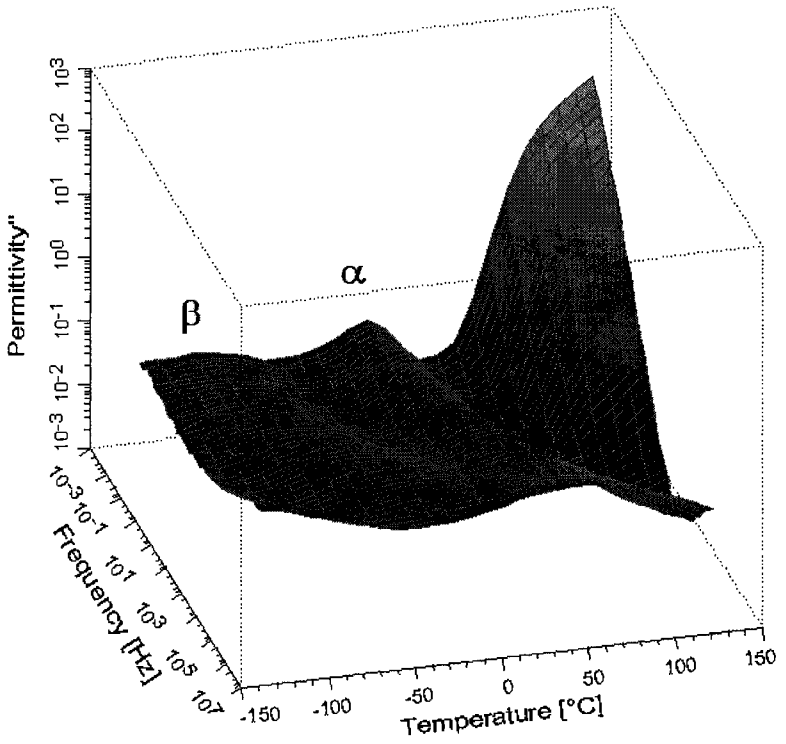

Figure 0-4. ε"– f –T surface for a 1200 EW unmodified, as-received Nafion® precursor sulfonyl fluoride film.

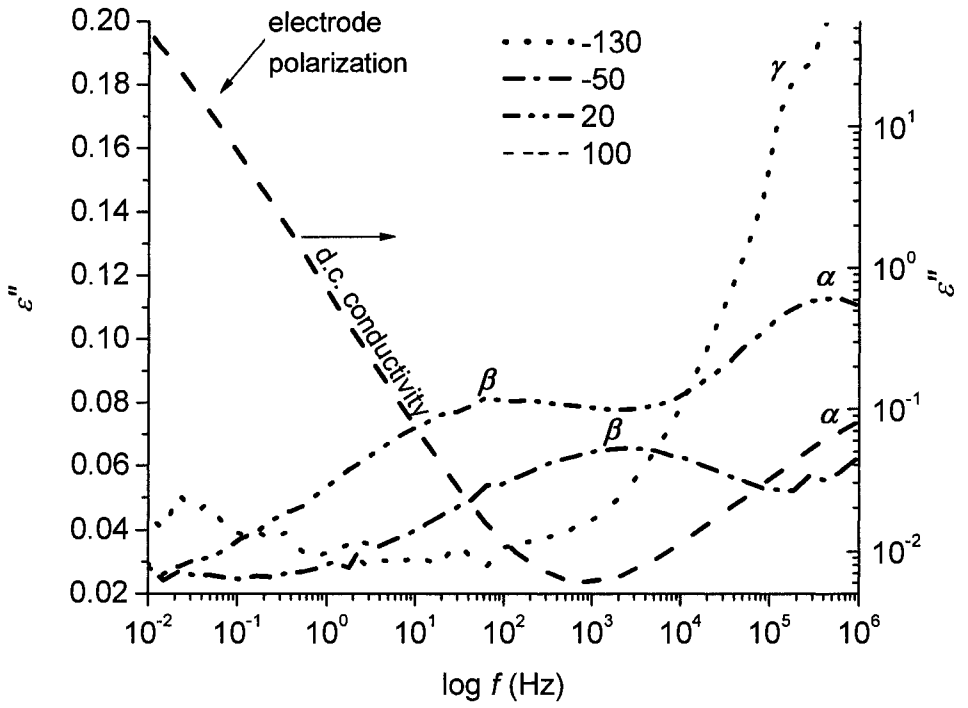

Figure 0-5. ε" vs. log10 f at various indicated temperatures (0° C) for a 1200 EW unmodified, as-received Nafion® sulfonyl fluoride precursor film.

The sharp rise in the response surface in proceeding to the high temperature/low frequency region is attributed to dc conductivity. Fitting the conductivity term of equation 3 to the linear low frequency sections of log ε'' vs. log f plots at constant T gives $N \approx 1$ which corresponds well with dc behavior. The fact that N is close to unity and not considerably less, suggests that membrane/electrode interfacial polarization is most likely not present to a large degree. The ε'' vs. f relationship for sample/electrode interfacial polarization is represented by a Debye-like equation that describes a peak with a relaxation time rather than monotonically decreasing ε'' behavior with increasing f, and this in fact is seen in the case of ionomers.[17]

Dielectric Relaxation Spectra of Diamine Modified Films at High Temperatures.

The reactions that introduce sulfonamide linkages significantly alter the dielectric spectra for all tested diamine species as seen on comparing the response surface in Figure 0-4 with that in Figure 0-6 for the example of 1,4 BDA modification to a depth of 10μm. Figure 0-7 consists of $\log \tau_{max}$ vs. 1/T plots using the data in Figure 0-6 with no thermal curing prior to testing in the BDS sample cell. The plots are not of a simple monotonically decreasing nature but have transitions. All modified films have at least one additional well-defined relaxation that appears at temperatures higher than the α peak temperature of the un-reacted sulfonyl fluoride precursor. It is reasonable that there should be more peaks considering that only a portion of the sample volume was reacted in this way and there are two distinct regions as seen in Figure 0-1. Interestingly, 1,2 PDA, 1,3 PDA and 1,4 BDA have yet a second additional relaxation peak that is even higher in temperature than the first additional peak as shown in Figure 0-8 and Figure 0-9 for EDA and 1,4 BDA, for brevity 1,2 PDA and 1,3 PDA plots are not shown. For the EDA reaction, this second relaxation peak is not as obvious as it is for the other diamine species modifications as peaks can be buried in the spectrum at high temperatures and low frequencies, i.e., dc conductivity region. In fact, two peaks do emerge following the EDA reaction upon subtracting the dc conductivity component, as seen in Figure 0-8 and Figure 0-9 for 1h cure. These are labeled amine-1-relaxation (A1R) and amine-2-relaxation (A2R), the former being the lowest in temperature of the two. Both A1R and A2R are affected by heat curing temperature and time as will be discussed.

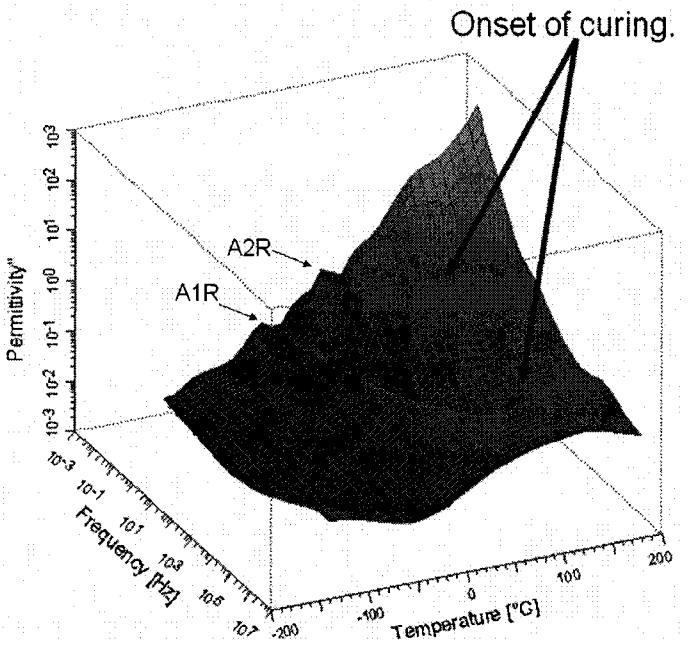

Figure 0-6. $\varepsilon'' - f - T$ surface for a Nafion® precursor sulfonyl fluoride film reacted symmetrically with 1,4 BDA to a depth of 10μm from both surfaces without prior heat treatment. 'Onset of curing' refers to the effect of heating in the BDS sample cell.

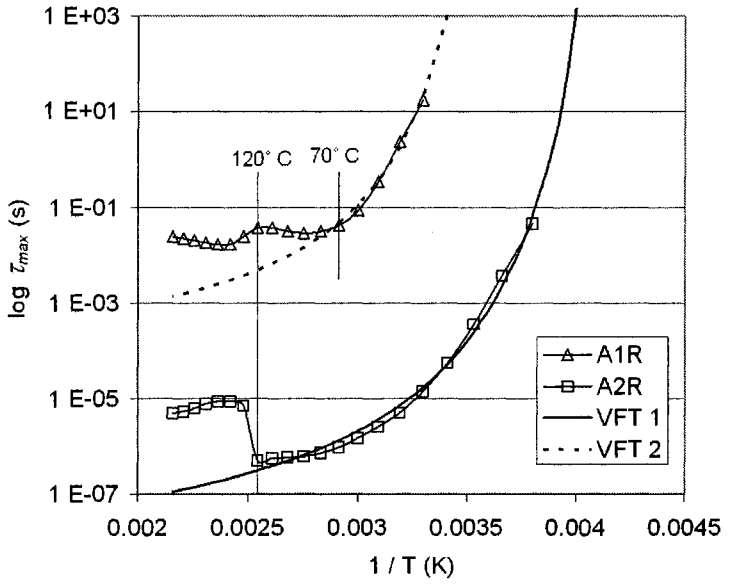

Figure 0-7. log τ_{max} vs. 1/T plots for the A1R and A2R relaxations for a Nafion® sulfonyl fluoride film reacted symmetrically with 1,4 BDA to a depth of 10μm from both surfaces without prior heat treatment. Superimposed curves are VFT equation fits to each relaxation across the appropriate lower temperature ranges.

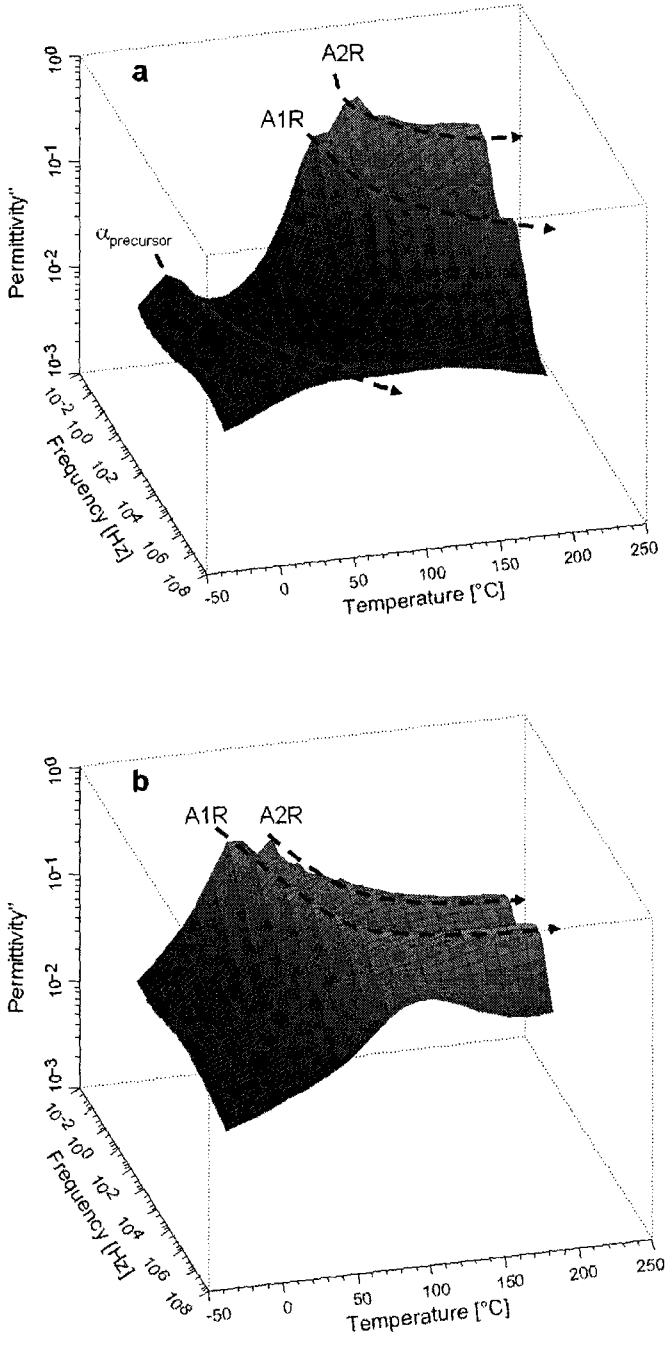

Figure 0-8. $\varepsilon''-f-T$ surfaces with d.c. subtracted for films cured for 1h at 200° C before dielectric measurements: a) EDA symmetrically reacted to a depth of 10μm; b) 1,4 BDA symmetrically reacted to a depth of 10 μm. The dashed black curves are the crests of the relaxation peaks at f_{max} over the range of T.

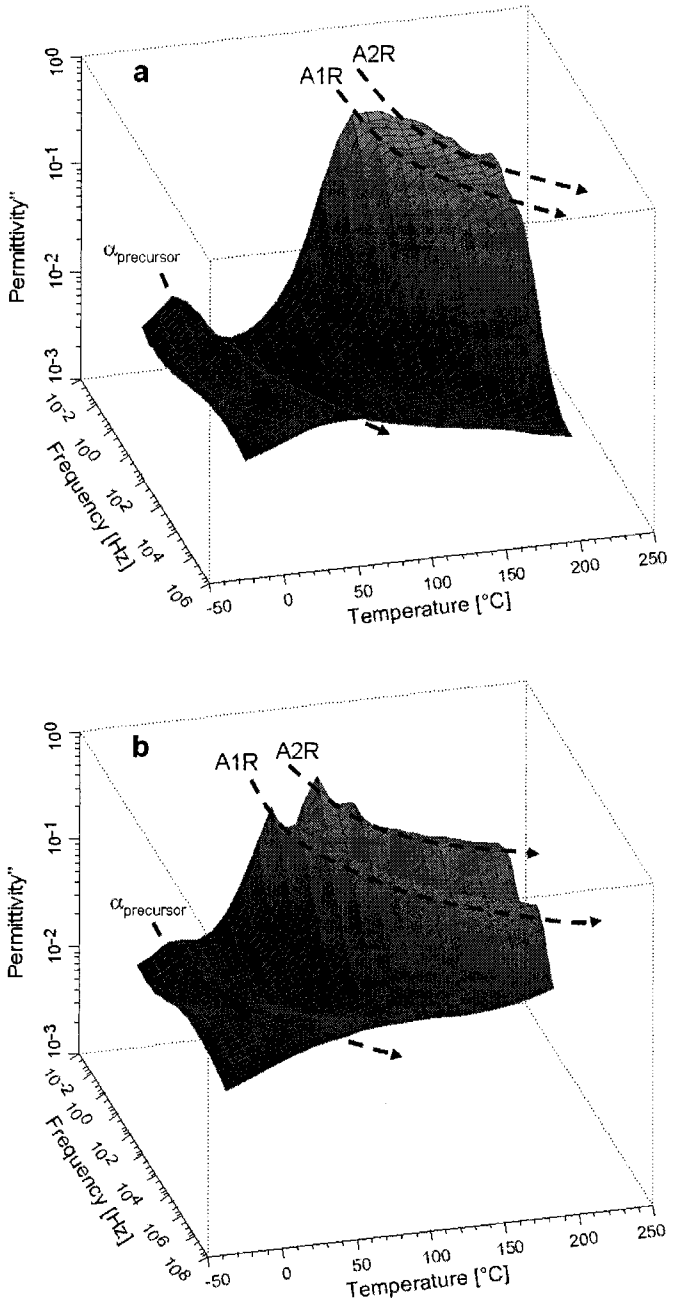

Figure 0-9. $\varepsilon'' - f - T$ surfaces with d.c. conductivity subtracted for films cured for 12h at 200° C before dielectric measurements: a) EDA symmetrically reacted to a depth of 10μm; b) 1,4 BDA likewise symmetrically reacted to a depth of 10μm. The dashed black curves are the crests of the relaxation peaks at f_{max} over the range of T.

For the HN equation to be well-fitted to spectra, the diamine modified films must be chemically stabilized by a full thermal cure before testing. Films tested without prior curing display irregular, unrepeatable results owing to incomplete reactions that are further driven with increase in temperature in the instrument. On the other hand, and in a useful sense, the curing process of diamine modified - but uncured - films can be studied in real time in this way. To this end, films with no prior curing, and for 1 and 12 h of prior curing were tested.

The onset of thermal curing during the dielectric data acquisition process is apparent in the spectra of a film reacted symmetrically with 1,4 BDA to a depth of 10μm on both surfaces, without prior heat treatment, as seen in the response surface in Figure 0-6. This means that the A1R and A2R ridges seen in Figure 0-6 were generated during the dielectic test as the sample cured. At T > 120° C the most prominent relaxations associated with the diamine modified region of the film shift to lower frequencies and higher temperatures, which indicates slower molecular motions, presumably due to the tethering of the 1,4 BDA molecule to the side chain, thereby hindering molecular mobility. After fitting the HN equation to the dielectric spectra, τ_{max}, was calculated. A plot of $\log_{10} \tau_{max}$ vs. 1/T , seen in Figure 0-7, reveals that the peaks for both A1R and A2R relaxations fit the VFT equation quite well until the temperature is increased to ~120° C, at which there is transitional behavior in the form of a rise, attributed to the onset of chemical reactions, namely, crosslinking. This initial shift in τ_{max} is not due to free NH_2 groups reacting with unreacted SO_2F groups, as previously mentioned. Covitch et al. demonstrated that for EDA only one amine group of the diamine molecule readily reacts with sulfonyl fluoride groups as it diffuses into the film at room temperature.[4] This

means that in the amine modified region there should be no sulfonyl fluoride functional groups, as confirmed by the ATR-IR data in Figure 0-2. These authors further suggest that the crosslinking reaction for EDA modified films involves two free amines reacting to form a diethylene*tri*amine crosslink as indicated above in mechanism 2.[4]

In situ heating of uncured films at constant temperature

This initial curing is clearly observed in evolving spectra when films with no prior thermal treatment – only partially reacted - are heated in the instrument to 200° C and then successive frequency sweep iterations are performed at this constant high temperature. The curing reaction was monitored by tracking τ_{max} vs. time in this way for the A1R and A2R relaxations and the results for A1R for the EDA and 1,3 PDA modifications, for example, are seen in Figure 0-10. All four diamines show an initial rapid increase in τ_{max} after which the first derivative decreases markedly. This reflects a condition where dipoles sensitive to chain motions become increasingly more restricted, most likely due to crosslink formation. In this chemically dynamic system the dipole moment associated with the SO_2F group disappears. According to Covitch et al., this reaction is accompanied by the release of 1 mole of NH_3 for every two equivalent moles of amine.[2] At ~50 min at 200° C the curve for EDA has an inflection point indicated by the arrow in Figure 0-10. After this inflection, τ_{max} for the EDA-reacted sample continues to shift to higher values, but more slowly.

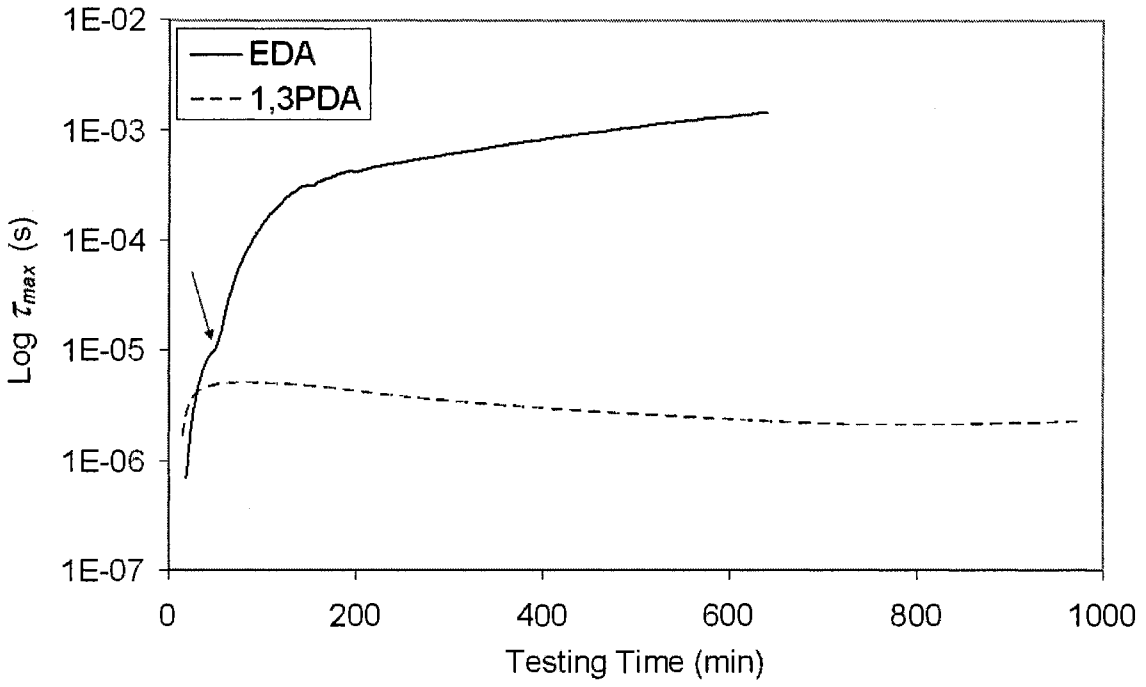

Figure 0-10. Log_{10} τ_{max} vs. BDS test time for the A1R relaxation for consecutive frequency sweep spectrum iterations at a constant temperature of 200° C for diamine modified films that were not heat cured before testing. Inflection point for the EDA curve is marked with arrow.

For 1,3 PDA, after a rapid short rise to a peak, the A1R curve slowly shifts and levels to lower τ_{max} indicative of faster chain motions. 1,2 PDA and 1,4 BDA curves show similar initial rapid shifts to higher τ_{max} values, but after ~ 150 and 230 min, respectively, peak resolution, and therefore relaxation time determination, is compromised due to peak broadening. However, this broadening does not always occur as evidenced by the distinct peaks in the 3D plot of Figure 0-8b and Figure 0-9b. The later situation may be due to difficulty in NH_3 molecules desorbing from of the sample as it is sandwiched between two electrodes that block most of the surface, except for the thin edges.

Heating films in the instrument at a lower temperature of 170° C reduces the overall curing rate, as seen in Figure 0-11. In addition to this the ε'' vs. f peak resolution is improved, no figure is provided to illustrate this later point. Similar to the behavior observed in Figure 0-10, all curves in Figure 0-11 display an initial rapid increase to higher τ_{max}; however, this occurs at slower rates due to the lower temperature of the sample holder. Again, the both the EDA and the 1,2 PDA modified films initially show similar behavior: a rapid rise in τ_{max} and an inflection point at approximately 250 mins. However, the 1,2 PDA curve differs from EDA in that after the initial rapid increase the τ_{max} values drop and then slowly increase again. In contrast to both the EDA and 1,2 PDA modified films the τ_{max} vs. time behavior is different for both the 1,3 PDA and 1,4 BDA modified films. Both curves of the 1,3 PDA and 1,4 BDA modified films asymptote. The difference in behavior between the EDA and 1,2 PDA modified films and the 1,3 PDA and 1,4 BDA modified films is peculiar. One possibility may be related to the diamine chain length such that 1,3 PDA and 1,4 BDA molecules are sufficiently long enough to a reach one or more sulfonyl fluoride groups forming a direct crosslink; whereas, the EDA and the 1,2 PDA molecules are not long enough to directly react rather they form an intermediate structure. This may imply that the inflection point for the EDA and the 1,2 PDA modified films is a chemical rearrangement from an intermediate structure to a more stable linkage. If this is true then it is possible that the inflection point may be due to the formation of the intermediate ring structure, described in mechanism 2,

which subsequently reacts to form the crosslink.

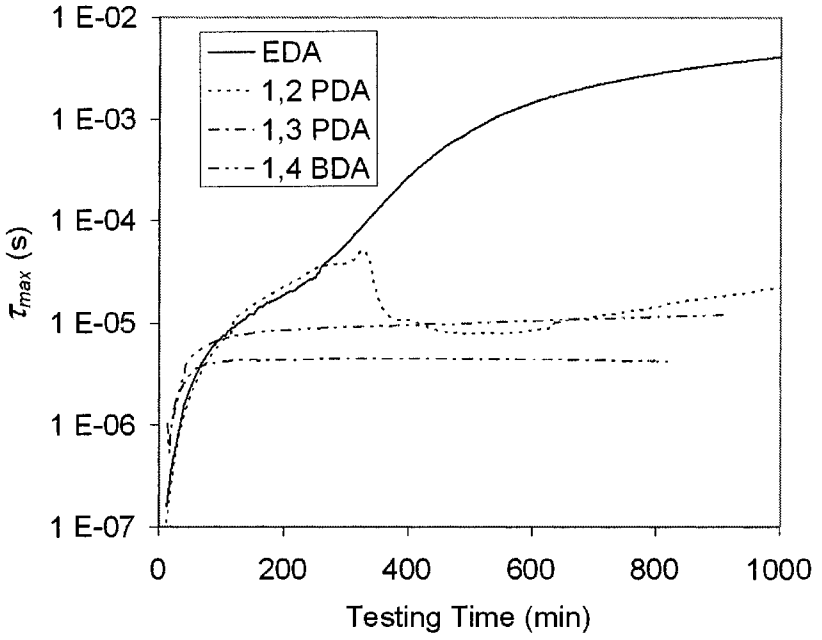

Figure 0-11. Log_{10} τ_{max} vs. test time in the BDS instrument for the A1R relaxation for consecutive frequency sweep iterations performed at the constant temperature 170° C for amine modified films that were not heated (cured) before testing.

Films cured prior to BDS testing

Diamine modified films cured for 1 and 12h at 200° C prior to BDS testing will now be discussed. All samples were symmetrically reacted with EDA, 1,2 and 1,3 PDA and 1,4 BDA to a depth of 10μm. Figure 0-8 and Figure 0-9 are examples of ε'' - f - T response surfaces for EDA and 1,4 BDA cured at 1h and 12h, respectively. 1,2 PDA and 1,3 PDA ε'' - f - T response surfaces are not shown, but show similar results. Figure 0-12 and Figure 0-13 are Arrhenius log τ_{max} vs. 1/T plots of the A1R and A2R peaks for all four amine modified films. These plots are sensitive to the molecular weight and branched character of the diamine reactant molecule. A1R relaxation times, of course, are lower than those for A2R. Generally speaking, both the A1R and A2R peaks of these

pre-cured films fit the VFT equation well at low temperatures, typically within 0.01 mean-square deviation (MSD). However, at higher temperatures A1R and A2R deviate from ideal VFT behavior. This is especially noticed for the 1h prior cured films. This implies that these relaxations are not characterized by activation energies but are reflective of glass-forming materials in the respective amine modified regions. Additionally the films cured for longer curing times have relaxations with a higher degree of ideal VFT behavior. Films cured for 1h will first be discussed followed by a similar discussion for films cured for 12h. After this the impact of these curing times on the fragility index will be analyzed.

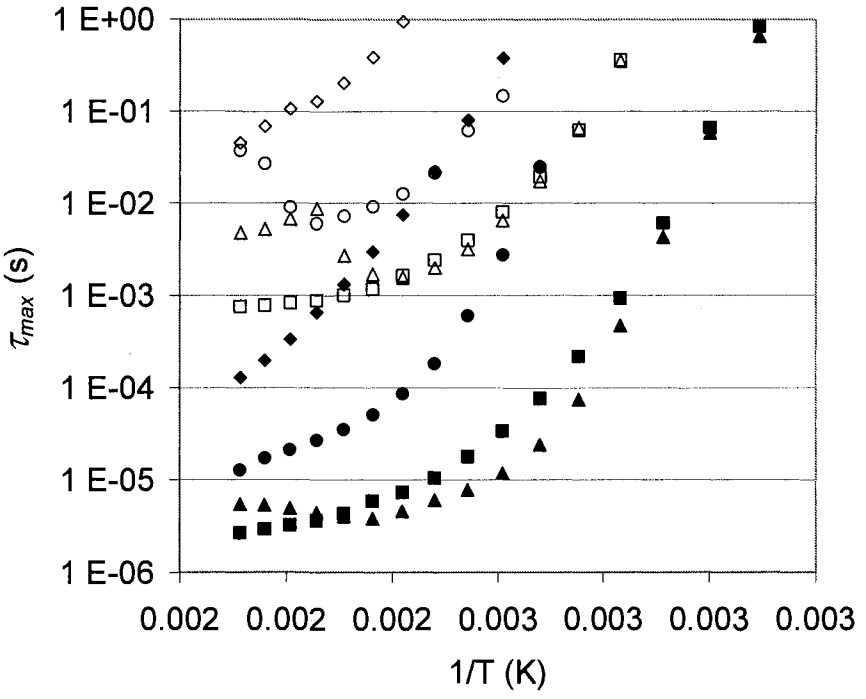

Figure 0-12. $\log_{10}\tau_{max}$ vs. 1/T for films symmetrically reacted to 10μm depth and cured for 1h: EDA (◊), 1,2 PDA (○), 1,3 PDA (Δ), 1,4 BDA (□). Closed symbols are A1R and open symbols are A2R.

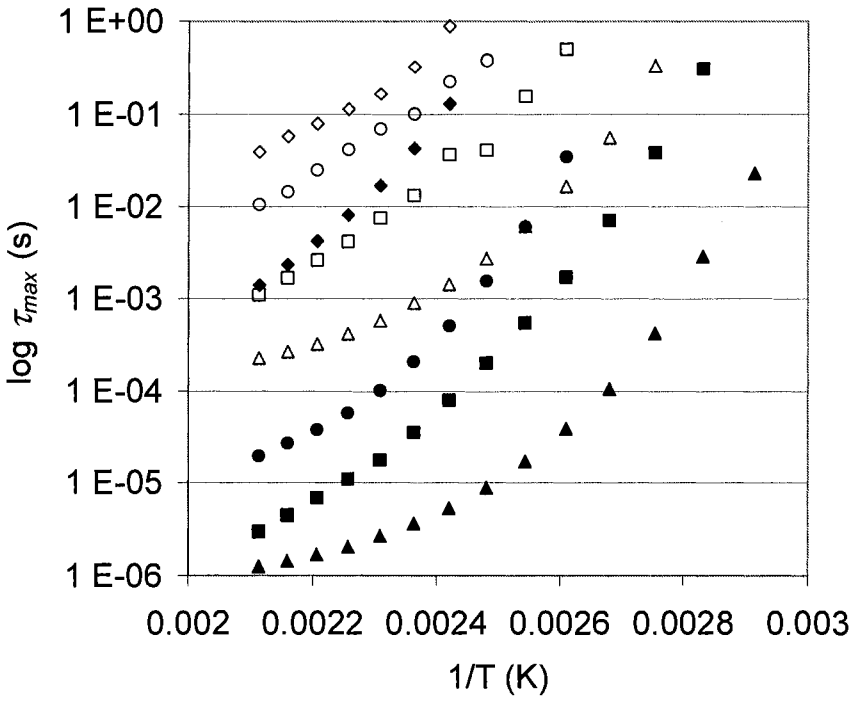

Figure 0-13. log τ_{max} vs. 1/T for films symmetrically reacted to 10μm depth and cured for 12h : EDA (◊), 1,2 PDA (○), 1,3 PDA (Δ), 1,4 BDA (□). Closed symbols are A1R and open symbols are A2R.

For the 1h cured films, increasing molecular weight from EDA to 1,3 PDA results in a shift of the both the A1R and A2R relaxations to lower τ_{max} at a given temperature, as indicated in Figure 0-12. This suggests that added carbons between the amine linkages impart mobility to the crosslinks, as is reasonable. However, there is no increase in τ_{max} for A1R and A2R with increased molecular weight from 1,3 PDA to 1,4 BDA. The A1R (and A2R) curves for 1,3 PDA and 1,4 BDA are essentially superimposed at lower temperatures. At higher temperatures the 1,3 PDA A1R and A2R curves deviate substantially from VFT behavior with an upswing to higher τ_{max}. This deviance might be due to further reactions that shift the linking structure.

When the amine modified films are heated for 12h, similar to the 1h cure, A1R and A2R of EDA have the greatest τ_{max} value at any given temperature. This is followed by 1,2 PDA. In contrast to the 1h cured films the 1,3 PDA modified film has the A1R and A2R lowest τ_{max} values for any given temperature, even lower than 1,4 BDA. Thus the order of highest to lowest τ_{max} values at any given temperature are EDA, 1,2 PDA, 1,4 BDA and 1,3PDA. Comparing the 1,3 PDA τ_{max} values of A1R in Figure 0-12 and Figure 0-13 seems to suggest that for this amine modified film that τ_{max} does not shift significantly with curing; rather, the overall shape of A1R obtains a more ideal VFT shape. This is apparent by noticing that the 1,3 PDA τ_{max} curves in Figure 0-13 does not have the upswing at higher temperatures like it goes in Figure 0-12. It is reasonable to assume that the longer heating time has driven the formation of bonds to a higher degree and *in situ* reactions have settled.

The fact that the 1,2 PDA modified film has higher τ_{max} values than the 1,3 PDA counterpart suggests that the 1,2 PDA molecule restricts the dipolar relaxation more than the 1,3 PDA molecule. This seems to be indicating that the steric effect of the bulkier pendent side group is restricting the motion. However, when compared with the smallest molecule EDA, the 1,2 PDA molecule seems to facilitate the motion, as the EDA modified film has higher τ_{max} values than the 1,2 PDA counterpart. These two molecules have the same number of carbon atoms directly between amine linkages suggesting that the pendent methyl group imparts mobility, facilitating the dipolar relaxation. The increased mobility resulting from the steric effect, i.e., bulkier stereochemistry, of the pendant methyl group is not as great as the effect of the increased molecular weight directly between two amines.

Although, the trends for A2R are similar to that for A1R for brevity only A1R relaxations will be discussed from this point forward.

The relationship between A1R log τ_{max} vs. 1/T curves and diamine molecular weight is better understood by quantifying the 'fragility' of each modified membrane. Fragility relates to the temperature dependence of the relaxation time for glass forming systems and is a measure of deviation from Arrhenius behavior. The opposite of a fragile glass is a 'strong' glass which has nearly Arrhenius (straight line) behavior. Amorphous silica is an example of a strong glass that has a near-linear log τ_{max} vs. 1/T behavior. Fragility, on a molecular level, relates to structure relaxation dynamics, chain segmental cooperative motions in the case of linear polymers, and short range order. For strong glasses, as temperature increases, short range order is maintained, whereas fragile glasses easily lose their local structure with increasing temperature owing to weak interactions.[18] SiO_2 glass maintains rigid local three-dimensional structure that is constrained by strong bonds.

The degree of fragility is quantified by the steepness index *m* which quantifies the shift in the time scale of structural dynamics with change in temperature:[19]

$$m = \left.\frac{d\log(\tau)}{d(T_g/T)}\right|_{T=T_g} \quad (6)$$

When *m* is high, the material is fragile; when it is low the material is 'strong'.

T_g, here, is taken as the dielectric relaxation-based glass transition temperature obtained by extrapolating the VFT equation to the long time of τ_{max} = 100s, at which long range structure is assumed to be frozen.[20] T_g values for the 12h cured specimens are reported in Table 0-2 along with the calculated VFT values for each relaxation. T_g at τ_{max}

= 100s decreases with increasing diamine molecular weight. The fragility index is quantified more specifically by the expression[20]:

$$m = \frac{E_a}{2.303R}\frac{T_g}{\left(T_g - T_V\right)^2} \quad (7)$$

Equation 7 is obtained by substituting the VFT equation in equation 6.

Table 0-2. Fitted VFT equation parameters and fragility the A1R relaxation of films cured for 1 and 12h after symmetric film reaction to a depth of 10μm from both surfaces.

	1h Prior Cure at 200°C				12h Prior Cure at 200°C			
	EDA	1,2 PDA	1,3 PDA	1,4 BDA	EDA	1,2 PDA	1,3 PDA	1,4 BDA
τ_0 (s)	2.1E-08	1.2E-06	1.2E-10	1.3E-08	7.3E-07	1.5E-07	8.7E-08	9.8E-10
E_a (kJ/mol)	13.6	2.6	11.7	6.7	10.1	5.8	3.4	13.4
T_V (°C)	12.5	68.8	-11.8	8.35	39.4	53.5	42.1	-2
T_g at 100s					104.2	87.9	61.8	61.6
m					47.3	92.8	146.5	47.4

Calculated *m* values, listed in Table 0-2, increase with increasing molecular weight from EDA to 1,3 PDA but then drops for 1,4 BDA to a value essentially equal to that for EDA. These values are comparable to those reported by Huang and McKenna, where, for comparison, *m* is low at 46 for flexible polyisobutylene and amorphous polyethylene and high at 214 for rigid polyetherimide.[19] High T_g is thought to be accompanied by high *m*. Extrapolated T_g values at τ_{max} = 100s for EDA, 1,2 PDA and 1,3 PDA are different, except that the values for 1,3 PDA and 1,4 BDA are essentially equal. For example, when increasing reactant molecular weight from EDA to 1,3 PDA, T_g at τ_{max} = 100s drops for 1,3 PDA—dropping even lower than 1,2 PDA. However, further increasing the molecular weight from 1,3 PDA to 1,4 BDA has practically no effect.

On inspecting the *linear* amines, the monotonic decrease in T_g at 100s with increasing molecular weight from EDA to 1,4 BDA (the value for the latter being essentially the same as for 1,3 PDA) suggests that additional carbons impart mobility to the crosslinks which, in turn, would seem to cause this relaxation at long times to occur faster. On the other hand, the corresponding increase, with increased crosslink size, in *m* suggests more complex behavior. The increase in *m* with increased crosslink length indicates increased fragility, which is also seen in Table 0-2 with the exception of 1,4 BDA. An increase in fragility indicates an increase in the rate that the relaxation approaches an apparent frozen state. It is interesting that an increase in molecule length from that of 1,3 PDA to 1,4 BDA does not affect this long time T_g although there is a profound decrease in *m*. The discrepancy between the T_g at 100s and *m* may relate to the degrees of freedom associated with each amine. For instance, the aliphatic content of the 1,3PDA may provide a sufficient distance to maximize the T_g reduction affect. However, motional processes incurred with increasing the aliphatic molecular weight may frustrate the cooperative motion such that it has a net reduction in T_g. But, the means in which that occurs is more convoluted. In other words, EDA and 1,4 BDA both have an even number of carbon atoms between the amines, but 1,3 PDA has an odd number of carbons between the amines. The odd number of carbons may intervene with the cooperative motional processes of the segmental relaxation thus increasing the fragility of the system.

The *nonlinear* 1,2 PDA modified materials have relaxations that are different from both EDA and 1,3 PDA. 1,2 PDA's lowered T_g from EDA may suggest that the 1,2 PDA molecule has more free volume than the EDA possibly from steric hindrance of the pendant methyl group. 1,2 PDA's increased *m* value from EDA further indicates that the

methyl group significantly interferes with the relaxation motions. Comparing 1,2 PDA with 1,3 PDA (i.e. the effect of constant molecular weight but different chemical structures) suggests that molecules with the same molecular weight but different chemical structures exhibit different dynamic cooperative motions. In other words, the methyl group on the 1,2 PDA reduces the T_g from that of EDA probably due to additional free volume at the expense of motional cooperation; yet, the free volume contribution is not as effective at reducing T_g as is the linear addition of another carbon on the amine backbone in 1,3 PDA.

Dielectric Relaxation Spectra of Amine Modified Films at Low Temperatures

Examining the 3D plots in Figure 0-8 and Figure 0-9, it is evident that the two new high-temperature/low-frequency relaxations with the diamine chemical modification do not replace the T_g relaxation or other lower temperature relaxations of the unreacted region of the film. This is in harmony with the visual evidence that these films have chemically distinct bi-layers as seen in Figure 0-1. When investigating the dynamic mechanical properties of the sulfonyl fluoride form of Nafion®, Kyu and Eisenberg observed a similar bilayer behavior upon partial conversion of the sulfonyl fluoride precursor to the $SO_3^-Na^+$ form. Na^+ ion exchange was said to occur "layer by layer" which is similar to the situation generated by the diamine diffusion-controlled reactions here.[21] These investigators saw, with increasing conversion of the sidechains to the ionic form, a decrease in the precursor layer T_g relaxation intensity with the simultaneous emergence of a β' shoulder on the β peak. With increasing conversion to the Na^+-form the shoulder became more distinct by shifting to higher temperatures. As previously stated, the *β*

relaxation is a conglomerate relaxation comprised of CF_2 relaxations and either side chain relaxations; with this in mind, Kyu correlated the new β' relaxation to ether side chain motions under the influenced of introduced ionic forces.

In the present study, a similar spectral feature occurs in the region of the $\beta_{precursor}$ relaxation for amine modified films, labeled β', at lower frequencies and higher temperatures. As apparent in Figure 0-14, at small reaction depths the β' relaxation appears as a shoulder on the lower frequency side of the $\beta_{precursor}$ relaxation peak. With increased reaction depth, the peak becomes better defined. On inspecting Figure 0-14 it is also apparent that the intensity of ε" depends more upon the total added reacted thickness of the film than the thickness of each side respectively. For instance, f_{max} increases in the order: EDA 10μm asymmetric < EDA 10μm symmetric < EDA 25μm asymmetric < EDA 25μm symmetric. Adding the total reacted thickness for the cross-section of each film is 10, 20, 25 and 50μm respectively. 1,4 BDA follows a similar pattern. It also appears that each 1,4 BDA sample on a whole has a higher loss permittivity than each respective EDA. It is logical to believe that the additional aliphatic carbons of the 1,4 BDA molecule impart increased mobility that is transferred to the dipole allowing the dipole to dissipate more energy. Interestingly, the f_{max} peak position of 300 Hz is the same for both the EDA and 1,4 BDA indicating that the peak shift is a phenomena that occurs between the sulfur and the nitrogen only, and it is not influenced by the molecular weight. (look into the 1,2 PDA and 1,3 PDA as the conformation my affect this; add that DMA data supports the peak shift idea).

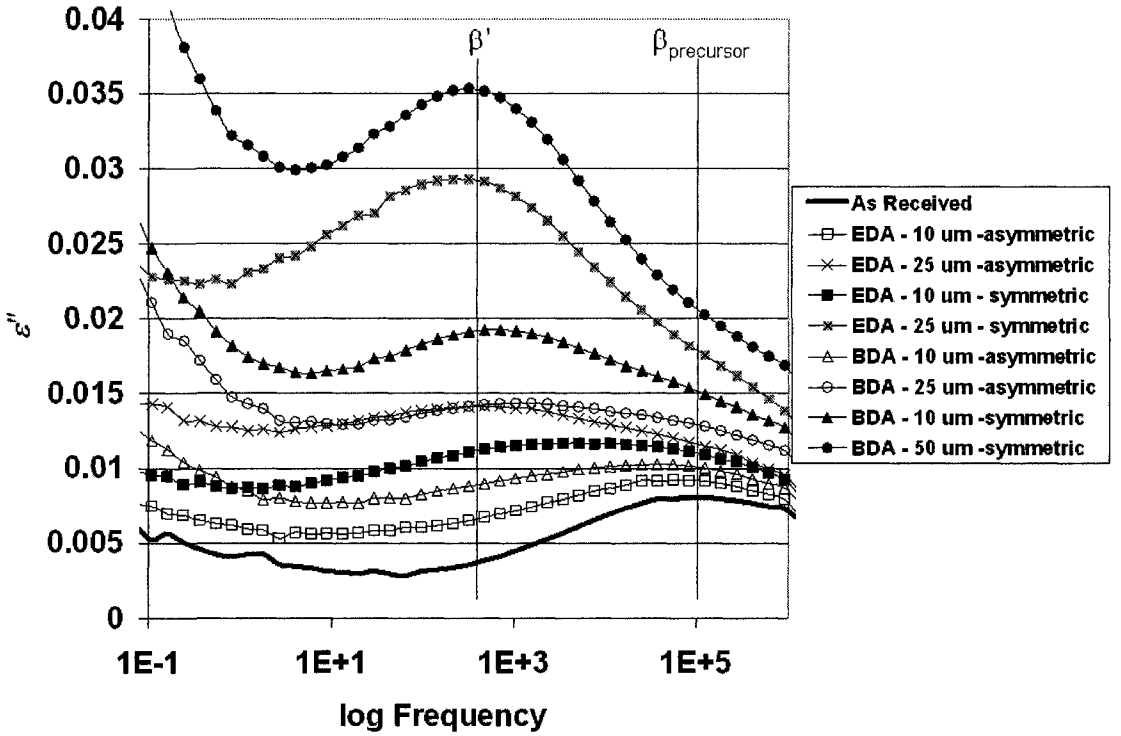

Figure 0-14. ε'' vs. log f at -10 °C for EDA and 1,4 BDA modified films at indicated reaction depths. The chemically unmodified sample curve (solid black) has two peaks at approximately 10^5 Hz. Amine modified films have an additional β' relaxation appearing as a shoulder at short reaction depths that sharpens with increasing reaction depth.

Dynamic Mechanical Analysis

Only the linear amine chemical modifications were analyzed using DMA and the results are displayed in Figure 0-15 through Figure 0-17. All three amine modified films show three distinct relaxations as in the dielectric spectra: one attributed to the glass transition of the unmodified region and two attributed to amine modified regions. These mechanical relaxations are designated the same as in corresponding dielectric spectra, e.g., A1R is the lowest temperature relaxation and A2R is the high temperature relaxation. Generally speaking, for all of the amines, with respect to cure time A1R shifts to higher temperatures and weakens in intensity, which is similar to the behavior observed in with BDS. The dimensioning peak intensity with up ward shift in temperature is most likely

due to higher degree conversion of the side groups resulting in more rigid structures. The A2R relaxation seen in dynamic mechanical spectra shifts to lower temperature with curing time.

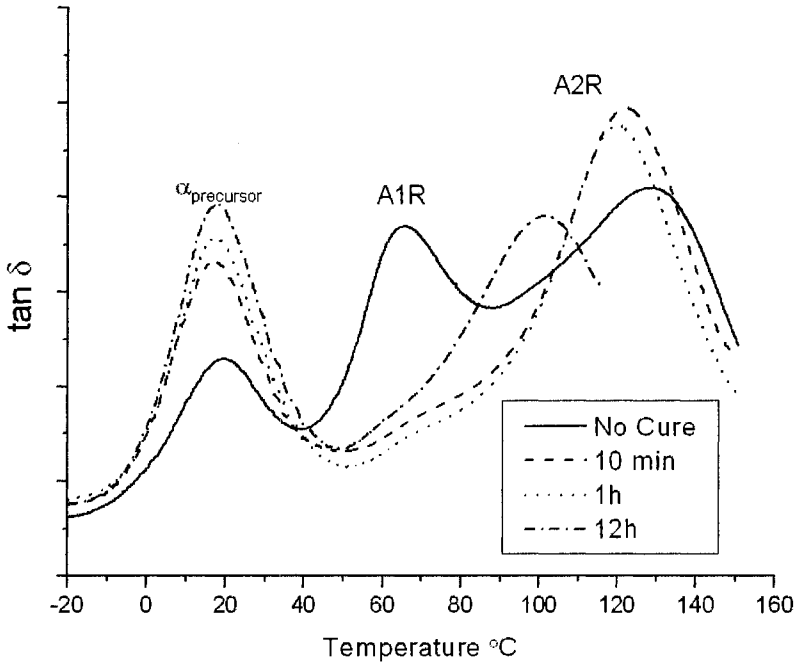

Figure 0-15. Dynamic mechanical tan δ vs. temperature at 1 Hz for indicated cure times of EDA films symmetrically-reacted to a depth of 10μm.

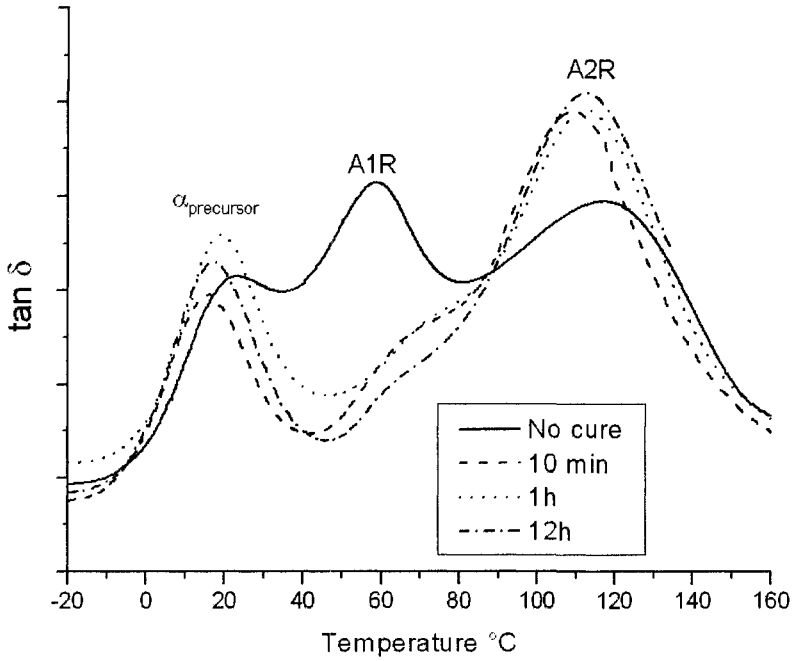

Figure 0-16. DMA tan δ vs. temperature at 1 Hz for indicated cure times for 1,3 PDA films symmetrically reacted to a depth of 10μm.

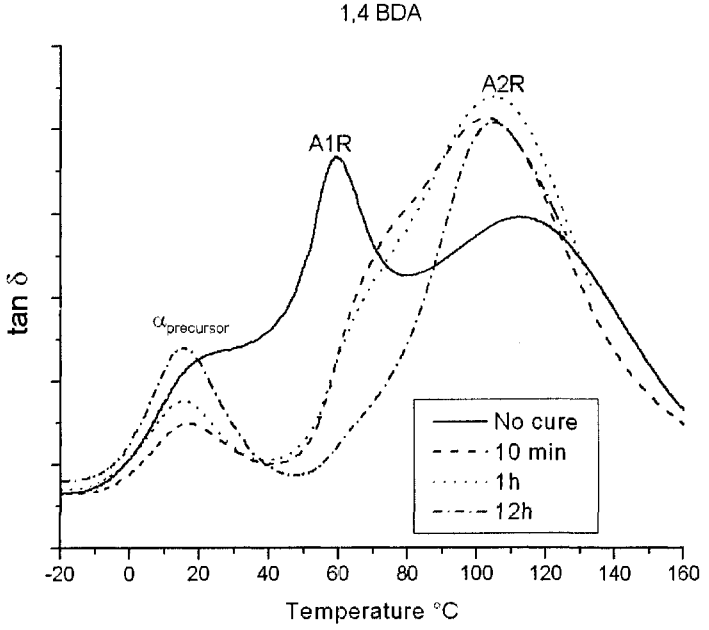

Figure 0-17. DMA tan δ vs. temperature at 1 Hz for indicated cure times for 1,4 BDA films symmetrically reacted to a depth of 10μm.

Conclusions

As demonstrated, all amine modified films discussed here have two relaxations (A1R and A2R). The fact that the A1R and A2R track each other with increasing temperature and frequency suggests that these two relaxations are closely linked to each other. The IR data from Figure 0-2 suggests that heating drives the free amine from a salt association to a covalent linkage. Correlating the disappearance of the A2R in the dielectric spectrum with the IR data could indicate that A2R stems from the reorientation of the dipole moment of the amine salt. Resultantly then, A1R would stem from the dipole reorientation of the amine covalent linkage. The shift of A1R to higher temperatures and frequencies implies restricted chain motion which further supports the idea that this relaxation is comprised of covalent linkages that are part of cross-links.

The presence of two relaxation peaks is reminiscent of the thermal transitions for the ionic forms of Nafion, which also have two high temperature relaxations. Moore et al. demonstrated that the highest temperature relaxation (i.e. the α-relaxation) was due to the on set of long range molecular motion of chains and side chains within a dynamically changing system. Using SAXS and DMA analysis they correlated the disappearance of the ionomer peak at the α transition with a loss in mechanical modulus to propose that the electrostatic network becomes dynamic at the α transition by an ion-hopping process. They attributed the β transition to the classic glass transition of the polymer; however, they defined the molecule motion process more precisely. Specifically, they stated that at the polymer T_g the main chain motions became thermally activated and facilitated by the motion of the side-chains within at physically static network.[22]

In the present study the amine modified films display a similar phenomenon where the dielectric relaxation tests indicate the presence of two high temperature amine relaxations for all of the amine modified films. It is quite possible the if A2R stems from a destabilization of an amine salt network that induces side chain mobility then the probability for two amine ends group to collide and covalently react is drastically increased at this relaxation temperature, thus driving the reaction to completion.

Acknowledgements

We acknowledge financial support of the NSF Materials Research Science and Engineering Center for Stimuli Responsive Materials (DMR–0213883) and E.I. DuPont Co. for donation of Nafion sulfonyl fluoride precursor film samples.

References

(1) Phillips, A. K.; Moore, R. B. *Polymer* **2005**, *46*, 7788-7802.

(2) Covitch, M. J.; Lowry, S. R.; Gray, C. L.; Blackford, B. *Polymer Preprints (American Chemical Society, Division of Polymer Chemistry)* **1980**, *21*, 120-121.

(3) Swaminathan, P.; Disley, P. F.; Assender, H. E. *Journal of Membrane Science* **2004**, *234*, 131-137.

(4) Covitch, M. J. In *Mebranes and Ionic and Electronic Conduction Polymers*; Yeager, E. B.; Schumm, B.; Mauritz, K. A.; Abbey, K.; Blankenship, D.; Akridge, J., Eds.; The Electrochemical Society, Incorporated: Cleveland, OH, 1982; Vol. 83-3, pp 31-49.

(5) Schonhals, A.; Kremer, F. *Broadband Dielectric Spectroscopy*, 1 ed.; Springer, 2003.

(6) Havriliak, S.; Negami, S. *Journal of Polymer Science, Polymer Symposia* **1966**, *14*, 99-103.

(7) Havriliak, S.; Negami, S. *Polymer* **1967**, *8*, 161-205, appendix 206-110.

(8) Schonhals, A., Application Notes Dielectric 1 ed.; Novocontrol, 1998; Vol. 2006.

(9) Diaz-Calleja, R. *Macromolecules* **2000**, *33*, 8924.

(10) Vogel, H. *Physik. Z.* **1921**, *22*, 645-646.

(11) Fulcher, G. S. *Journal of the American Ceramic Society* **1925**, *8*, 339-355.

(12) Tamman, G.; Hesse, W. *Zeitschrift fuer Anorganische und Allgemeine Chemie* **1926**, *156*, 245-257.

(13) Conley, R. T. *Infrared Spectroscopy*, 2nd ed.; Allyn & Bacon: Boston, 1972.

(14) Rhoades, D. W.; Mauritz, K. A. *In Press.* **2007**.

(15) Hodge, I. M.; Eisenberg, A. *Macromolecules* **1978**, *11*, 289-293.

(16) McCrum, N. G.; Read, B. E.; Williams, G. *Anelastic and Dielectric Effects in Polymeric Solids*; Dover Publications, Inc.: New York, 1967.

(17) Klein, R. J.; Zhang, S.; Dou, S.; Jones, H. H.; Colby, H. H.; Runt, J. P. *Journal of Chemical Physics* **2006**, *124*, 144903.

(18) Casalini, R.; Roland, C. M. *Physical Review E* **2005**, *72*, 0315031-0031503-0315034.

(19) Huang, D.; McKenna, G. B. *Journal of Chemical Physics* **2001**, *114*, 5621-5630.

(20) Vilgis, T. A. *Physical Review B* **1993**, *47*, 2882-2885.

(21) Kyu, T.; Hashiyama, M.; Eisenberg, A. *Canadian Journal of Chemistry* **1983**, *61*, 680-687.

(22) Page, K. A.; Cable, K. M.; Moore, R. B. *Macromolecules* **2005**, *38*, 6472-6484.

CHAPTER IV

DIELECTRIC RELAXATION STUDIES ON THE β RELAXATION OF H^+ NAFION® UNDER DEHYDRATION

Abstract

Fuel cell operating performance is dependent and influenced by a large number of variables including membrane preparation and conditioning. In this work broadband dielectric spectroscopy was used to study the β relaxation, viz. the glass transition, of dehydrated H^+ Nafion® membranes. The studies described here demonstrate that the macromolecular motions in H^+ Nafion® membranes depend on the thermal history, hydration during preparation steps and method of conversion to the acid form through different salt forms. To obtain repeatable results H^+ Nafion® membranes must be dried at temperatures higher than their α relaxation which is ~110° C. Furthermore, proper selection of the chemical nature of the acid during the acid wash step directly impacts the β and α relaxations.

Introduction

A number of factors affect fuel cell operating performance. Proton conductivity depends on temperature, relative humidity, gas crossover, water management, electrode kinetics, and chemical and physical degradation. Membrane preparation and conditioning affects performance. The studies described here demonstrate that the macromolecular motions in H^+ Nafion® membranes depend on the thermal history, hydration during preparation steps and method of conversion to the acid form through different salt forms.[1]

Yeo and Yeager initially demonstrated that drying at elevated temperatures reduces H^+ Nafion® water absorption[2] and classified membranes as having the following three morphological forms dependent upon preconditioning. These conditions were classified as as-received, boiled in water and dried at elevated temperature, referred to as the normal (N), expanded (E), and shrunken (S) forms, respectively. Later, Hinatsu et al. confirmed that at room temperature membranes that were vacuum dried at 80 and 105° C prior to testing absorbed less water than membranes that were vacuum dried at room temperature[3] and samples dried at 105° C absorbed the least water. Furthermore, they reported that upon immersion in liquid water, samples dried at 80 and 105° C absorbed water differently than at temperatures below 100° C.[3] Samples dried at 80° C absorbed water linearly with temperature whereas samples dried at 105° C absorbed water non-linearly vs. temperature. However, at temperatures greater than 100-110° C, both samples had the same uptakes and it was suggested that morphological differences attributed to drying temperature disappeared at temperatures greater than 100-110 °C, suggesting that the E-form was recovered by submerging in boiling water. It should be remembered that these early studies involved rather old H^+ Nafion® grades.

In a recent study using small angle neutron scattering (SANS), Kim et al. reported the effects of pretreatment on H^+ Nafion® morphology[4] and concluded that extruded membranes have oriented ionic clusters while solution-cast membranes do not. In addition, thick extruded membranes (>183μm) have crystallites, but thinner extruded membranes and solution cast membranes do not. They determined that crystallization is related to the longer cooling times associated with thicker membranes. Instrument - *in situ* swelling of membranes from water vapor did not affect the crystallites. As expected,

ionic domain spacing increased with swelling. Pretreatment affected sorption behavior of extruded membranes. Specifically, pre-treating membranes by boiling in dilute H_2SO_4 at 80° C, as compared to those not boiled before testing increases the long spacing between ionic clusters and reduces total water absorption. These membranes were dried under vacuum at RT for one day and then subsequently at 40° C for several hours prior to testing. This last point suggests that pretreated membranes were in the E-form during SANS testing. From these and other studies[5,6] it is evident that the combination of water content and temperature influence morphology and directly affect the physical properties of H^+ Nafion®.

Recently, the highest temperature (α) relaxation for acid form H^+ Nafion® was associated with long range chain motions coupled to destabilization of hydrogen bonded acid group associations.[7] Furthermore, by increasing the size of alkylammonium counter ions, Moore et al. showed that, at the α transition, the electrostatic forces that give ionic aggregates cohesion weaken, thus rendering long-range main chain and side chain motions more facile.[8] The α transition is thought to be a change from a static to dynamic ion-hopping network allowing for morphological reorganization while the β relaxation is thought to occur within a static network where the ion associations are frozen and the molecular motions resemble those above a polymer glass transition. These assignments will be adopted in the analysis of macromolecular motions in H^+ Nafion® membranes using broadband dielectric spectroscopy (BDS) as presented here.

The dielectric relaxation behavior of H^+ Nafion® was originally investigated by Yeo and Eisenberg[9] who reported that a β relaxation was comprised of a major and minor peak that was highly sensitive to water. At low water contents (~ 0.7 H_2O/SO_3H) the

major peak of the glass transition relaxation was at ~ 50° C while the minor peak was at ~ 25° C. Increasing water content to 2.1 H_2O/SO_3H reduced the temperature of both major and minor peaks to approximately -20 and -10 °C, respectively. Both peaks were very sensitive to small fluctuations in water contents with the minor peak being slightly more so. Increasing the water content to 4.1 H_2O/SO_3H further reduced the temperature of the major and minor peaks to ~ -85 and -70 °C.

This present study was performed to establish the dependence of macromolecular motions in H^+ Nafion®, especially at low degrees of hydration, at different temperatures. Such information is essential in understanding the dynamic state of H^+ Nafion® in PEM fuel cells at high temperatures. Furthermore, it is important to understand how repeatable 'dry' pre-conditioned membranes actually are, under given conditions, for the purpose of experimental reproducibility.

Experimental

Materials

H^+ Nafion® chemical structure is comprised of a perfluorinated backbone with perfluoroalkylether side chains terminated with sulfonic acid groups:

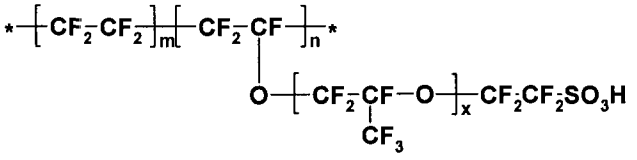

2 mil thick, 1100 EW H^+ form H^+ Nafion® in cast form was obtained from E.I.DuPont Co. for these studies.

Membrane Preparation

Membranes were cut from an as-received sheet to 2.2 cm in diameter and boiled in either nitric acid or hydrochloric acid for 2h. After this acid washing, samples were rinsed in DI water and then refluxed in DI water for 1h. The samples were removed from the water, positioned approximately 1 cm apart on a glass sheet and placed in vacuum for 12h at 0, 50, 70, 90 and 110° C. Membranes boiled in hydrochloric acid were only vacuum dried at 90° C. Upon sample removal from the vacuum oven they were immediately placed in a dry glove box at < 0.2% RH for a minimum of 7d.

All samples were tested with the following three step sequence. In the first step, labeled *in situ* drying (IS), a sample was *in situ* dried at a constant temperature of either 70 or 90° C. At this step frequency sweeps iterations were constantly taken with the culmination of this step occurring when 250 frequency sweeps were taken. One frequency sweep iteration took approximately 2min20 sec. Subsequently in the second step, labeled cycle 1, the temperature was reduced to -130° C. After the temperature equilibrated one frequency sweep was performed. The temperature was then increased in increments of 10° C up to 200° C with a frequency sweep occurring at each increment after thermal equilibration. The second step was repeated once and this data is labeled cycle 2.

Samples are labeled according to the manner in which they were dried in the vacuum oven (VO) and further dried *in situ* (IS) in the BDS sample chamber. For instance, a sample labeled VO30-IS70 indicates the sample was dried in the vacuum oven at 30° C and then dried in the BDS at 70° C for 250 frequency sweep iterations or approximately 9h. VO110-IS90 designates a sample that was dried in the vacuum oven at

110° C and then dried in the BDS at 90° C for 250 frequency sweep iterations. All samples were placed in a dry glove box (< 0.2% RH) for a minimum of 7d between the vacuum oven and BDS testing.

In our initial studies it was determined that large T_g shifts occurred due to atmospheric water absorption while loading the sample in the BDS chamber. To minimize this, sample thickness was measured and sandwiched between the electrodes in the glove box. Pressure was maintained on the electrodes to reduce surface area exposure. After the sample was removed from the glove box its total exposure to environmental atmosphere was less than 2 min. The purpose of the *in situ* drying step is to remove water absorption that might take place during the sample loading step.

Instrumentation

A Novocontrol GmbH Concept 40 broadband dielectric spectrometer was used over the frequency (f) range 0.1Hz - 3MHz at fixed temperatures from -130 to 190° C. Temperature (T) was controlled to within +/- 0.2° C. Samples were tightly pressed between two 20mm aluminum sheets that were further sandwiched between two 20mm diameter brass electrodes.

Dielectric spectroscopy is a powerful technique in being able to interrogate molecular and charge motions over a very wide range of time and distance scales.[10] The complex dielectric permittivity is given by the following equation in which ω, the angular frequency, $= 2\pi f$ and $i = \sqrt{1}$.

$$\varepsilon^*(\omega) = \varepsilon'(\omega) - i\varepsilon''(\omega) \qquad (1)$$

ε' reflects material polarizability, usually due to orientation of dipoles in polymers but can also reflect interfacial polarization; ε'' is proportional to energy dissipated per cycle during these molecular motions.

The Havriliak-Negami (HN) equation, below, is used to represent dielectric spectra with an additional term to account for possible dc conductivity at low f: [11,12]

$$\varepsilon^*(\omega) = \varepsilon' - i\varepsilon'' = -i\left(\frac{\sigma_0}{\varepsilon_0 \omega}\right)^N + \sum_{k=1}^{n}\left[\frac{\Delta\varepsilon}{\left(1+(i\omega\tau_{HN})^{\alpha_{HN}}\right)^{\beta_{HN}}}\right] \quad (2)$$

Each term in the sum represents a different relaxation process. Parameter values result from fitting this equation to experimental data. $\Delta\varepsilon = \varepsilon_o - \varepsilon_\infty$ is the difference between the low and high frequency limits of ε' for a given process. τ_{HN} is a time related to the actual relaxation time, τ_{max}, associated with the frequency at peak maximum, f_{max}. α_{HN} and β_{HN} are measures of the breadth and symmetry, respectively, of the given relaxation such that $\alpha_{HN} < 0 \leq 1$ and $0 < \beta_{HN} \leq 1$. α_{HN}, β_{HN} and τ_{HN} are used to determine τ_{max} using equation 3:[13]

$$\tau_{\max} = \tau_{HN}\left[\frac{\sin\left(\frac{\pi\alpha_{HN}\beta_{HN}}{2(\beta_{HN}+1)}\right)}{\sin\left(\frac{\pi\alpha_{HN}}{2(\beta_{HN}+1)}\right)}\right]^{\frac{1}{\alpha}} \quad (3)$$

When present, dc conductivity can obscure polymer relaxations that occur at low frequencies resulting in a superposition with the α relaxation. This superposition is removed once N (≤ 1) and the dc conductivity σ_0 are determined by curve fitting in the low f regime so that this term is subtracted point-by-point from ε'' curves to reveal un-obscured relaxation peaks.

Isothermal dielectric permittivity data were fitted to the HN equation including the dc term to obtain τ_{HN}.[12]

Results and Discussion

Figure 0-1 is a typical three dimensional tan δ - T - *f* response surface for 'dry' H^+ H^+ Nafion®. On this surface are three distinct ridges that correspond to three macromolecular relaxations labeled α, β, and γ.[9] The α ridge corresponds to the relaxation associated with long range motions as influenced by sulfonic acid aggregates assigned by Moore et al.[7] The β peak is identified with main chain segmental motions (glass transition) and the γ peak with CF_2 and side chain motions.[9] Comparing the β relaxation peak with that previously reported by Yeo and Eisenberg suggests that this material has a water content value, λ, of approximately 1.5 H_2O/SO_3H, or less.[9]

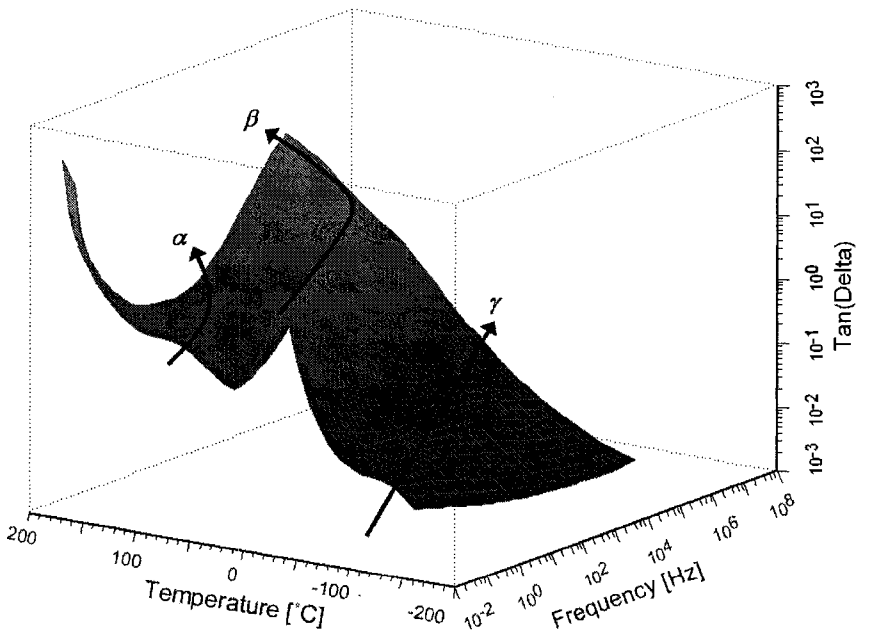

Figure 0-1. Tan δ - *f* - T surface of dry H^+ Nafion®. Curved arrows follow α, β and γ relaxation crests.

As described, samples were loaded into the BDS and heated (dried) *in situ* at a constant temperature for approximately 9.74 h. During this heating time, frequency sweeps obtained permittivity data (ε' and ε'') on a continuous basis to track the dehydration of the membrane. After this heating was complete, the samples were thermally cycled twice from -130 to 200° C, and frequency sweep data was collected at 10° C increments.

The impact of the *in situ* heating on the H^+ Nafion® membrane will be discussed first in section A. Following that the impact of the thermal cycling from -130 to 200° C will be discussed in sections B and C, relating to cycle 1 and cycle 2, respectively. After this in section D the impact of thermal drying in the vacuum oven, which was conducted prior to testing the in BDS, will be discussed. Section E details the non-linear response of the β relaxation. Finally section F discusses how the type of acid the H^+ Nafion® membranes are boiled in during preconditioning affects both the α relaxation and β relaxation of the dielectric spectra.

A. In situ heating at constant temperature.

The first series of experiments indicate that the time the sample was held at a constant temperature of 70° C in the BDS prior to thermal cycling impacts the glass transition of the material. To evaluate the impact of small amounts of absorbed moisture on the glass transition, after the sample was thoroughly dehydrated, the samples used for this testing were not sandwiched into the electrode setup in the drybox, rather they were intentionally exposed to atmospheric moisture for 5 minutes after removal from the glove box before testing. Figure 0-2, a plot of ε'' vs. $\log f$ at 70° C for five specific time increments, displays the glass transition, viz. the β relaxation, shifting to higher

frequencies with respect to drying time in the instrument. For this sample the β peak is not entirely in the test window at the start of *in situ* drying. With increased time at 70° C the β peak monotonically shifts leftward into the frequency test range. Figure 0-3 is a plot of τ_{max} vs. testing time at 70° C for the β relaxation for the same sample. τ_{max} monotonically shifts upward over a decade with decreasing rate. It is theorized that at 70° C small amounts of water desorb from the membrane resulting in a sort of deplasticization and increase in T_g.[9] The rate of water desorption is slow because the sample is sandwiched between two solid electrodes with only a small area at the edges for water molecules to escape. To reduce absorbed atmospheric moisture in subsequent testing all samples, thereafter, were immediately transferred from the glove box to the instrument with less than 30 s exposure to atmospheric moisture.

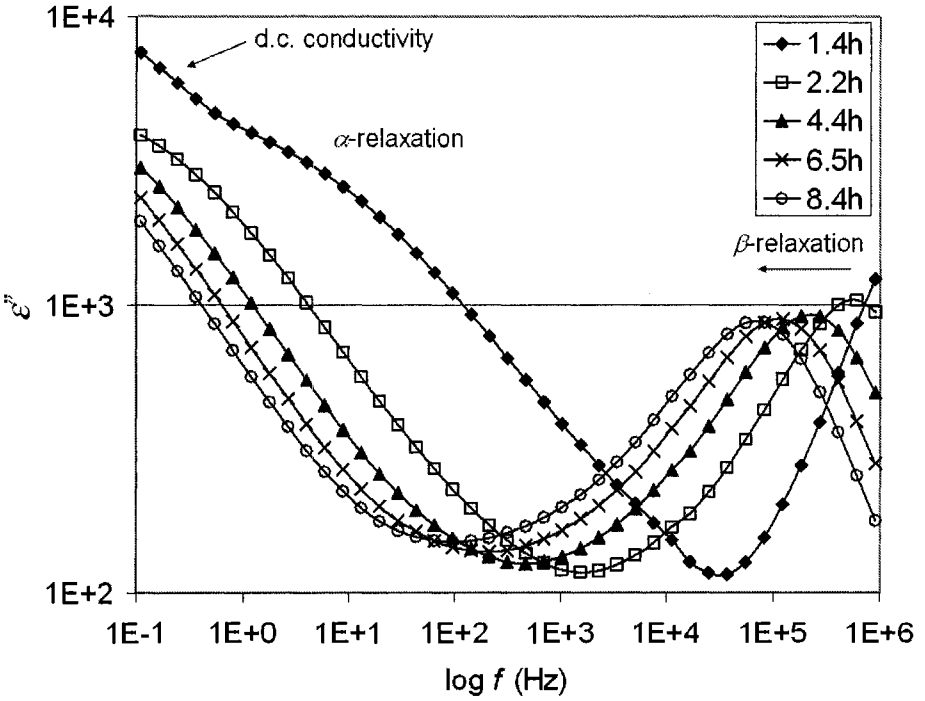

Figure 0-2. $Log_{10}\ \varepsilon''$ vs. $log_{10} f$ for *in situ* membrane drying at 70° C for different times after exposure to atmospheric moisture for ~ 5 min.

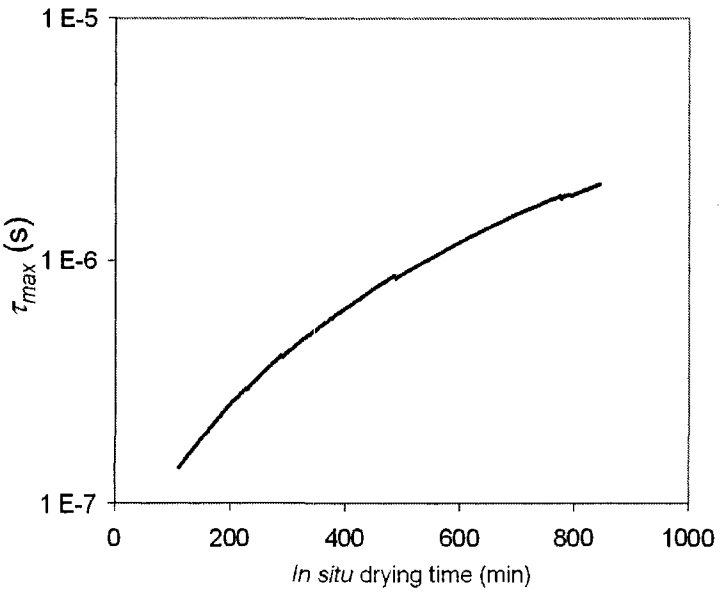

Figure 0-3. $Log_{10}\tau_{max}$ for β relaxation vs. drying time for same sample/conditions as in Figure 0-2.

To investigate the impact of drying temperature on H^+ Nafion® relaxation behavior, samples that were prepared at an *in situ* drying temperature of 70° C are compared to samples that were prepared at an *in situ* drying temperature of 90° C. Figure 0-4 is a plot of τ_{max} vs. time for *in situ* drying of the six VO30 samples, three for an *in situ* heating temperature at constant 70° C and three for an *in situ* heating temperature at constant 90° C. τ_{max} shifting is not as great for these samples because the initial moisture content is less than that of the sample of Figure 0-3. The general trend for both *in situ* drying at constant 70 and 90° C is an initial shift to higher τ_{max} followed by an approach to constancy. This trend is representative for all VO-IS samples regardless of temperature in the vacuum oven. Overall, IS70 membranes have greater τ_{max} values at longest tested time compared to their IS90 counterpart as indicated in Table 0-1. This is theorized to be due to more thermal energy associated with the higher

temperature facilitating the relaxation. The fact that τ_{max} for the IS70 and IS90 samples reaches an asymptote by 200 and 100 min, respectively, verifies that the moisture content has equilibrated at this temperature and has implications with regard to careful sample preparation.

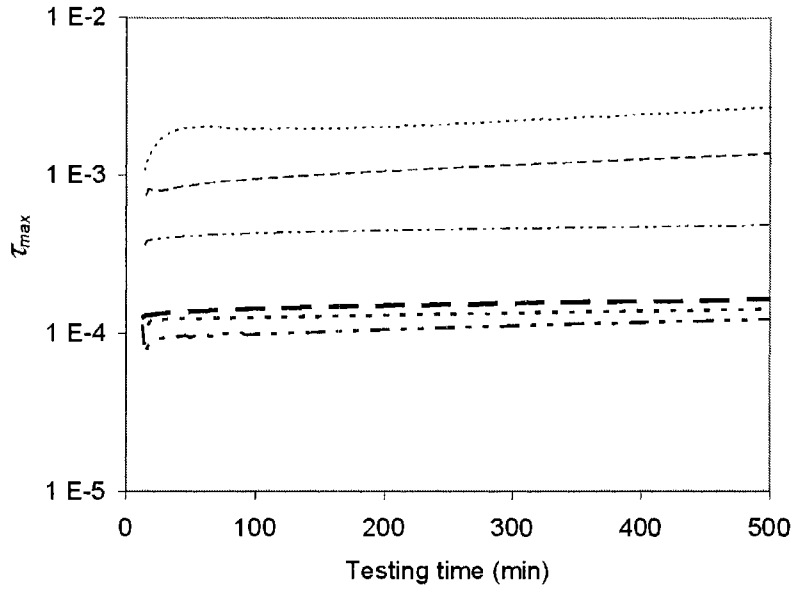

Figure 0-4. $Log_{10}\tau_{max}$ for β relaxation vs. drying time for six VO30 samples: three dried *in situ* at 70° C (light curves, top) and three dried *in situ* at 90° C (bold curves, bottom).

Table 0-1. τ_{max} (s) for the β relaxation of each vacuum oven + *in situ* drying combination. Three samples, labeled S1, S2 and S3, were tested for each testing condition.

Specimen	VO	IS	S1	S2	S3	Average	StDev
VO30-IS70	30	70	2.81E-3	4.89E-4	1.42E-3	1.57E-3	1.17E-3
VO30-IS90	30	90	1.45E-4	1.25E-4	1.65E-4	1.45E-4	2.00E-5
VO50-IS70	50	70	8.35E-4	1.76E-4	4.35E-4	4.82E-4	3.32E-4
VO50-IS90	50	90	3.34E-4	1.77E-4	2.03E-4	2.38E-4	8.38E-5
VO70-IS70	70	70	2.83E-3	1.96E-3	1.31E-3	2.03E-3	7.62E-4
VO70-IS90	70	90	8.26E-5	9.86E-5	6.65E-5	8.26E-5	1.60E-5
VO90-IS70	90	70	7.45E-4	1.11E-3	1.57E-3	1.14E-3	4.14E-4
VO90-IS90	90	90	1.77E-4	4.05E-4	3.34E-4	3.05E-4	1.16E-4
VO110-IS70	110	70	4.31E-4	7.24E-4	4.35E-4	5.30E-4	1.68E-4
VO110-IS90	110	90	1.17E-4	3.19E-4	1.40E-4	1.92E-4	1.11E-4

B. Temperature cycling from -130 to 200 C: cycle 1.

Holding the material at a constant temperature prior to thermal cycling allows the material to reach an equilibrium that is then interrupted by thermal cycling. This is confirmed by observing both the polarizability and energy dissipation of H^+ Nafion® as a function of temperature. The effects of the *in situ* heating are clearly observed during the first heating cycle that occurs immediately after the *in situ* heating is completed. Figure 0-5 is a plot of ε' and ε'' vs. T for the first temperature cycle after the *in situ* heating of a VO30-IS70 sample. Both the ε' and ε'' curves show a two-stage increase in permittivity. The first stage increase is the onset of the β relaxation around 0° C and results in ε' and ε'' increasing by over two orders of magnitude reflecting considerable polarizability. The second stage increase is the onset of the α relaxation, occurring between 60 and 100° C, and once again the ε' and ε'' increase by over two orders of magnitude. These β and α peak positions are in agreement with those observed using dynamic mechanical analysis.[7] The ε' values are greater than what might be expected on the basis of a simple fixed dipole reorientation process caused by liberated macromolecular degrees of freedom. Also, it must also be considered that dc conduction could contribute to a curve rise at the highest temperatures of ~T>160° C.

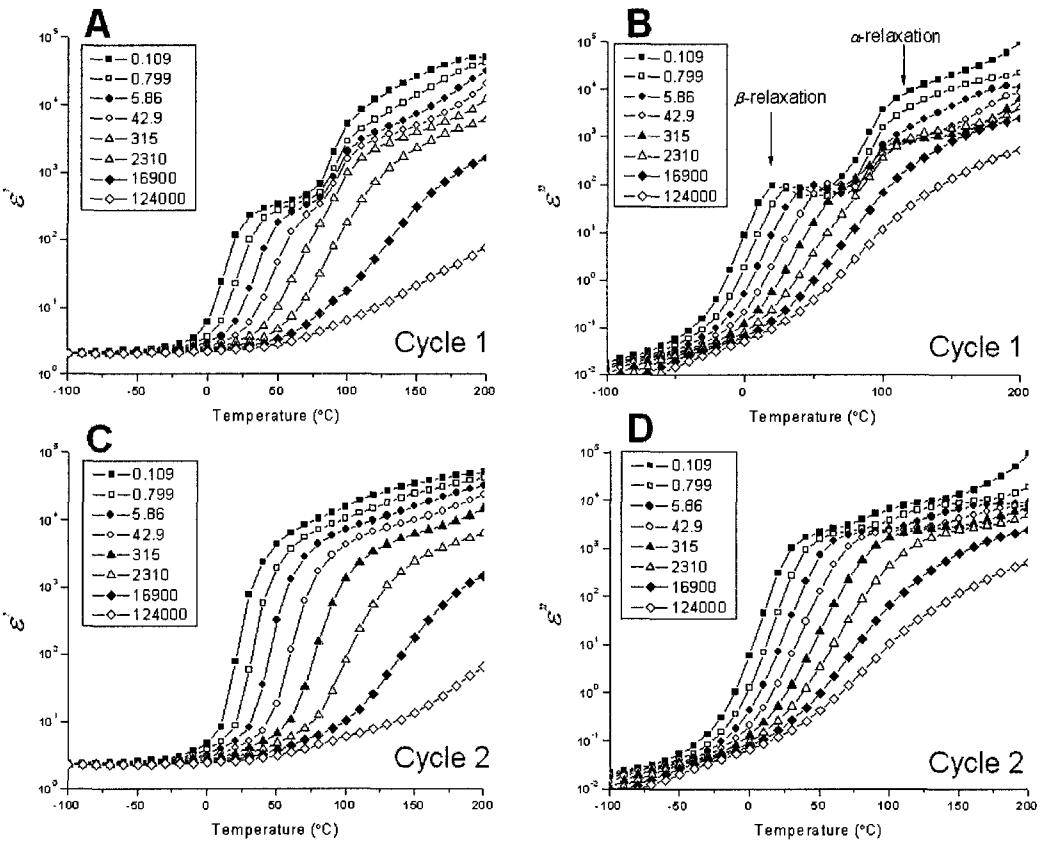

Figure 0-5. Log_{10} ε' vs. T (left) and log_{10} ε'' vs. T of VO30-IS70 at indicated frequencies (Hz). A series of frequency sweeps were performed at 10° C increments from -130 to 200° C after *in situ* drying. Plots A,B are for cycle 1 and plots C,D are for cycle 2.

The second stage increase in ε'' occurs at temperatures higher than the β relaxation peak and lower than the α relaxation peak. Fundamentally this increase in energy dissipation indicates that the polymer segmental motions are impacted or facilitated by the α relaxation. This is better illustrated in Figure 0-6 by isolating VO30-IS70 and VO30-IS90 ε'' vs. log f curves below the β relaxation, i.e. at 40° C, and above the α relaxation peak, i.e. at 120° C. Notice first the IS90 curves. The curves at 40 and 120° C have similar ε'' values despite being shifted for different temperatures. Notice second that the curve at 120° C for the IS70 sample which is very similar to both of the

curves for the IS90. However, the IS70 curve at 40° C is much different—it has much lower ε'' values. The ε'' values for the curve at 40° C are approximately 3 orders of magnitude lower than the values at 120° C for the same sample. Furthermore, the ε'' values at 120° C for the IS70 sample are of similar intensity to those of the IS90 curves. These results suggest that *in situ* heating at 70° C does not provide sufficient thermal energy to permit the structures to rearrange to the degree achieved by *in* situ heating at 90° C.

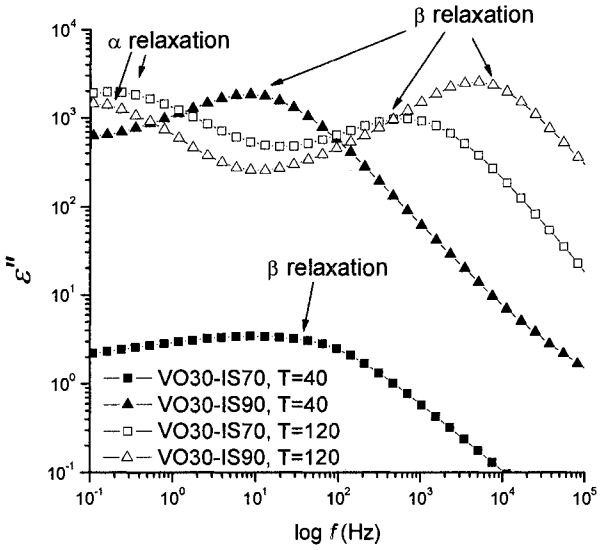

Figure 0-6. $\text{Log}_{10}\ \varepsilon''$ vs. $\log_{10} f$ with dc contribution subtracted for 1st temperature cycle for samples VO30-IS70 and VO30-IS90 both at 40° C and 120° C.

Figure 0-7 contains plots of $\log_{10}\ \varepsilon''$ vs. $\log_{10} f$ in the region of the β peak at successive 20° C temperature increments for cycle 1 of VO30-IS70 and VO30-IS90 samples. In both cases the peak shifts to higher frequencies with increasing in-cell heating temperature. For clarity sake it is restated here that the incremental temperature increases occur only after the *in situ* heating is completed. Furthermore, the d.c. conductivity contribution was not subtracted as it is not present until temperatures greater

than 160° C. The sample that was *in situ* dried at 90° C does not show the dramatic increase in ε'' with increasing temperature like the sample *in situ* dried at 70° C. *In situ* drying at 90° C is much closer to the dynamic α relaxation which allows for the structures to rearrange themselves to accommodate the loss of water. *In situ* drying at 70° C does not provide enough thermal energy to cause this structural rearrangement, i.e. the sample has not entered the low temperature wing of the α relaxation.

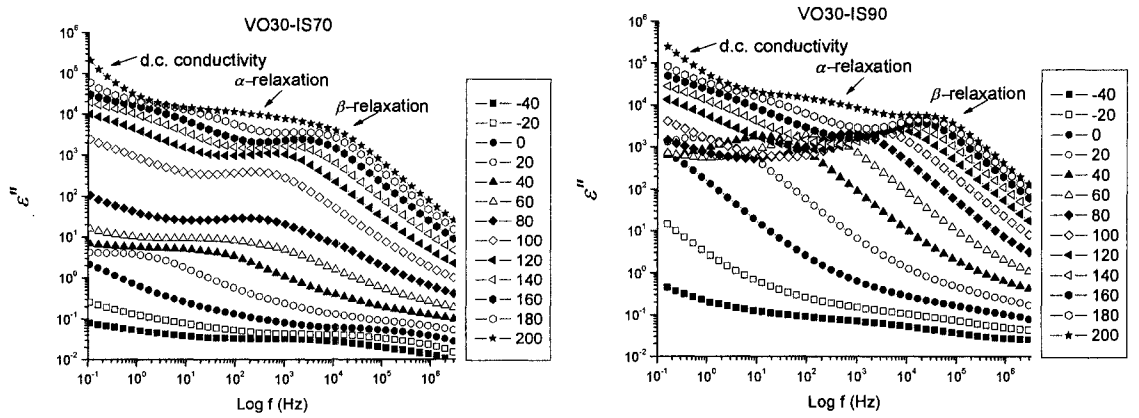

Figure 0-7. $\text{Log}_{10}\ \varepsilon''$ vs. $\log_{10} f$ in the region of the β relaxation for the first temperature cycle of VO30-IS70 (left) and VO30-IS90 (right) with curves being separated by consecutive 20° C increments. The dc contribution has not been subtracted. For clarity both samples were vacuum oven dried at 30° C and then placed in the glove box for 7 days. The difference between the two samples comes after the samples are loaded in the BDS. The IS70 specimen was *in situ* dried at 70° C whereas the IS90 specimen was *in situ* dried at 90° C. It's apparent by contrasting these two plots that the IS90 specimen does not show the dramatic increase in the ε'' for the β relaxation.

Another way to examine this structural change is by examining the breadth and asymmetry of the β relaxation via the HN equation. However, before that can be done the major and the minor peaks of the β relaxation must first be illustrated. Figure 0-8 is a plot at 60° C of log ε'' vs. log f with the accompanying HN fit parameters for the same VO30-IS90 sample. The α relaxation is the peak furthest to the left at the lowest frequency. No d.c. conductivity is present at this temperature. The β relaxation is the

peak to the right at higher frequencies. As is apparent from Figure 0-8 the β relaxation is best fit with two HN parameters labeled major and minor respectively. Early on in the relaxation study of H^+ Nafion® Yeo and Eisenberg discovered that the β-relaxation was comprised of two relaxation peaks whose temperature position and relaxation to each other depended on hydration level.[9] Using dielectric relaxation techniques on K-form Nafion® membranes at various hydration levels Tsonos et al. suggested that the high frequency *β*-relaxation was directly related to the rotation of the SO_3-H_20 dipole.[14] Furthermore, by expanding upon an earlier study by Mauritz et al.[15] Tsonos used blocking electrodes and non-blocking electrodes to demonstrate that the low frequency/higher temperature β-relaxation disappeared when the non-blocking electrodes were used.[16] This suggested that the low frequency/higher temperature *β*-relaxation was related to interfacial polarization between the hydrophilic/hydrophobic regions. Ironically, despite these later two points and confirming that the *β*-relaxation was sensitive to water Tsonos did not discuss the *β*-relaxation as stemming from or relating to segmental motions of the main polymer chain. It is possible that this β relaxation minor peak corresponds to the population fraction of chains influenced by interfacial polarization forces. Furthermore, heating causes this peak to increase which may be suggesting an increase in surface area to volume ratio (i.e. a larger interface).

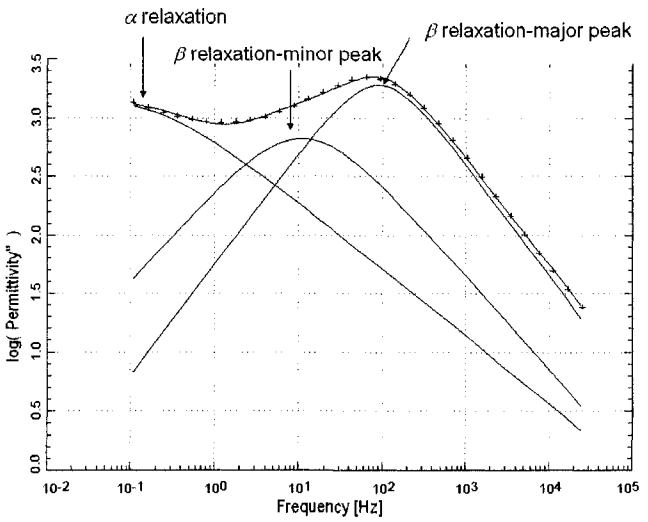

Figure 0-8. Log_{10} ε" vs. log_{10} *f* for a VO30-IS90 sample at 60° C. The glass transition is best fit with two HN parameters. The (+) symbols are actual data points.

Now the discussion that the structural change of the β relaxation is illustrated by examining the breadth and symmetry terms of the HN function is resumed. The breadth and asymmetry fitted terms for HN function for the VO30-IS70 and VO30-IS90 samples at 40 and 120° C are contained in Table 0-2. For the curves in Figure 0-6, the breadth terms (α_{HN}) for the major and minor peaks are much lower for the VO30-IS70 sample at 40° C compared to that at 120° C. For instance, for the minor peakα_{HN} = 0.53 at 40° C whereas α_{HN} = 0.88 at 120 °C. However, the β relaxation peak breadth value for the VO30-IS90 sample at 40° C is very similar to that at 120° C: α_{HN} = 0.85 at 40° C and α_{HN} = 0.78 at 120° C. Additionally, the α_{HN} values for the IS70 sample at 120° C are very similar to values for IS90 at 40 and 120° C. This latter fact points out that the α_{HN} value narrowing for both major and minor peaks of the IS70 sample is the result of the heating with respect to drying history. This indicates that the β relaxation distribution is narrowing signify that the relaxation is becoming more uniform. The main (only visible)

peak positions for both T = 40° C spectra are at lower *f* than those for the 120° C spectra, which indicates slower motions, as is reasonable. This may be suggesting that the structural rearrangement facilitated by the α relaxation allows the β relaxation to be more uniform. Heating causes a redistribution of ion chains which allow for an increase in the uniformity of the β relaxation. Lastly, this implies that before heating the chains are not in equilibrium.

Table 0-2. Havriliak-Negami α and β parameters for samples VO30-IS70 and VO30-IS90 for cycle 1.

	Major Peak				Minor Peak			
	α		β		α		β	
	40°C	**120°C**	**40°C**	**120°C**	**40°C**	**120°C**	**40°C**	**120°C**
IS70	0.78	0.98	0.99	1.00	0.53	0.88	1.00	1.00
IS90	0.96	0.98	1.00	1.00	0.85	0.78	1.00	1.00

C. Temperature cycling from -130 to 200° C: cycle 2.

As discussed, significant molecular motions occur during initial post-drying thermal cycling. Subsequent thermal cycling, i.e. cycle 2, however, does not cause a similar polarization or energy dissipation response at any of the frequencies tested such as that which occurs for cycle 1. For example, the cycle 2 plots in Figure 0-5, i.e., C and D, do not show the two stage increase in the ε' and ε'' vs. T curves as is seen for the cycle 1 plots in Figure 0-5, i.e. A and B. Figure 0-5 plots C and D show a single stage increase of ε' and ε'' over approximately four orders of magnitude, which begins at the onset of the β relaxation and levels off at approximately 25° C. Furthermore, for cycle 2, a dramatic increase of ε' and ε'' is not observed at the onset of the α relaxation as the β and α relaxations are not well differentiated (no multiple inflections on the former or distinct peaks on the latter). Figure 0-9 shows ε'' vs. T at a frequency of 0.109 Hz for

cycles 1 and 2. At this low frequency, a half cycle of applied field oscillation is rather long (4.6s) so that long range macromolecular motions can be captured. For cycle 2, ε'' increases at the onset of the β relaxation which is not manifested as a complete peak but rather there is a monotonic increase thereafter such that the curve lies close to that for cycle 1. This is an example of thermal-drying history in that cycle 2 data reflects the history of greater drying at higher temperature. This later behavior is probably the result of the cumulative effect of water being liberated in cycle 1 at temperatures greater than the α relaxation in combination with structural rearrangement which is facilitated by the α relaxation. For cycle 1 the initial increase in the β relaxation with heating is directly related to the fact that these samples were dehydrated at lower temperatures, i.e., the vacuum oven temperature was 30° C and *in situ* constant heating was 70° C. The increase in temperature above that of the *in situ* drying causes a structural rearrangement apparent by the second increase in $\varepsilon''$and ε''. This stepwise increase is only attainable by first drying below the α relaxation and then increasing the temperature to the α relaxation region. These curves are elevated to higher values with decreasing frequency because polarization becomes increasingly more facile with increasing thermal kinetic energy as the period of voltage oscillation becomes longer. This means that increasing thermal kinetic energy increases the dipole mobility so that the dipoles can align with the field easier and the fact that the frequency is low means that there is a long time scale in which to sample these motions and register a high polarization.

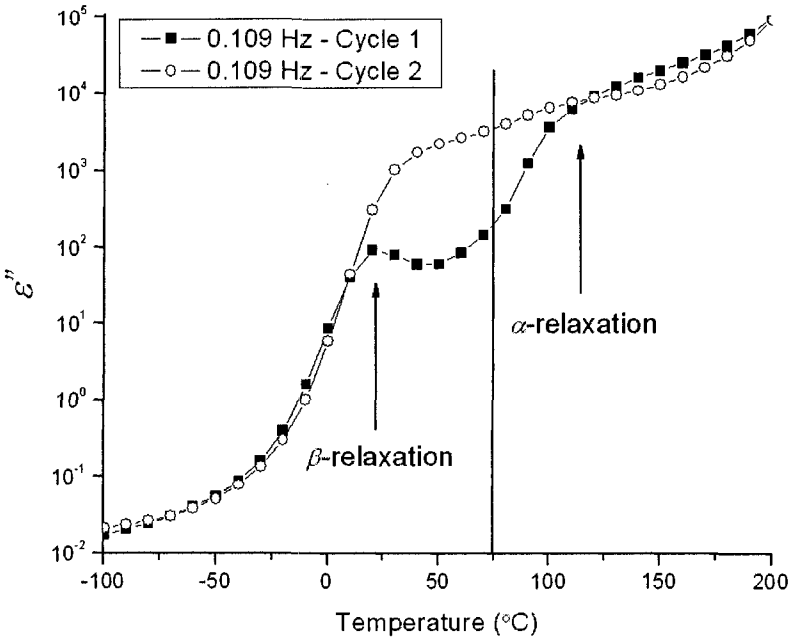

Figure 0-9. Log_{10} ε'' vs. T at 0.11Hz for two consecutive temperature cycles from -130 to 200° C with frequency sweeps at 10° C increments. The temperature is held constant at each frequency sweep. Before testing, the sample was dried in a vacuum oven at 30° C for 12h. Before the temperature was reduced to -130° C the sample was dried at 70° C for approximately 9.75 h.

Examining cycle 1 log ε'' vs. T plots in Figure 0-10 through Figure 0-14 indicates more variability for IS70 than IS90 samples demonstrating that *in situ* drying affects experimental repeatability. Each plot has data displayed for each respective cycle. For both IS70 and IS90 three samples were analyzed for each conditioning criteria to illustrate repeatability. For all vacuum oven treatments (except VO110) cycle 1 curves from IS70 have more variability than 1) the IS70 cycle 2 curves and 2) the IS90 cycle 1 and cycle 2 curves. IS90 curves for cycle 1 and cycle 2 appear to have more similarities than the IS70 counterparts. Qualitatively speaking, IS90 sample results are more repeatable than IS70 samples for temperature cycle 1. This conclusion is illustrated by

comparing IS70 and IS90 samples for cycle 1 in Figure 0-10 of the six samples conditioned at VO30. The maximum ε'' values of the three samples of IS70 cycle 1 are 4.20, 685 and 93.4 which average to 261 with a standard deviation of 370, as reported in Table 0-3. Note that these three values span three orders of magnitude. In contrast, the maximum ε'' values of the three samples of IS90 cycle 1 are 1590, 1350 and 1740 that average to 1560 and a standard deviation of 197. These values have the same order of magnitude as was previously suggested indicating that *in situ* drying at 70° C produces unstable structures that are not in thermodynamic equilibrium. This results in a reduction of sample reproducibility and an increase in error. However, *in situ* drying at 90° C provides sufficient thermal energy allowing chains to reach *more* favorable structures. This is why the three ε'' vs. T curves for the IS90 samples are typically more similar than the IS70 curves, which show more variability.

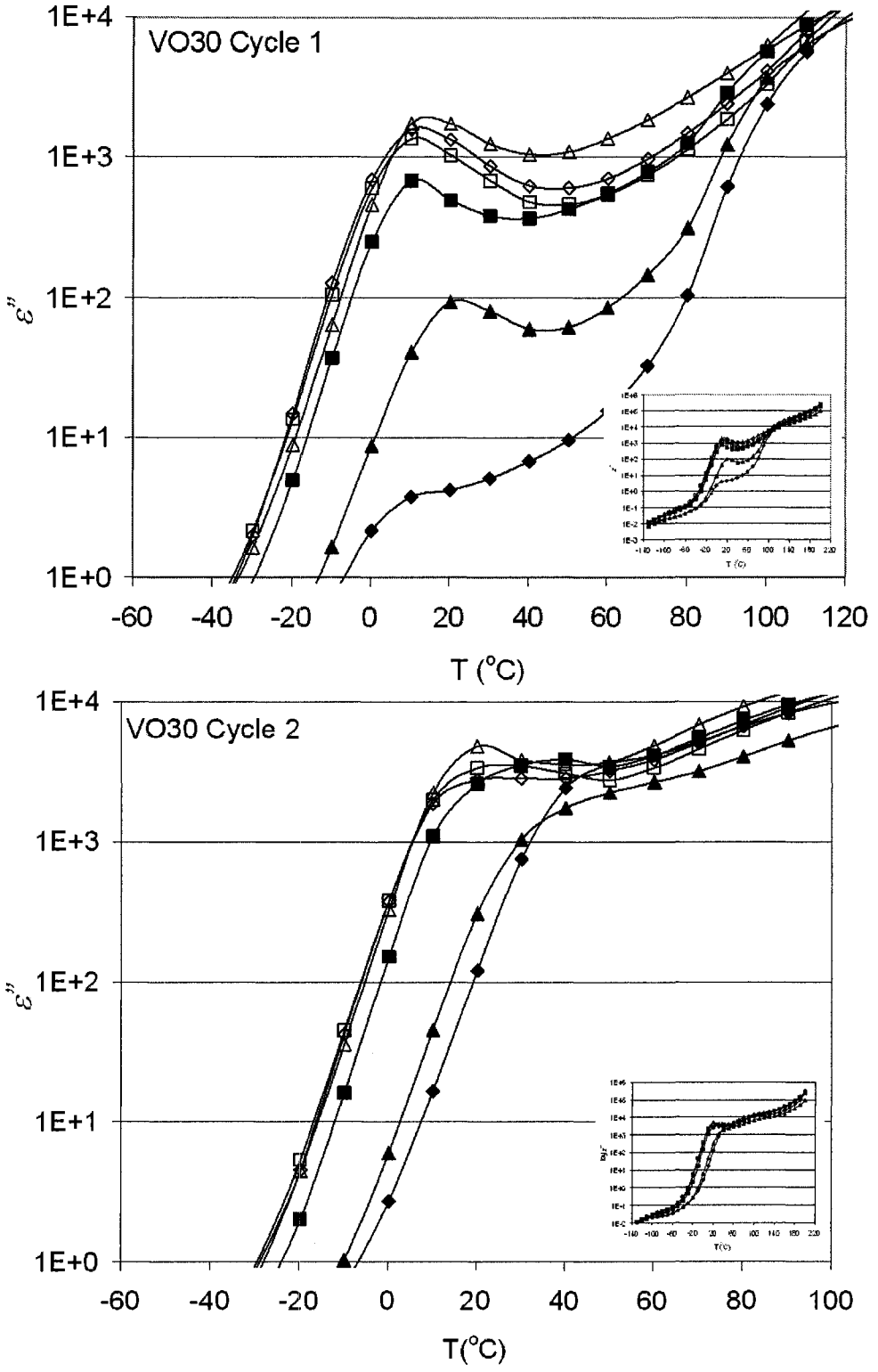

Figure 0-10. Log_{10} ε'' vs. T (°C) for samples dried in vacuum at 30° C, then tested *in situ* in the BDS at 70° C (filled triangles) and 90° C (open squares). Left plot designates first temperature cycle and right plot designates the second temperature cycle. Different shapes designate different specimens.

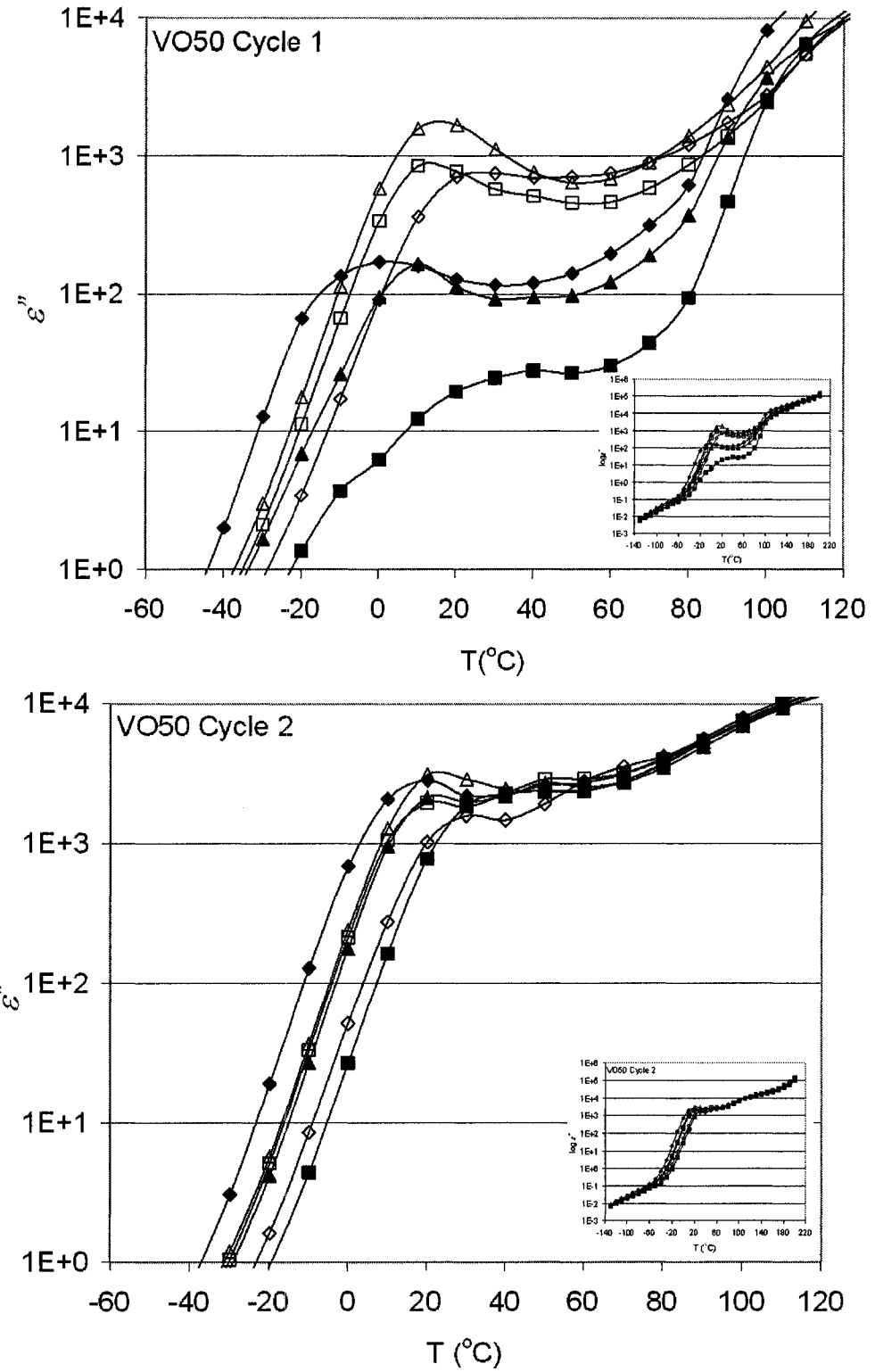

Figure 0-11. Log_{10} ε'' vs. T (°C) for samples dried in the vacuum oven at 50° C and then *in situ* in the BDS at 70 °C (filled triangles) and 90 °C (open squares). The left plot is for the first temperature cycle and the right plot is for the second cycle. Different shapes designate different specimens.

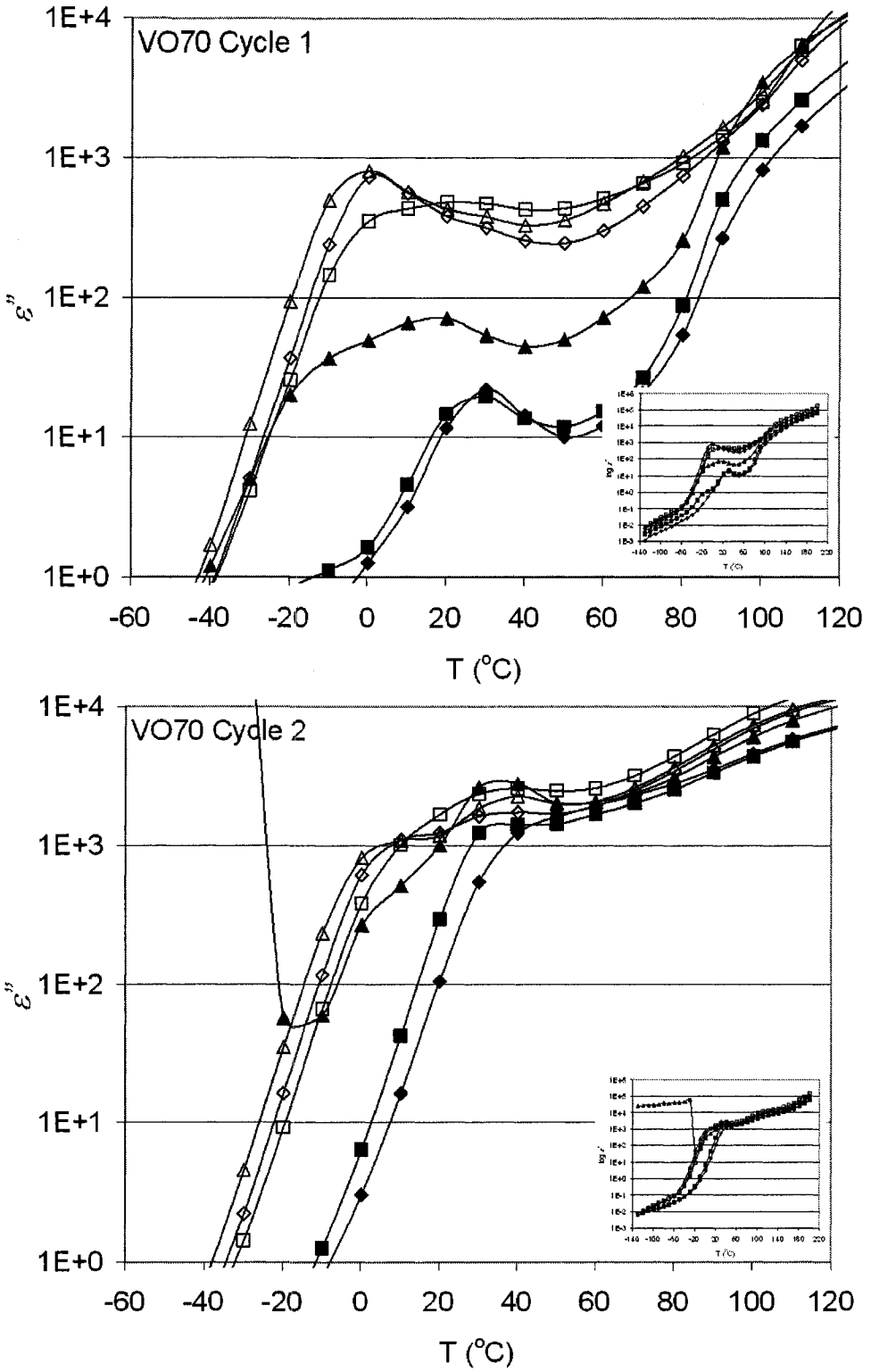

Figure 0-12. Log_{10} ε'' vs. T (°C) for samples dried in vacuum oven at 70° C, then *in situ* in the BDS at 70° C (filled triangles) and 90 °C (open squares). Left plot is for first temperature cycle; right plot is for second temperature cycle. Different shapes designate different samples.

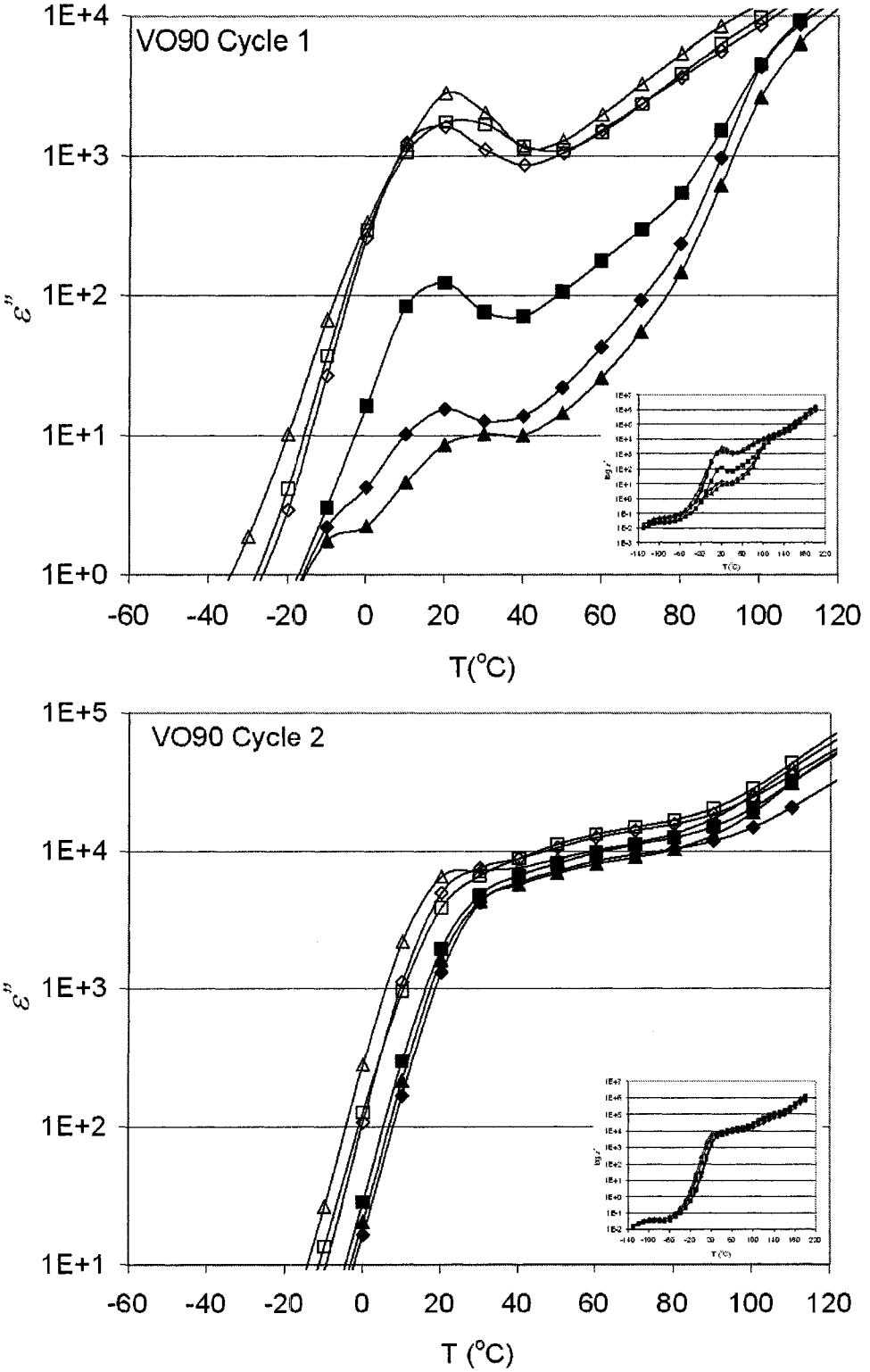

Figure 0-13. Log_{10} ε'' vs. T (°C) for samples dried in vacuum oven at 90° C, then *in situ* in BDS at 70° C (filled triangles) and 90° C (open squares). Left plot is for first temperature cycle; right plot is for second temperature cycle. Different shapes designate different specimens.

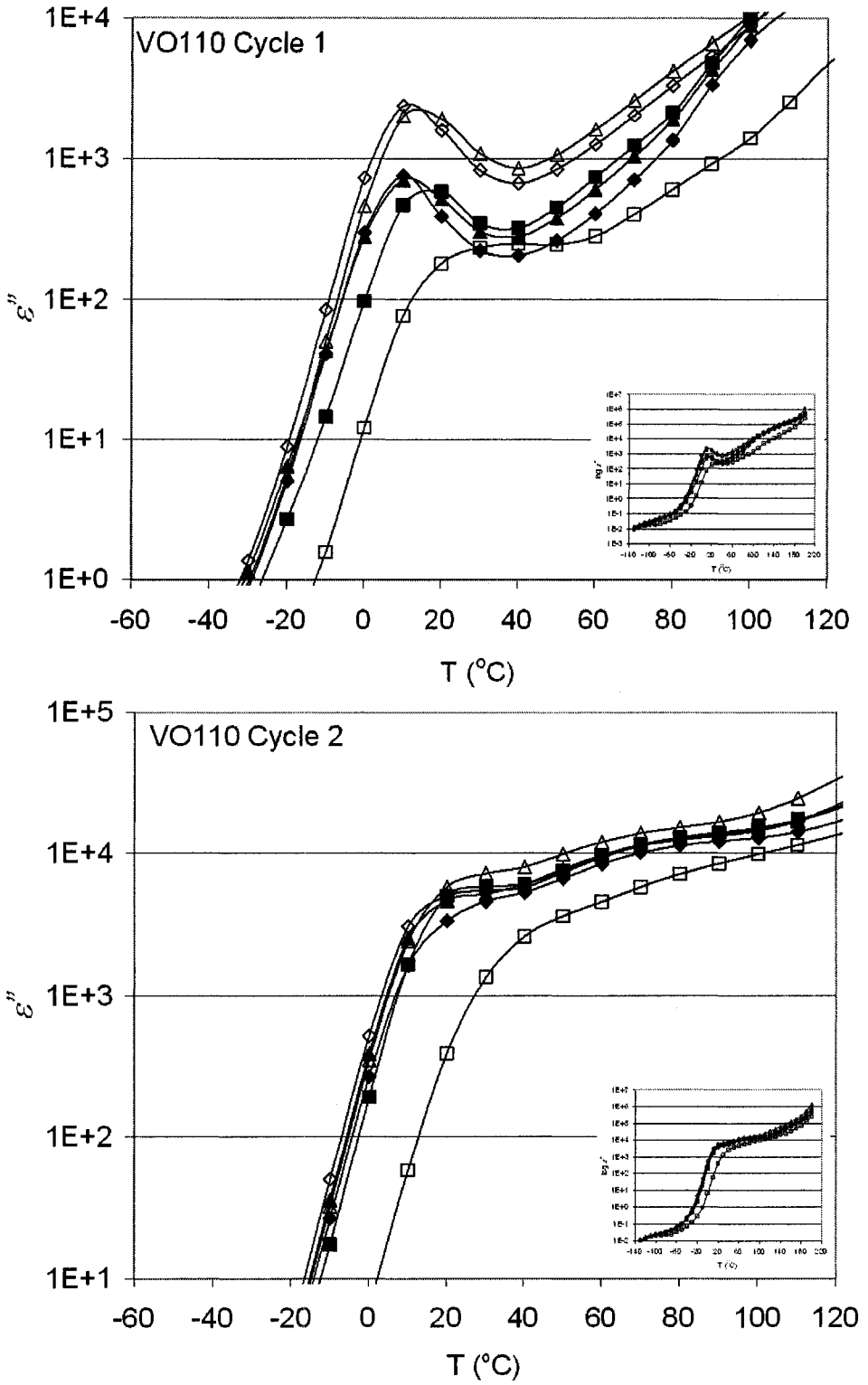

Figure 0-14. Log_{10} ε'' vs. T (°C) for samples dried in vacuum oven at 110° C, then *in situ* in BDS at 70° C (filled triangles) and 90° C (open squares). Left plot is for 1st temperature cycle; right plot is for 2nd temperature cycle. Different shapes designate different specimens.

Table 0-3. ε'' vs. T peak values of glass (β) transition at f= 0.109 Hz.

		Cycle 1				Cycle 2			
		IS70		IS90		IS70		IS90	
	Specimen	**ε''**	**T**	**ε''**	**T**	**ε''**	**T**	**ε''**	**T**
VO30	1	4.2	20	1590	10	3600	50	2850	30
	2	685	10	1350	10	3510	30	3380	20
	3	93.4	20	1740	10	1740	40	4840	20
	average	**261**	**17**	**1560**	**10**	**2950**	**40**	**3690**	**23**
	StDev	370	6	197	0	1049	10	1031	6
VO50	1	169	0	755	30	2780	20	1560	30
	2	27.6	40	849	10	2250	40	1930	20
	3	163	10	1690	20	2110	20	3070	20
	average	**120**	**17**	**1098**	**20**	**2380**	**27**	**2187**	**23**
	StDev	80	21	515	10	353	12	787	6
VO70	1	22.1	30	729	0	1220	40	1730	40
	2	19.6	30	478	20	1410	40	2560	40
	3	71.1	20	807	0	2770	40	2230	40
	average	**38**	**27**	**671**	**7**	**1800**	**40**	**2173**	**40**
	StDev	29	6	172	12	845	0	418	0
VO90	1	15.5	20	1620	20	4190	30	7570	30
	2	122	20	1750	20	4760	30	6620	30
	3	10.2	20	2840	20	5670	30	7160	30
	average	**49**	**20**	**2070**	**20**	**4873**	**30**	**7117**	**30**
	StDev	63	0	670	0	746	0	476	0
VO110	1	763	10	2400	10	3340	20	5050	20
	2	586	20	181	20	4980	20	2600	40
	3	710	10	2030	10	4680	20	7170	30
	average	**686**	**13**	**1537**	**13**	**4333**	**20**	**4940**	**30**
	StDev	91	6	1189	6	873	0	2287	10

Examining cycle 2 in Figure 0-10 through Figure 0-14 indicates that *in situ* drying does not affect repeatability for the second thermal cycle to as great an extent as it does for the first cycle. Overall, IS70 and IS90 are much more similar for cycle 2 suggesting that the heating of cycle 1 results in permanent or semi-permanent change. The results of this annealing are a consistent increase of ε'', for all samples regardless of vacuum oven temperature and *in situ* drying, to values between 10^3 and 10^4 as shown in Table 0-3.

Generally speaking, for the β relaxation, the low temperature wing of the peak on the ε'' vs. T curve (Figure 0-10 through Figure 0-14) is well defined but on the high temperature side it is very broad. This high temperature wing merges with another higher temperature relaxation believed to be the α relaxation.

D. Analysis of hydration & thermal conditioning prior to testing.

All IS70 samples, regardless of vacuum oven temperature (except VO110) have increased variability compared with the IS90 samples, as illustrated in Figure 0-10 through Figure 0-14. The maximum ε'' values at 0.109Hz for the β relaxation of each sample are tabulated in Table 0-3. All of the ε'' average values are lower for IS70 samples when compared with the IS90 samples suggesting that the ε'' increase is dependent upon the temperature of the *in situ* drying. As was previously mentioned, the increase in ε'' for the IS70 samples is not observed upon a subsequent BDS testing cycle (i.e. cycle 2), implying that the alteration is irreversible with respect to temperature alone.

The different results stemming from different vacuum oven drying procedures, *in situ* heating at constant temperature, and *in situ* thermal cycling show the interplay relationship between hydration and temperature. Whether the membrane's morphology is in the E, N, or S form as originally described by Yeo and Yeager directly depends on the hydrothermal history.[2] Simply stated, at a constant temperature the ionic side chains rearrange themselves to accommodate any increase or decrease in water content. For instance, if the ionic clusters gain water then the molecules will rearrange themselves to accommodate more water, and vice versa if water is lost. This notion is not so straight forward when hydration and temperature are changing simultaneously. Before the data can be discussed in this light two basic scenarios will be considered.

Scenario 1: drying at temperatures higher than the α relaxation. When water leaves the membrane the ionic chains have sufficient thermal energy to seek out their most favorable conformations by molecular rearrangement. This is because at the α relaxation the hydrogen bonded network is destabilized resulting in a dynamic polymer network with ionic side chains freely moving.[7] Upon cooling, the morphology remains stable, as long as no water is absorbed. Drying under these conditions gives the most tightly packed structures.

Scenario 2: Drying beneath the α relaxation temperature. At sub-α temperatures the polymer side chains, according to the most recent view, are in static associations.[7] As such, the polar side chains are not able to rearrange to accommodate new hydration levels; therefore, the morphology remains locked in a frustrated state until the temperature is raised to activate the α relaxation. Upon heating at temperatures close to the α relaxation, the side chains will begin to rearrange to attain their most favorable conformations under the new hydration level. The closer the temperature is to the α relaxation the faster the rate of rearrangement. However, it must be remembered that as the temperature increases additional water desorbs from the system convoluting the isolation of the hydration and thermal processes.

The molecular significance of the increase in ε'' with increasing temperatures seems to suggest that the *in situ* drying at 70 °C produces structures that are unstable when temperature cycling begins as this is well below the α relaxation as described in scenario 2. However, *in situ* drying at 90° C is in the low temperature wing of the α relaxation as this temperature is much closer to the α relaxation peak. Therefore more thermal energy is available which generates a greater population of chains like that which

is described in scenario 1. Activating the dynamic network allows the chains to approach more equilibrium packing. As a result the three ε'' vs. T curves for IS90 samples in cycle 1 are more similar to each other than their IS70 counterparts which show more variability (in Figure 0-10 through Figure 0-14). In line with Yeo and Yeager's [2] classification it is believed DI-water refluxing of membranes erases prior conditioning, i.e. thermal history, of ionic aggregates and places the ionic cluster in the expanded (E) form.[3] Thus, before *in situ* drying in the BDS the samples that were vacuum oven dried at 30° C are assumed to be in the E-form. However, as the vacuum oven temperature increased to 50 and 70° C it is believed that the morphology of the samples should increasingly have greater S-form characteristic, respectively. Theoretically, the morphology of the VO110 samples should all be in the S-form probably indicating why the VO110 samples in Figure 0-14 do not match the trends of the vacuum oven samples in Figure 0-10 through Figure 0-13.

If the ε'' increase of the β relaxation peak is attributed to a transition of morphology from the E-form or N-form to the S-form, then logically the VO110 samples should not have the increase in ε'' of the β relaxation peak when comparing cycle 1 to cycle 2. Examining Figure 0-10 through Figure 0-14 it is evident that the increase in ε'' of the β relaxation peak is least pronounced of all the vacuum oven treatments. Additionally, the ε'' vs. T curves for the VO110-IS70 samples resemble the VO110-IS90 much more than the other vacuum oven treatments. Thus it is thought that the increase in ε'' with increasing temperature for the IS70 samples is related to the morphology changing from the E-form to the S-form through ion-hopping. However, if that is true then the question still remains, that if the increase in ε'' is due to the morphology transitioning from the E-form to the S-form and the VO110 samples are in the S form

prior to testing then why do the VO110 samples still show some ε'' increase, even though it is reduced? This paradox may be suggesting that the 110 °C vacuum oven temperature may not provide sufficient thermal energy to fully mobilize all of the ionic domains. This may be related to the α relaxation being a distribution and the high temperature wing is not completely activated at the 110° C. In other words, the morphology of the ionic clusters may obtain an ultra-shrunken (US) morphology as a result of going to temperatures higher than the 110° C as occurs in cycle 1. Upon cooling, the morphology attained from the higher temperature heating is preserved for the start of the subsequent cycle (i.e., cycle 2), which has also been suggested by other authors.[4,17] With this in mind it is believed that the morphology is US for all the samples at the start of cycle 2. It is suggested that to obtain the US morphologies prior to testing that the samples be dried at temperatures 40 to 50 °C above the peak of the α relaxation. This later point will ensure sufficient thermal energy is present to activate all populations of ionic side chains.

E. Non-linear response of the β relaxation.

The glass transition can be observed using BDS over many frequency orders of magnitude.[18] For most glass-forming materials, this transition does not display Arrhenius behavior with respect to temperature and is commonly studied using the Vogel-Fulcher-Tamman equation (VFT) and the fragility index.[19] As previously stated, IS90 samples appear closer to an equilibrium state than IS70 samples. For this reason only the IS90 samples will be discussed from this point on, unless specifically stated otherwise.

This section is divided into three parts. The first part (i) describes the procedure for HN equation fitting and rationale. The second part (ii) details fitting τ_{max} vs. 1/T data to the VFT equation and associated complexities, and resultant data. The third part (iii)

deals with quantifying the degree of non-linearity, also known as the 'fragility' which will be explained.

(i) HN equation fitting procedure

As mentioned, the HN function has two parameters that quantify the breadth and degree of asymmetry of dielectric relaxation curves. For simple polymers, fitting to data is uncomplicated, but not so for H^+ Nafion® owing to its polar/nonpolar character as well as superposition of α and β relaxations and usual presence of d.c. conduction at higher temperatures. Moreover the glass transition (β relaxation) can be resolved into a major and a minor peak as illustrated in Figure 0-8. When H^+ Nafion® is very dry, as required for BDS, these two peaks are greatly affected by small changes in moisture content, as previously described. One or two additional H_2O molecules per SO_3H group can reduce T_g by as much as 70° C and shift the relative position and intensity of the two peaks.[9] In addition, as will be discussed later, the relative positions and intensities of the major and minor peak, and with respect to each other, also depend on the preconditioning and testing procedure. For example, for a given procedure the intensity of the major peak may be much greater than the minor peak and the corresponding τ_{max} values for each peak are discernible, thus clearly distinguishing the major peak from the minor peak. However, this may not be the case for a different procedure where the major and minor peaks may have similar intensities or similar f_{max} values leading to confusion with peak identification. Thus, it is difficult to absolutely determine the true f_{max} peak positions for the major and minor peaks. This leads to the possibility of several logical fitting scenarios for a single data set all with different f_{max} peak positions for the major and minor peaks. The possibility that one set of data can be fit with several different curve

sets necessitates a standardized fitting procedure, as will be immediately detailed, or all of the subsequent data and calculations will be erroneous.

On a log-log plot, by definition, for a single HN parameter the slope of the high frequency wing on a peak can only be equal to or less steep than the low frequency side.[19] In this study, all H^+ Nafion® samples inherently have a very steep high frequency wing as illustrated in Figure 0-8, with typical α_{HN} values being 1.00. Thus by definition the β_{HN} term must also equal unity. Fortunately, the peak corresponding to the steep high frequency wing is almost always the one with greatest intensity, although not always so. For the sake of standardizing the HN fitting process, and corresponding VFT equation fitting process, the highest frequency peak, which inherently has α_{HN} and β_{HN} fit values near unity, is here identified as the primary (major) peak that will be used for the VFT fitting process of the polymer T_g. The peak that is lower in frequency from this primary peak is identified as the secondary (minor).

(ii) The VFT process

Log τ_{max} vs. $1/T$ plots for the glass transition relaxation are characteristically nonlinear (non-Arrhenius) and obey the empirical Vogel-Fulcher-Tamman (VFT) equation commonly used for glassy materials:[20-22]

$$\tau(T) = \tau_0 \exp\left(\frac{E_a}{k_B(T - T_V)}\right) \qquad (5)$$

Where τ_0 is a hypothetical relaxation time at infinite temperature. Theoretically speaking τ_0 is related to phonon vibrations and for simple systems is 10^{-14}s.[23] k_B is the Boltzmann constant. E_a is a fitting constant that, although having the same units, is not a real activation energy in the sense of rate processes. T_v, the Vögel temperature, is often considered to be related to, and typically 30 to 70 °C below, the glass transition temperature, T_g.

VFT data is generated as follows: First, ε'' vs. log f plots are fit with the HN equation, at each temperature increment. Second, the frequency that corresponds to the ε'' peak maximum for the β relaxation major peak is extracted from the model function. This frequency is related to the relaxation time at that temperature by $\tau_{max} = 1/2\pi f_{max}$. Then, the log τ_{max} is plotted vs. $1/T$ and the VFT equation is fitted to this data to determine the extent of non-linearity, i.e., deviation from Arrhenius behavior. VFT plots for a VO30-IS90 sample will now be discussed.

Figure 0-15 is a VFT plot of the 1^{st} cycle of a VO30-IS90 sample and Figure 0-16 is a plot for the 2^{nd} cycle for the same VO30-IS90 sample. The VFT equation for both cycles 1 and 2 are fit in two ways. The first VFT fitting process is over the entire BDS testing temperature range up to 200° C. The second VFT fitting process is only up to 120° C. The rationale for the reduced VFT temperature fitting window is that it is believed that the α relaxation process may influence the β relaxation at higher temperatures, thus compromising the quality of the VFT fit.

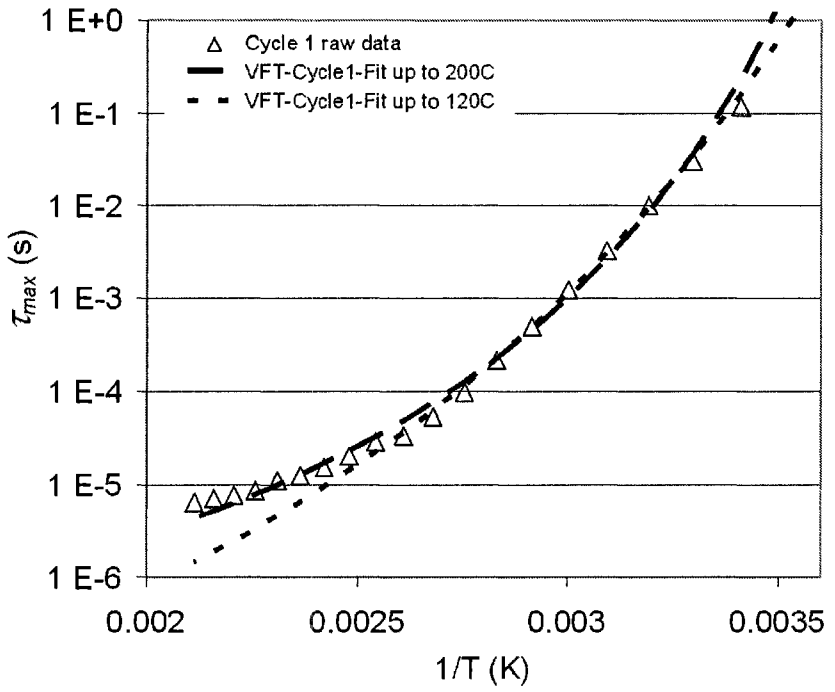

Figure 0-15. VFT plot of $\log_{10} \tau_{max}$ for the β relaxation vs. $1/T$ for the 1st cycle of a VO30-IS90 specimen.

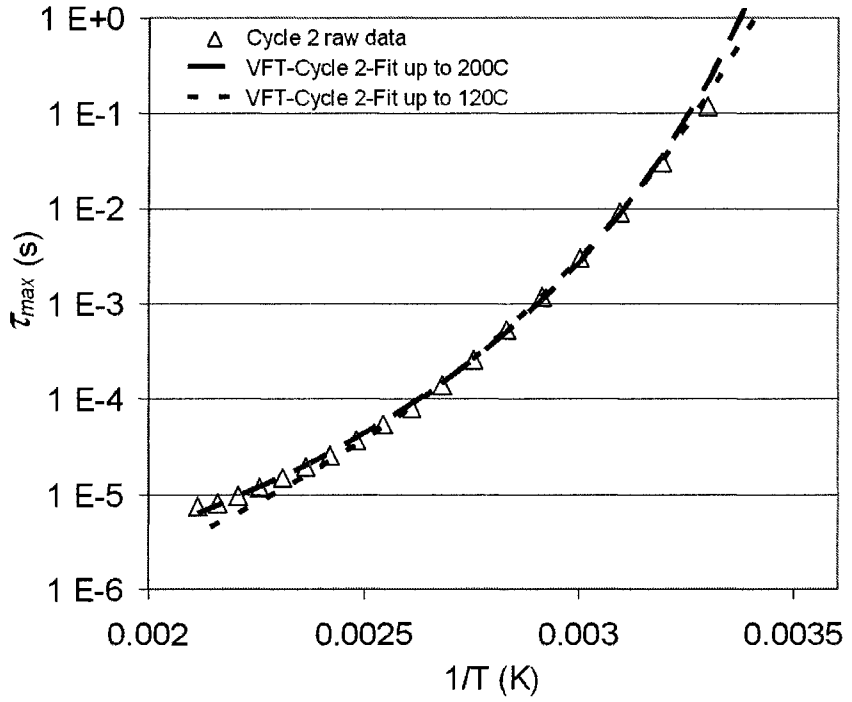

Figure 0-16. VFT plot of $\log_{10} \tau_{max}$ for the β relaxation vs. $1/T$ for the 2nd cycle of a VO30-IS90 sample.

Mean square deviations (MSD) for each of these fits are shown in Table 0-4. MSD is a measure of how accurately the VFT curve fits the experimental points. MSD is calculated in the y-direction at each data point by subtracting the fit function from the actual data and squaring the difference. These squared values are then averaged together to give MSD. The lower the MSD, the better is the fit. As indicated in Table 0-4, reducing the temperature window of VFT fitting improves the overall fit for both cycles 1 and 2, i.e. the MSD values are lower when fitting to a maximum temperature of only 120 °C. This improvement may occur because at high temperatures the α relaxation overlaps the β relaxation since the τ_{max} for the former is around 100-110 °C. It is possible that if the α relaxation did not overlap the β relaxation the data points would follow the single VFT curve that was fit over the reduced temperature window as illustrated in Figure 0-15 and Figure 0-16. The VFT curve fitted over the shorter *T* range falls beneath the data points at higher temperatures. Its important to note that this is the opposite of what typically occurs for a single relaxation, which is τ_{max} usually shifts to lower values.

Table 0-4. MSD values of the VFT equation fit log τ_{max} vs. 1/T data for cycle 1 and cycle 2 of VO30-IS90 specimen fit with VFT function under two scenarios: 1.) over the entire BDS testing temperature range (i.e,. up to 200° C) and 2.) only up to 120° C.

	Scenario 1: up to 200° C	Scenario 2: up to 120° C
Cycle 1	0.0932	0.0551
Cycle 2	0.0312	0.0149

As previously mentioned, the cycle 1 VFT fit over the entire temperature range (up to 200° C) was the poorest. However, fit quality improves with cycle 2 indicated by the lower MSD value. Thus, additional cycling suggests that the additional heating at temperatures higher than that of the α relaxation improves the repeatability and

subsequent VFT quality. It is believed that the mobility gained at temperatures higher than the α relaxation impacts the β relaxation resulting in a shift in the β relaxation to higher τ_{max}. The result of this is the data fits the VFT curve better suggesting that the data for cycle 2 is an improvement over that of cycle 1. We intend to investigate if additional heating cycles (i.e. cycle 3 or cycle 4) should be conducted to see if eventually the system reaches equilibrium, or if the same effect can be studied by annealing the sample *in situ* for various times and temperatures.

As discussed, for most polymer systems variability is reduced in the VFT fitting procedure by setting τ_0 equal to 10^{-14} s which allows for the other variables, E_a and T_V, to be optimized more easily. However, locking $\tau_0 = 10^{-14}$ s does not work for any H^+ Nafion® samples as it gives very poor fits. The VFT parameters in Table 0-5 and Table 0-6 were all generated with all three VFT parameters free to adjust, including τ_0. Averaging all τ_0 values in Table 0-5, which were generated with τ_0 free to adjust, yields $\tau_{0,ave} = 2 \times 10^{-7}$ s, which is seven orders of magnitude higher than that which is typically expected for a glass relaxation. $\tau_{0,ave} = 3 \times 10^{-8}$ s for VFT fits established over the reduced temperature range (i.e. a maximum temperature of 120° C) also with τ_0 free to adjust, as listed in Table 0-6. This is one order of magnitude lower than the value obtained fitting with a maximum temperature of 200° C, but it is still much higher than 10^{-14}. To better understand the result of VFT equation fitting to data for a fixed τ_0 value, the raw BDS data was refit by locking to $\tau_0 = 2 \times 10^{-7}$s for VFT fits over the entire testing temperature range up to 200° C. The same was done for VFT fits over the reduced temperature range by setting $\tau_0 = 3 \times 10^{-8}$ s.

Table 0-5. VFT fitted parameters fit over temperature range 30 to 200° C.

		τ_0 (s)		E_a (kJ/mol)		T_v (°C)		
	Vac-oven temp °C	Average	Stdev	Average	Stdev	Average	Stdev	Average MSD
cycle 1	30	1.49E-07	1.83E-07	8.9	2.7	222	22	1.02E-01
	50	1.55E-07	4.70E-08	7.6	0.3	238	4	7.89E-02
	70	2.50E-07	3.18E-07	7.7	3.3	214	11	1.12E-01
	90	5.60E-07	4.80E-07	6.6	2.2	243	9	1.11E-01
	110	5.10E-07	5.95E-07	6.4	0.8	242	4	1.11E-01
cycle 2	30	9.33E-08	8.51E-08	9.9	2.8	223	20	4.48E-02
	50	1.22E-07	9.04E-08	9.3	2.2	235	17	5.39E-02
	70	6.83E-08	6.44E-08	10.3	1.9	216	14	4.56E-02
	90	3.33E-07	2.28E-07	7.5	1.3	241	9	6.10E-02
	110	1.90E-07	1.98E-07	9.2	0.6	228	10	6.10E-02

Table 0-6. VFT fit parameters fit over temperature range 30 to 120° C.

		τ_0 (s)		E_a (kJ/mol)		T_v (°C)		
	Vac-oven temp °C	Average	Stdev	Average	Stdev	Average	Stdev	Average MSD
cycle 1	30	4.47E-09	6.81E-09	19.4	8.4	205	22	5.35E-02
	50	8.16E-09	1.11E-08	15.1	3.2	199	16	5.17E-02
	70	3.94E-09	5.69E-09	17.8	7.1	178	32	6.13E-02
	90	2.60E-08	2.14E-08	12.4	3.8	212	12	3.67E-02
	110	1.42E-07	2.40E-07	14.7	7.5	204	37	6.42E-02
cycle 2	30	7.56E-09	4.80E-09	14.9	2.9	198	17	1.75E-02
	50	4.89E-09	4.42E-09	17.8	5.3	194	24	2.84E-02
	70	2.16E-08	3.27E-08	14.8	4.5	194	24	2.26E-02
	90	2.65E-08	1.92E-08	12.6	1.4	212	7	2.76E-02
	110	2.84E-07	2.33E-07	7.0	6.4	228	18	4.47E-02

One plausible explanation for the τ_0 discrepancies is that for most glassy polymer systems the segmental relaxation is assigned as the α relaxation, as it is usually the highest temperature relaxation. However, recent data give compelling evidence to the idea that for H^+ Nafion® membranes the glass transition relaxation of the polymer matrix is not the highest temperature relaxation.[7,8] Rather, the destabilization of the ionic network is the highest temperature relaxation for H^+ Nafion®. It is possible that the

destabilization of the ionic network (i.e. the α relaxation) disrupts the lower temperature segmental relaxation (β relaxation) preventing it from approaching $\tau_0 = 10^{-14}$.

(iii) Fragility

The degree of deviation from Arrhenius behavior is quantified by the fragility index or steepness index, *m*, which measures the temperature shift on the chain dynamics, in the case of linear polymers:[24]

$$m = \left.\frac{d\log(\tau)}{d(T_g/T)}\right|_{T=T_g} \quad (6)$$

T_g is the dielectric relaxation based glass transition temperature obtained by extrapolating the VFT equation to τ_{max} = 100s, at which time the macromolecular structure is assumed to be essentially frozen in place. An easy way to compare fragility indexes of various glassy materials is by substituting the VFT equation into equation 6 leading to the expression [25]:

$$m = \frac{Ea}{2.303R}\frac{T_g}{(T_g - T_V)^2} \quad (7)$$

Calculated T_g values at τ_{max} = 100s are listed in Table 0-7 and Table 0-8 along with corresponding *m* values. In Figure 0-17 and Figure 0-18 these *m* values are plotted in bar chart format with one standard deviation error bars on either side of the average. Generally speaking, fragility values range from 35 to 61 depending on the cycle and the fitting process used. The range of fragility values probably stems from the dynamic structural nature of the ionomer changing with respect to thermal and hydration history during testing, as was previously discussed. In addition the activation of the α relaxation at higher temperatures and the fact that the β relaxation has two transitory peaks, namely

the major and minor peaks, further complicates matters. The notion that the molecular motions associated with the two peaks rearranging themselves with different hydration levels and histories misconstrues their identity, making the fitting process more difficult and possibly reducing the accuracy of the fitting process. On average fragility values are lower for cycle 2 than cycle 1, which may suggests that the β relaxation is more flexible and restricted as a result of the structural rearrangement that was previously suggested to occur with increased heating. Additionally, the average fragility increases slightly with increasing vacuum oven temperature for both cycle 1 and cycle 2. However, this is not as pronounced when τ_0 is locked to equal 2×10^{-7} s. Fragility values calculated from VFT fits up to 120° C tend to have less error (i.e. lower standard deviations) than those fragility values calculated up to 200° C. This is probably related to the α relaxation interfering with the β relaxation. Furthermore, locking $\tau_0 = 2 \times 10^{-7}$ s, as opposed to letting τ_0 be a free variable, reduces the standard deviation as well—emphasizing the importance of fitting consistency. Based on this information, for standardization purposes it is recommended that *m* values should be calculated from cycle 2 data that is fit up to 120° C with 2×10^{-8} s.

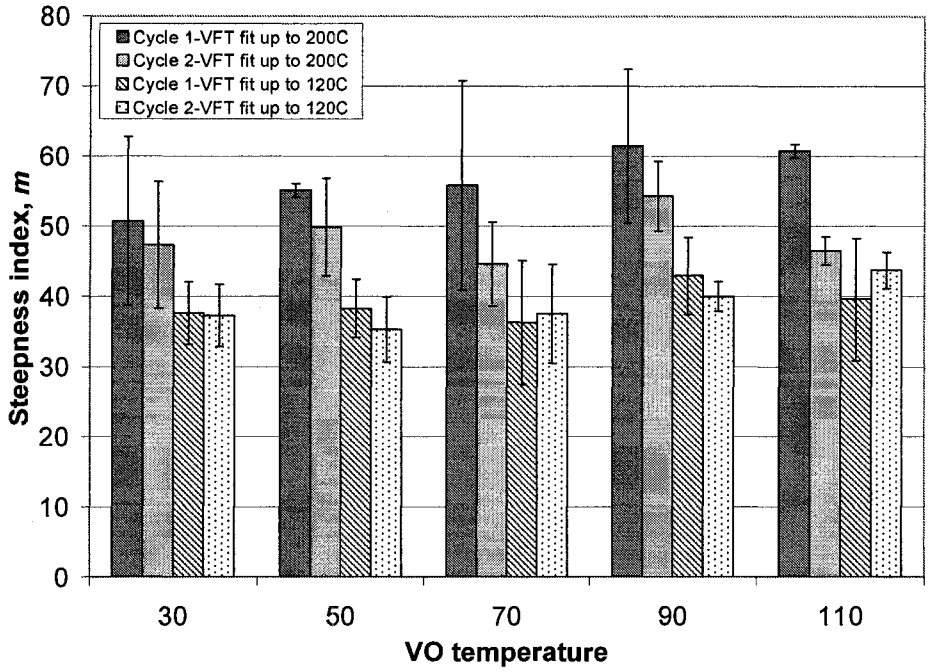

Figure 0-17. Fragility indices averaged at each vacuum oven (VO) temperature with error bars representing one standard deviation. These values are based on VFT equations fit with adjustable τ_0.

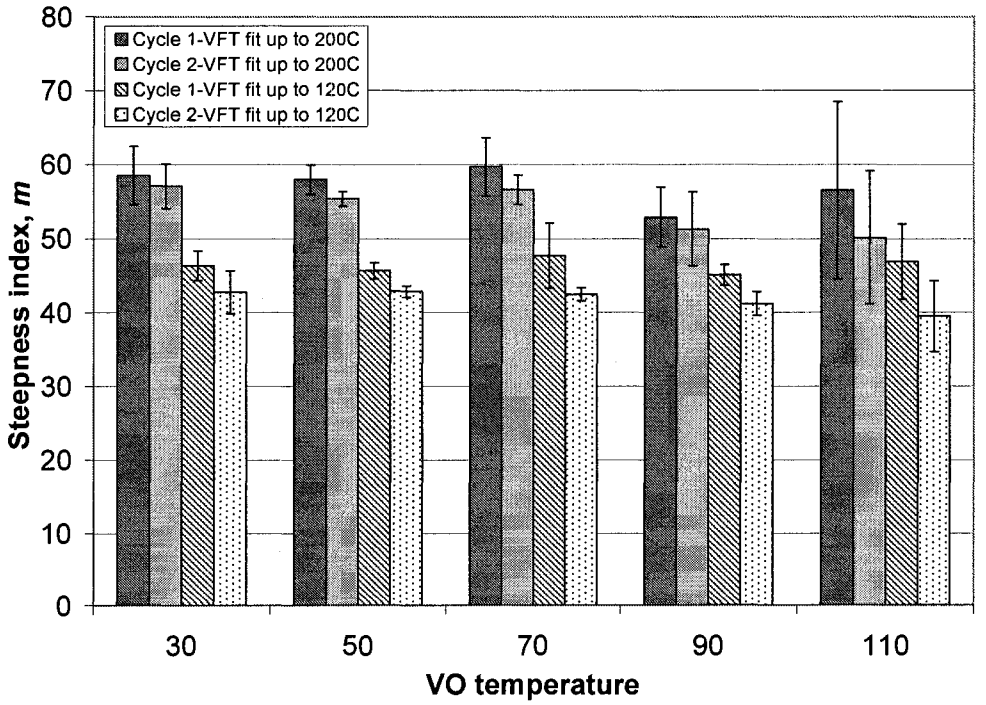

Figure 0-18. Fragility indices averaged at each vacuum oven temperature with one standard deviation error bars. Values from VFT equations fit with $\tau_0 = 2 \times 10^{-7}$s or VFT equations fit up to 200° C and $\tau_0 = 3 \times 10^{-8}$ s for VFT equations fit up to 120° C.

Table 0-7. T_g calculated at τ_{max} = 100s from VFT equation and corresponding fragility index, m. Values based on VFT equations fit with adjustable τ_0.

		VFT fit up to 200 °C				VFT fit up to 120 °C			
		T_g (K) @ τ_{max}=100s		m		T_g (K) @ τ_{max}=100s		m	
	VO	Average	Stdev	Average	Stdev	Average	Stdev	Average	Stdev
cycle 1	30	273	9	51	12	294	43	38	4
	50	283	3	55	1	275	5	38	4
	70	258	15	56	15	261	7	36	9
	90	283	2	61	11	277	3	43	6
	110	282	2	61	1	278	12	40	9
cycle 2	30	279	8	47	9	274	5	37	4
	50	288	8	50	7	280	7	35	5
	70	273	6	45	6	269	7	38	7
	90	287	3	54	5	280	2	40	2
	110	282	9	46	2	286	11	44	3

Table 0-8. T_g calculated at τ_{max} = 100s from VFT equation and corresponding fragility index, m. Values based on VFT equations fit with $\tau_0 = 2 \times 10^{-7}$s for VFT equations fit up to 200° C and $\tau_0 = 3 \times 10^{-8}$s for VFT equations fit up to 120° C.

		VFT fit up to 200° C				VFT fit up to 120° C			
		T_g (K) @ τ_{max}=100s		m		T_g (K) @ τ_{max}=100s		m	
	VO	Average	Stdev	Average	Stdev	Average	Stdev	Average	Stdev
cycle 1	30	273	9	51	12	271	7	46	2
	50	283	3	55	1	279	2	46	1
	70	258	15	56	15	268	4	48	4
	90	283	2	61	11	278	6	45	1
	110	282	2	61	1	277	1	47	5
cycle 2	30	281	5	49	6	277	5	43	3
	50	288	8	50	7	285	5	43	1
	70	273	6	45	6	273	2	42	1
	90	287	3	54	5	280	1	41	2
	110	282	9	46	2	278	6	39	5

Compared with other common polymers, the fragility values reported here for H^+ Nafion®, ranging from 35-61, are rather low. For instance poly(methylmethacrylate), polystyrene, polypropylene, and polycarbonate have fragility values of 145, 139, 137 and 132, respectively.[24,26] Many factors influence fragility: molecular weight, polymer

flexibility/rigidity, excess entropy and even T_g.[27] However, there are no hard rules for trends as many exceptions exist for each factor. For instance, for both polystyrene and poly(methyl methacrylate) fragility increases with increases in molecular weight. Yet, for poly(dimethyl siloxane), poly(propylene oxide), and polyisoprene fragility is independent of molecular weight. Generally speaking two observations are made: 1) when T_g increases with molecular weight fragility usually increases as well and 2) polymers with rigid backbones and high T_gs are typically fragile.[27] Low *m* values correspond to strong glasses where as high *m* values correspond to fragile glasses. The low fragility values reported here indicates that the H^+ Nafion® membrane is a rather strong polymeric glass. This is more common for polymers with low T_gs and flexible backbones. For instance polyisobutylene has a low fragility value of 46 and corresponding T_g of approximately -74° C. [24,26] Furthermore, pure polytetrafluorethylene, the hydrophobic phase of H^+ Nafion®, has a very flexible backbone and a similar glass transition of -73° C,[28] which support the notion that H^+ Nafion® should also have a low *m* value.

Another common way to quantify fragility is with the $F_{1/2}$ value which is a ratio of the temperature at $\tau_{max}=10^{-6}$s to the temperature at $\tau_{max}=10^{2}$ s:[29]

$$F_{1/2} = 2\frac{T_g}{T_{1/2}} - 1, \quad \tau(T_g)=10^{2}\text{ s};\ \tau(T_{1/2})=10^{-6}\text{ s} \qquad (8)$$

Nominally speaking the $F_{1/2}$ ratio is named in relation to fact that $\tau_{max}=10^{-6}$s is a realistically measurable value at approximately the half way point between the assumed low temperature frozen in value at $\tau_{max}=10^{2}$s and the theoretically limiting high temperature microscopic phonon value at $\tau_{max}=10^{-14}$s.

For all of the different testing scenarios utilized here the $F_{1/2}$ fragility values range from approximately -0.01 to -0.7. Based on the definition of the $F_{1/2}$ fragility equation $F_{1/2}$ values should range from 0 for strong materials to unity for fragile systems. SiO_2 is one of the least fragile vitreous materials having an $F_{1/2}$ value of 0.13. Therefore, either the H^+ Nafion® membranes are less fragile than SiO_2 or the H^+ Nafion® membrane fundamentally breaks the assumptions required for the $F_{1/2}$ fragility analysis. The curvature of the τ_{max} values graphed against 1/T in Figure 0-15 and Figure 0-16 is compelling evidence to disprove the former point. Therefore, the later notion, that H^+ Nafion® fundamentally breaks several $F_{1/2}$ analysis assumptions, is believed to be the reason for the flawed $F_{1/2}$ values of the H^+ Nafion® membranes. A basic assumption of the $F_{1/2}$ test is that the E_a and T_V parameters for the VFT fits are generated by locking τ_0 $=10^{-14}$. However, as pointed out in a previous section for the β relaxation of H^+ Nafion® typically τ_0 ranges from 10^{-7} to 10^{-8}. Consequently, the $T_{1/2}$ values calculated for the H^+ Nafion® membranes are much higher than typical which, when used for calculating $F_{1/2}$ values, generate negative values. This later point may further support the notion that the α relaxation is interfering with the β relaxation at higher temperatures and may be construing the fragility values.

F. Influence of acid wash on α and β relaxations.

For all of the preceding sections all of the H^+ Nafion® membranes were preboiled in HNO_3. However, as will be detailed in this section the type of acid the H^+ Nafion® membranes are boiled in during preconditioning also affects both the α relaxation and β relaxation of the dielectric spectra. Figure 0-19 through Figure 0-21 are plots of log ε''

vs. log f for two series of H^+ Nafion® samples preconditioned exactly the same way—the only difference between the two is that one set was boiled in HCl and the other was boiled in HNO_3. In contrast to the HNO_3 samples, those samples boiled in HCl prior to testing have higher frequency β relaxations and lower frequency α relaxations. For instance, at 120 °C, as illustrated in Figure 0-20, for the HCl preconditioned membranes the difference between the average τ_{max} of the α relaxation and that of the β relaxation is 0.75, see Table 0-9 and Table 0-10. However, for the HNO_3 membranes the difference is only 0.018—an order of magnitude lower. Thus for the HCl preconditioned samples this renders the two relaxations much more distinct than those of the HNO_3 samples. Particularly, for the for the HNO_3 samples, as indicated in Figure 0-19, the high frequency wing of the α relaxation and the low frequency wing of the β relaxation are superimposed on each other.

Table 0-9. Average τ_{max} values at various temperatures for H^+ Nafion specimens preconditioned with boiling HNO_3 or HCl.

	α-relaxation		β-relaxation	
°C	HNO_3	HCl	HNO_3	HCl
90	1.37E-01	n/a	4.75E-04	3.00E-05
120	1.77E-02	7.48E-01	8.83E-05	3.11E-05
170	6.10E-03	3.99E-02	2.32E-05	7.48E-06

Table 0-10. The average difference between the average τ_{max} values of the α-relaxation and β-relaxation for those specimens boiled in HNO_3 and HCl.

°C	HNO_3	HCl
90	1.36E-01	n/a
120	1.76E-02	7.48E-01
170	6.07E-03	3.99E-02

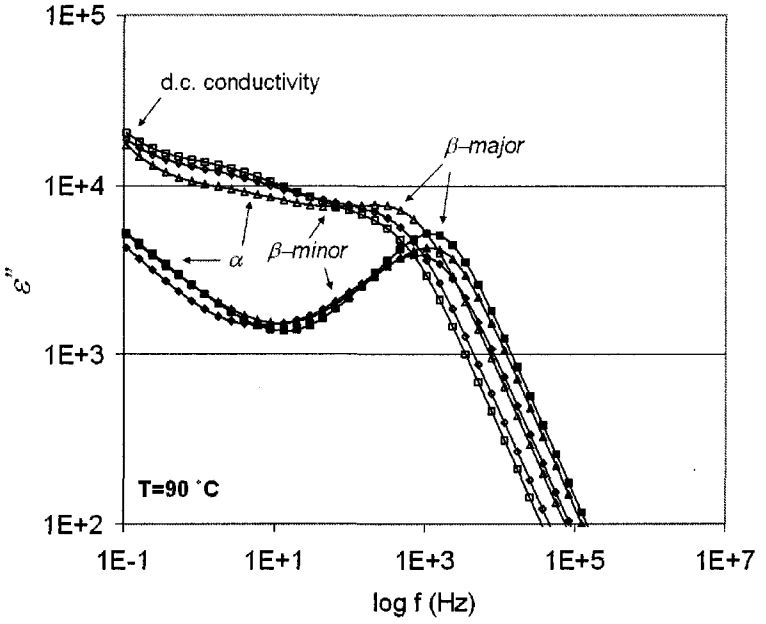

Figure 0-19. BDS spectra of log ε'' vs. log f at 90 °C for H^+ Nafion boiled in a) HCl (solid symbols) b) HNO_3 (open symbols).

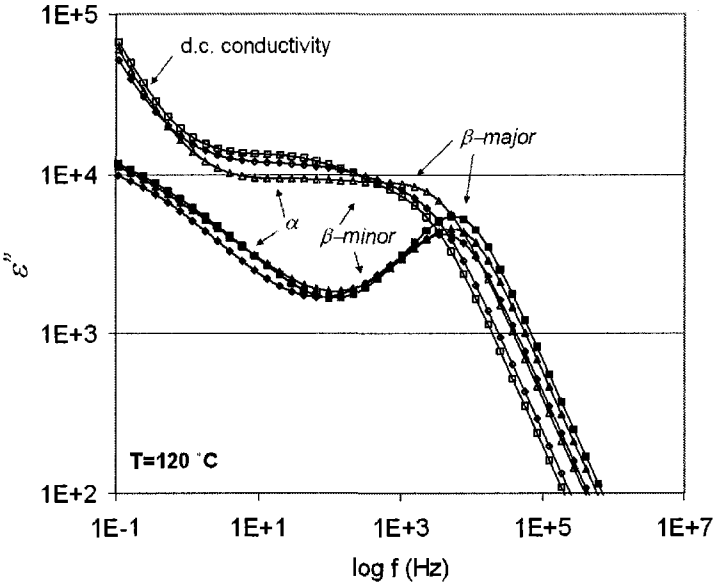

Figure 0-20. BDS spectra of log ε'' vs. log f at 120 °C for H^+ Nafion boiled in a) HCl (solid symbols) b) HNO_3 (open symbols).

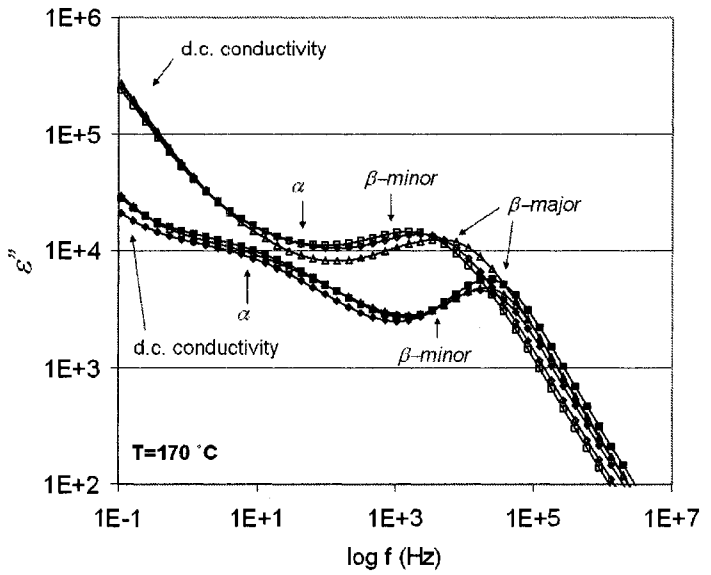

Figure 0-21. BDS spectra of log ε" vs. log f at 170 °C for H^+ Nafion boiled in a) HCl (solid symbols) b) HNO_3 (open symbols).

As indicated in Figure 0-19 d.c. conductivity begins at 90 °C for the HNO_3 samples. However, for the HCl samples d.c. conductivity does not begin until approximately 30 or 40°C higher as indicated in Figure 0-20. Stemming from charge carriers d.c. conductivity characteristically arises at low frequencies as the mobile ions are capable of moving from one electrode to the other electrode in one half electric pulse cycle. The movement of these ions is facilitated by the destabilization of the ionic network, i.e. the α relaxation. Resultantly, since the HNO_3 has a lower α relaxation, i.e. destabilization of the ion network, the α relaxation begins at a lower temperature for the HNO_3 samples than that for the HCl samples. Interestingly though, the fitted d.c. conductivity values from the log ε" vs. log f plots are approximately 0.7 for both acids treatments. The conductivity value is an indication of the ease of passage the charge travels. For instance, $\sigma = 1$ is indicative of an unobstructed pathway, or 'ideal' conductor.

As σ values decrease, conductivity pathways become more tortuous. $\sigma \approx 0.7$ suggests haphazard charge conducting pathways with randomly connected interconnections and charge traps.[30] The similar values for the different pretreatment samples may indicate that the charge travels through similar morphological structures in the different preconditioned membranes, with the onset differences occurring at dissimilar temperatures.

It is believed that the temperature at which the acid boils is of importance here. Nitric acid boils at ~83 °C whereas hydrochloric acid boils at ~116 °C. If the α relaxation for dynamic rearrangement is at approximately 110 °C, as previously discussed, then the temperatures at which nitric acid boils is approximately 25 °C below the α relaxation. However, the temperature at which HCl boils is approximately at or slightly above the peak of the α relaxation. This means that the HCl boil yields sufficient thermal energy to permit the ionic side chains to dynamically rearrange in the hydrated state—expansion from hydration occurs with ion hopping. However, for the HNO_3 boil the ionic side chains are more restricted—expansion from hydration occurs without the full extent of ion hopping gained by the α relaxation. In other words, for membranes swollen with HNO_3 hydration occurs with more restrictions and, furthermore, stresses resulting from hydration are difficult to relieve because there is not sufficient energy to allow the chains to rearrange. A counter argument to this notion is that residual acid remains in the H^+ Nafion® membrane during the BDS testing which possibly could induce shifting of the relaxations by offsetting the acidity of the membrane. This later point is a possibility, but, it is unlikely to occur as the membranes were rinsed and subsequently boiled in an abundance of de-ionized water after the acid boiling. However, if it is in fact true then

the data further indicate how small changes in pKa resulting from preconditioning drastically influence the α relaxation and proton movement.

Conclusions

Processing conditions used to prepare H^+ Nafion® films for testing under very dry conditions have a direct impact on the β and α relaxations and degree of E-form or S-form substance. In this study, drying temperatures, hydration history and chemical nature of the acid pretreatment were investigated. Understanding the influence of drying temperature is very important for production of H^+ Nafion® membranes with consistent repeatable properties. To achieve consistent property performance in the dry state, membranes must be dried at temperatures greater than the high temperature wing of the α relaxation. Failure to do this leaves the structures in an entropically frustrated state that is susceptible to rearrangement if the temperature is raised to any temperature higher than the onset of the α relaxation. This rearrangement is believed to occur to accommodate the loss of water that transpired during dehydration. If membranes are dehydrated below the α relaxation they will not be in their most favorable conformations and packing of sidechains. Rather they will be in a frustrated state until the temperature is raised to the α relaxation where the ionic network destabilizes allowing the side chains to rearrange to a minimum free energy state. Any characteristics determined via testing of samples dried below the α relaxation will show increased variability and poor reproducibility. Therefore, it is recommended that when working with H^+ Nafion® in the very dry state the specimens be dried at temperatures higher than the high temperature wing of the α relaxation, or at a minimum, increase the temperature after drying to the α relaxation

region to allow the frustrated structures to relax to optimal packing. Furthermore, if the thermal and hydration condition is conducted *ex situ* caution must be exercised to prevent the addition of atmospheric water which will, at minimum, distort if not erase any results of prior conditioning history.

Samples dried at temperatures less than that for the onset of the α relaxation show a two stage increase in ε' and ε'' with increasing temperatures. The first stage is identified as the β relaxation. It is theorized that the second stage increase is evidence for structural rearrangement from the E-form to the S-form as originally characterized by Yeo and Yeager.[2] It is reasonable that for drying at temperatures between the β relaxation and the α relaxation a gradient of structures will exist. For example, drying at temperatures closer the α relaxation produces membranes with greater S-form structures, whereas, drying at temperatures closer to the β relaxation produces membranes with greater E-form structures. The molecular mobility gained from increasing the temperature through the β relaxation is not enough to allow the rearrangement to occur as H^+ Nafion® is morphologically stable at temperatures in the vicinity of the β relaxation.[31] This is indicated by the distinct β relaxation observed at lower temperatures for the first heating cycle of the IS70 samples, and to a lesser extent, the IS90 samples. This onset of rearrangement begins at the start of the low-temperature wing of the α relaxation. In the low temperature wing of the α relaxation the system begins to transition from a static network where the ionic chains are locked in at specific locations to a dynamic network where the ionic side chains are free to molecularly rearrange. In contrast, drying at temperatures well above the α relaxation produces structures that are completely converted to the S-form, or US-form. Upon cooling the structures obtained at the highest

temperature will be maintained with subsequent heating as long as no additional water is absorbed.

Although the full nature of the minor β peak is unknown it is known that it is identified with the interfacial region between the ionic and non-ionic regions. The notion that the β minor peak increases with heating may further be suggesting that the clusters are shrinking in size. This decreased size would increase the surface area to volume ration of the clusters resulting in an increased interfacial region with corresponding relaxation.

The dynamic nature of the H^+ Nafion® membrane network at higher temperatures and the possibility that one set of data can be fit with several different VFT curve sets makes quantifying the β relaxation's degree of non-Arrhenius behavior difficult. However, steps can be taken to reduce the fitting error by 1) ramping the temperature above the high temperature wing of the α relaxation prior to testing, 2) locking τ_0 at 10^{-8} s, 3) fitting to a maximum temperature of 120° C or lower. In addition, concerning the two peaks which comprise the β relaxation, little information is available on their nature and how they differ in mechanism. Once these peaks are better understood it is believed that VFT fitting accuracy will greatly improve. The fact that the β relaxation is capable of being fit with the VFT equation gives further support to the identification of the β relaxation as the polymer glass transition and the α relaxation as the destabilization of the hydrogen bonded network.

Some of the typical assumptions associated with the VFT equation in polymer systems prove irrelevant for H^+ Nafion® relaxation behavior. The notion that τ_0 ranges from 10^{-7} to 10^{-8} for H^+ Nafion® is rather peculiar as it is expected to be very different at

10^{-14} s, which is typical polymers. This may be related to the α relaxation interfering with the β relaxation as temperature is increased and the two overlap. It is quite possible that destabilization of the ionic network (i.e., the α relaxation) disrupts the lower temperature segmental relaxation (β) preventing it from approaching $\tau_0 = 10^{-14}$ s.

The fragility values reported here for H^+ Nafion®, ranging from 35-61, are rather low for polymers indicating that H^+ Nafion® is a rather strong glass which is probably related to the restricted flexibility of the polytetrafluorethylene backbone and the low glass transition. The range of fragility values probably stems from the dynamic structural nature of the ionomer changing with respect to thermal and hydration history during testing.

It is important to remember that these tests were conducted on H^+ Nafion® in the very dry state and the relaxations, especially the β relaxation, are influenced by incorporated water.[9] It is not known if the differences in the α and β relaxations for the two acid preconditioning treatments persist in the hydrated state as observed here in the dry state. However, if it does persist, then it is possible that some discrepancies and performance differences of H^+ Nafion® reported in the literature[1,6] may stem from the acid boiling precondition step as discussed here. For instance, it's well known that H^+ Nafion® suffers from localized dehydration in fuel cell operation. It may be possible that the d.c. conductivity differences observed here, which stem from the different acid pretreatments, may affect the H^+ Nafion® fuel cell performance by facilitating this dehydration. Furthermore it may be possible to mitigate inconsistent conductivity measurements during the preconditioning by proper acid selection.

The notion that different acid treatments generate different structures is highly probable. It would be ideal to be able to identify the morphology that corresponds to each acid treatment; however without the addition of scattering data any conclusions drawn here would be speculation. Lastly, it must be remembered that the present data does not provide direct information on the actual morphological structures of ionic domains as that extracted from small angle scattering data.

References

(1) Borup, R.; Meyers, J.; Pivovar, B.; Kim, Y. S. *Chemical Reviews* **2007**.

(2) Yeo, R. S.; Yeager, H. L. In *Modern Aspects of Electrochemsitry, No.16*; Conway, B. E.; Bockris, R. E., Eds.; Plenum Press: New York, 1985; pp 437-504.

(3) Hinatsu, J. T.; Mizuhata, M.; Takenaka, H. *Journal of the Electrochemical Society* **1994**, *141*, 1493-1498.

(4) Kim, M.-H.; Glinka, C. J.; Grot, S. A.; Grot, W. G. *Macromolecules* **2006**, *39*, 4775-4787.

(5) Rollet, A.-L.; Gebel, G.; Simonin, J.-P.; Turq, P. *Journal of Polymer Science: Part B: Polymer Physics* **2001**, *39*, 548-558.

(6) Majsztrik, P. W.; Satterfield, M. B.; Bocarsly, A. B.; Benziger, J. B. *Journal of Membrane Science* **2007**, *301*, 93-106.

(7) Osborn, S. J.; Hassan, M. K.; Divoux, G. M.; Rhoades, D. W.; Mauritz, K. A.; Moore, R. B. *Macromolecules* **2007**, *40*, 3886-3890.

(8) Page, K. A.; Cable, K. M.; Moore, R. B. *Macromolecules* **2005**, *38*, 6472-6484.

(9) Yeo, S. C.; Eisenberg, A. *Journal of Applied Polymer Science* **1977**, *21*, 875-898.

(10) Kremer, F.; Schonhals, A. *Broadband Dielectric Spectroscopy*; Springer: Heidelberg, Germany, 2003.

(11) Havriliak, S.; Negami, S. *Journal of Polymer Science, Polymer Symposia* **1966**, *14*, 99-103.

(12) Havriliak, S.; Negami, S. *Polymer* **1967**, *8*, 161-205, appendix 206-110.

(13) Diaz-Calleja, R. *Macromolecules* **2000**, *33*, 8924.

(14) Tsonos, C.; Apekis, L.; Pissis, P. *Journal of Material Science* **2000**, *35*, 5957-5965.

(15) Su, S.; Mauritz, K. A. *Macromolecules* **1994**, *27*, 2079-2086.

(16) Tsonos, C.; Apekis, L.; Pissis, P. *Journal of Material Science* **1998**, *33*, 2221-2226.

(17) Nosaka, A. Y.; Watanabe, S.; Toyoda, I.; Nosaka, Y. *Macromolecules* **2006**, *39*, 4425-4427.

(18) McCrum, N. G.; Read, B. E.; Williams, G. *Anelastic and Dielectric Effects in Polymeric Solids*; Dover Publications, Inc.: New York, 1967.

(19) Schonhals, A.; Kremer, F. *Broadband Dielectric Spectroscopy*, 1 ed.; Springer, 2003.

(20) Vogel, H. *Physik. Z.* **1921**, *22*, 645-646.

(21) Fulcher, G. S. *Journal of the American Ceramic Society* **1925**, *8*, 339-355.

(22) Tamman, G.; Hesse, W. *Zeitschrift fuer Anorganische und Allgemeine Chemie* **1926**, *156*, 245-257.

(23) Angell, C. A. *Polymer Papers* **1997**, *38*, 6261-6266.

(24) Bohmer, R.; Ngai, K. L.; Angell, C. A. *Journal of Chemical Physics* **1993**, *99*, 4201-4209.

(25) Vilgis, T. A. *Physical Review B* **1993**, *47*, 2882-2885.

(26) Huang, D.; McKenna, G. B. *Journal of Chemical Physics* **2001**, *114*, 5621-5630.

(27) Sokolov, A. P.; Novikov, V. N.; Ding, Y. *Journal of Physics: Condensed Matter* **2007**, *19*, 205116-205124.

(28) Lau, S.-F.; Wesson, J. P.; Wunderlich, B. *Macromolecules* **1984**, *17*, 1102-1104.

(29) Richert, R.; Angell, C. A. *Journal of Chemical Physics* **1998**, *108*, 9016-9026.

(30) Mauritz, K. A. *Macromolecules* **1989**, *22*, 4483-4488.

(31) Page, K. A.; Landis, F. A.; Phillips, A. K.; Moore, R. B. *Macromolecules* **2006**, *39*, 3939-3946.

CHAPTER V

CHEMICAL DEGRADATION OF NAFION® MEMBRANES

Abstract

1100 EW acid form Nafion® was degraded with Fenton's reagent solution and analyzed with broadband dielectric relaxation spectroscopy (BDS), SEM and ATR-FTIR. All three analysis methods indicate that substance non-uniform degradation begins to occur only after 45h of exposure to Fenton's reagent solution. However, the F-ion release rate is constant with respect to exposure to Fenton's reagent solution. BDS results indicate regional increases in fragility the segmental relaxation. FTIR results further support the notion that the degradation process is not uniform across the film. Specifically, spectroscopic differences are observed for the sulfonate functional groups and the water surrounding these groups. SEM images indicate that bubbles are widespread on the interior and surface of the membranes only at 60 and 75h of degradation.

Introduction

Nafion® perfluorosulfonic acid proton exchange membranes (PEM) are currently the benchmark against which other membranes are compared for use in automotive fuel cells. Historically, this membrane was developed for fuel cell utilization because of its good chemical resistance and high proton conductivity. However, the Nafion® still does not exhibit sufficient chemical stability for this use.

Reviews have summarized the state of understanding of PEM degradation, which can be physical and chemical, the two being coupled. [1-3] Membrane creep and microcrack formation, in combination with degraded structure and morphology all play a

part in PEM physical deterioration. Elevated temperature, reduced humidity and RH, temperature and voltage cycling in a cell contribute to degradation.[3] Peroxide radical attack on –COOH end groups in Nafion® is believed to be the primary route of chemical degradation.[2] LaConti et al. proposed the *in situ* production of peroxide via reduction of oxygen molecules at the Pt anode.[4] H_2O_2 molecules subsequently react with impurities found in fuel cells, such as Fe^{2+} and Cu^{2+}, generating highly reactive hydroxyl (•OH) and hydroperoxy (•OOH) radicals. Several studies suggested that peroxide is much less reactive in the absence of the metal ions. However, in the presence of the metals, which are found in small quantities in the PEM, peroxide radicals are created easier. These free radicals subsequently attack the –COOH polymer end groups and unzip the chain with –COOH regeneration according to the following reactions:[5]

$$R_f\text{-}CF_2COOH + \bullet OH \rightarrow R_f\text{-}CF_2\bullet + CO_2 + H_2O$$

$$R_f\text{-}CF_2\bullet + \bullet OH \rightarrow R_f\text{-}CF_2OH$$

$$R_f\text{-}CF_2OH \rightarrow R_f\text{-}COF + HF$$

$$R_f\text{-}COF + H_2O \rightarrow R_f\text{-}COOH + HF$$

This mechanism was advanced based on degradation studies on model compounds with –COOH end groups that were found to degrade at least one order of magnitude faster than similar compounds with no –COOH end groups.[6] Previous studies demonstrated that H-end group formation in perflourinated membranes could be minimized by treating the PEM with elemental fluorine, thus removing the reactive end groups.[5] In addition Du Pont (proprietary) studies have further indicated that special treatment of the H-end groups reduces degradation and improves PEM performance.

Despite the belief that peroxide radical attach on –COOH end groups is is the primary route of degradation - even if all –COOH end groups are eliminated - fluoride release during operation persists. This later point suggests that radical attack also occurs at different locations on the chemical structure.[2] Several alternative modes of degradation have been suggested. Schlick et al. UV irradiated model compounds of the sulfonic acid ether sidechain in the presence of Cu(II) and Fe(III). They found that independent of peroxide concentration Fe(III) facilitated sulfonic acid decomposition generating a $\bullet CF_2$ radical species. The Cu(II) on the other hand was believed to attack tertiary C-F bonds that are present where the side chain attaches to the main chain.

Studies of membranes degraded from actual fuel cell usage are preferred. However, the PEM degradation process during FC operation occurs slowly—over thousands of hours rather than seconds and minutes. Fenton's reagent is commonly used *ex situ* to accelerate the degradation process.[3] The primary step of this reaction is the oxidation of iron (II) to iron (III) by the peroxide. The peroxide radical subsequently decomposes into a hydroxyl ion and radical:

$$Fe^{2+} + H_2O_2 \rightarrow Fe^{3+} + \bullet OH + OH^-$$

$$H_2O_2 + HO\bullet \rightarrow H_2O + \bullet OOH$$

Although quantifiable data is lacking for the direct correlation of this *ex situ* test to FC- *in situ* life tests, the Fenton's reagent method is widely used. Part of its acceptance is due to the inherent presence of metal cations in the PEMs during fuel cell operation which Fenton's reagent mimics. Furthermore, it is accepted that F^- release rate is strongly correlated to degradation. Thus, upon placing a PEM in a Fenton's reagent solution the F^- release rate can be used to monitor degradation rate.

Here we present a study of monitoring the PEM degradation process using broadband dielectric spectroscopy (BDS). BDS is powerful in being capable of interrogating molecular motions in samples over very wide ranges of time and distance scales. In an electric field, dielectric materials dissipate energy by orienting their dipoles to align approximately with the electric field. As we previously reported, the chemical degradation process creates shorter macromolecular chains, which affects the time scale of dipole relaxation. In a previous publication we reported on chemically degraded Nafion® as analyzed with BDS.[7] We described how such degradation, affected by Fenton's reagent, shifts the β relaxation (glass transition) to higher temperatures and postulated that this could be due to low molecular weight fragments being leached out into the electrolyte, leaving a molecular weight distribution that is then skewed toward longer chains. While the results reported in that former publication are valid and accurate, here we detail an improved sample preparation with analysis method and conclusions. Specifically, we demonstrate that the degradation process non-uniformly degrades the polymer matrix causing regional differences not only in the fragility of the polymer matrix but also in the sulfonate-water network.

Experimental

Materials

Nafion® chemical structure is comprised of a tetrafluoroethylene backbone with perfluorovinyl ether side chains terminated with sulfonic acid groups.

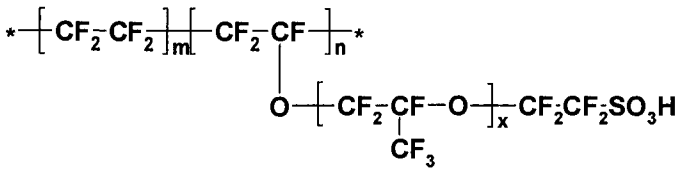

1100 equivalent weight (EW) H^+ form Nafion®, 2 mils thick, was obtained from E.I DuPont Co. This material was melt-extruded in sheets.

Membrane Preparation.

As illustrated in Figure 0-1, acid form membranes were degraded by submerging a 2.5 x 20 cm piece in 50mL of 30% H_2O_2. 0.005g of Fe^{2+} was used for every 1g of dry Nafion®. This Fenton's reagent solution was refreshed every 15h.

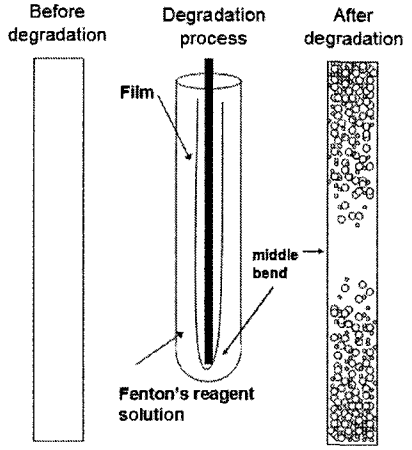

Figure 0-1. Schematic of Nafion® membrane submerged in a test tube containing Fenton's reagent solution. After degradation, the concentration of bubble formation is higher at the top of the membrane than at the middle where the film is bent.

Control membranes were cut into circles with diameters of 2.2 cm and boiled in 2M hydrochloric acid for 2h. The HCl wash is necessary to remove iron that may have complexed with the sulfonic acid side chains during the degradation process. After the acid washing, the membranes were rinsed in DI water and subsequently refluxed in DI water for 1h. Membrane specimens were removed from the DI water, placed 2 cm apart

on a Teflon sheet, and placed in a vacuum at 90° C for 12h. Upon removal of the specimens from the vacuum oven they were immediately placed in a dry glove box (< 0.2%RH) for a minimum of seven days.

We earlier determined that large variations in T_g occurred due to water absorption while loading the sample in the BDS.[7] To reduce this undesired variability, sample thickness was measured in the glove box and then the sample was sandwiched between the electrodes in the glove box. Pressure was maintained on the electrodes to reduce surface area exposure to atmospheric moisture. After the sandwiched sample was removed from the glove box its total time of exposure to environmental atmosphere was less than 2min and typically less than 1min.

Instrumentation

Scanning electron microscopy (SEM).

SEM images were gathered using an FEI Quanta 200 Environmental Scanning Electron Microscope under high vacuum. For all images the electron beam was 10.0 kV and the spot size was 7.2 nm.

FTIR/ATR Spectroscopy.

FTIR-ATR spectroscopic analyses were conducted using a Bruker Equinox 55. The films were allowed to equilibrate at room temperature and 35% relative humidity for two days; prior to that they were kept under dry nitrogen gas for at minimum two weeks. The films were clamped on top of a germanium crystal, and spectra were collected in 9-bounce reflectance mode. All of the spectra that were acquired are the result of at least 32 scans with the background subtracted from the spectra to enhance peaks.

Broadband dielectric spectroscopy (BDS).

A Novocontrol GmbH Concept 40 broadband dielectric spectrometer was used over the frequency range 0.1Hz - 3MHz. Before loading samples in the spectrometer, they were tightly pressed between two 20mm aluminum sheets that were sandwiched between two 20mm diameter brass electrodes. Once each specimen was loaded each was *in situ* dried at 90° C for 250 frequency sweep iterations. The purpose of the *in situ* drying step is to remove any water absorption that may have occurred during the sample loading step. After this step, the temperature was reduced to -130° C and frequency sweeps were performed at consecutive 10° C increments up to 200° C. To enhance sample reproducibility two consecutive temperature cycles were used and referred to as cycle 1 and cycle 2. Typically, only the results of cycle 2 are discussed. The temperature (T) was controlled to within +/- 0.2 °C.

The complex dielectric permittivity, ε^*, is given by the following equation in which ω, the angular frequency, is $2\pi f$ and $i = \sqrt{1}$.

$$\varepsilon^*(\omega) = \varepsilon'(\omega) - i\varepsilon''(\omega) \qquad (1)$$

ε' reflects material polarizability, usually due to orientation of dipoles attached to polymers, but can also reflect interfacial polarization. ε'' is proportional to the energy dissipated per cycle during these dipole orientations that are coupled to chain motions.[8]

The Havriliak-Negami (HN) equation, often used to represent dielectric relaxation spectra, is shown below with an additional term to account for possible d.c. conductivity at low frequencies. [9,10]

$$\varepsilon^*(\omega) = \varepsilon' - i\varepsilon'' = -i\left(\frac{\sigma_0}{\varepsilon_0 \omega}\right)^N + \sum_{k=1}^{n}\left[\frac{\Delta\varepsilon}{\left(1+(i\omega\tau_{HN})^{\alpha}\right)^{\beta}}\right] \qquad (2)$$

Each term in the sum represents a different relaxation process such as glass and sub-glass transitions in polymers. The values of the parameters result from a fit of equation 2 to experimental data. $\Delta\varepsilon = \varepsilon_o - \varepsilon_\infty$ is the difference between the low- and high frequency limits of ε' for the given process. τ_{HN} is a time that is related to the actual relaxation time, τ_{max}, which is associated with the frequency at the respective peak maximum, f_{max}. α and β are measures of the breadth and symmetry, respectively, of the given relaxation such that $\alpha < 0 \leq 1$ and $0 < \beta \leq 1$. Data-fitted α, β and τ_{HN} parameters are then used to determine τ_{max} using the following equation.[11]

$$\tau_{\max} = \tau_{HN}\left[\frac{\sin\left(\frac{\pi\alpha\beta}{2(\beta+1)}\right)}{\sin\left(\frac{\pi\alpha}{2(\beta+1)}\right)}\right]^{\frac{1}{\alpha}} \qquad (3)$$

When present, d.c. conductivity can obscure weak polymer relaxations that occur at low frequencies. This obscuration is removed as follows: Once the exponent $N \leq 1$ and the d.c. conductivity σ_0 are determined by curve fitting in the low f regime, this term is subtracted point-by-point from ε'' curves to reveal relaxation peaks.

Isothermal dielectric permittivity data were fitted to the Havriliak-Negami equation with a d.c. loss contribution to obtain τ_{HN}, the *H-N* relaxation time.[10] The d.c. loss contribution arose at temperatures higher than T_g and typically was subtracted to better visualize actual relaxation peaks. Figure 0-2 is a typical BDS spectrum of $\log_{10}\varepsilon''$ vs. $\log f$ plot of a 75h degraded film. An in depth analysis of the fitting process is provided in previous publication of ours.[12]

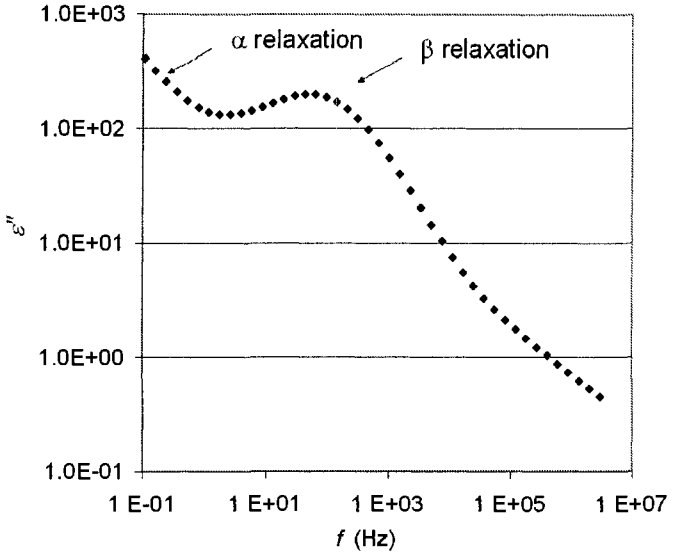

Figure 0-2. A typically relaxation plot of $\log_{10}\varepsilon''$ vs. $\log f$ for H+ Nafion that was chemically degraded for 75h.

For the relaxation associated with the glass transition $\log \tau_{max}$ vs. $1/T$ is characteristically nonlinear (non-Arrhenius-like) and obey the empirical Vogel-Fulcher-Tamman (VFT) equation for glass-forming materials: [13-16]

$$\tau(T) = \tau_0 \exp\left(\frac{E_a}{k_B(T - T_V)}\right) \qquad (4)$$

τ_0 is a hypothetical relaxation time at infinite temperature, k_B is the Boltzmann constant. E_a is a fitting constant and not an activation energy. T_v, the Vögel temperature, is often considered to be related to, and typically 30 to 70 °C below, the glass transition temperature, T_g. Theses three fitted parameters are used to quantify the degree of deviation from linearity, which is more commonly known as the fragility of the material.

Results

F^- ion release.

Table 0-1 lists fluorine ion concentration measured after every 15h during the Fenton's degradation process. The solution was refreshed every 15h. The F^- concentration is practically constant at each solution refreshment regardless of degradation time. This suggests that the degradation process is continuous with respect to time and not incremental. If the later were observed then a significant increase in F- concentration would be expected at a specified time.

Table 0-1. Fluorine ion release concentration (ppm) at specified time with two samples per sample set. The time represents the total time exposed to Fenton's reagent solution. The solution was refreshed every 15h when the fluorine ion concentration was measured.

sample set	15h		30h		45h		60h		75h	
1	23.1	22.9	-	-	-	-	-	-	-	-
2	24.1	23.7	24.1	24.1	-	-	-	-	-	-
3	24.5	24.8	24.2	24.5	24.1	24.8	-	-	-	-
4	23.6	24.5	22.5	22.8	23.6	23.4	27.7	27.4	-	-
5	14.5	16.9	14.6	15.1	15.9	16.1	19.9	16.6	22.8	22.9

Scanning electron microscopy.

As shown in Figure 0-3, the surfaces of as-received films are naturally smooth. In contrast, degraded films are rough with micron sized bubbles erupting from the film interior, the degree of which depends on aging time. A relatively small number of ruptures appear on the surface of films after 45h exposure to Fenton's reagent solution. The bubbles are small (< 25 μm), sporadic, and not on the interior, as shown in Figure 0-4. This is in sharp contrast to membranes degraded for 60 and 75h. As shown in Figure 0-5, after 60h of exposure to Fenton's reagent, large and small bubbles are

widespread on the surface and interior. There are no notable differences between the 60 and 75h degraded specimens upon comparing Figure 0-6 with Figure 0-5.

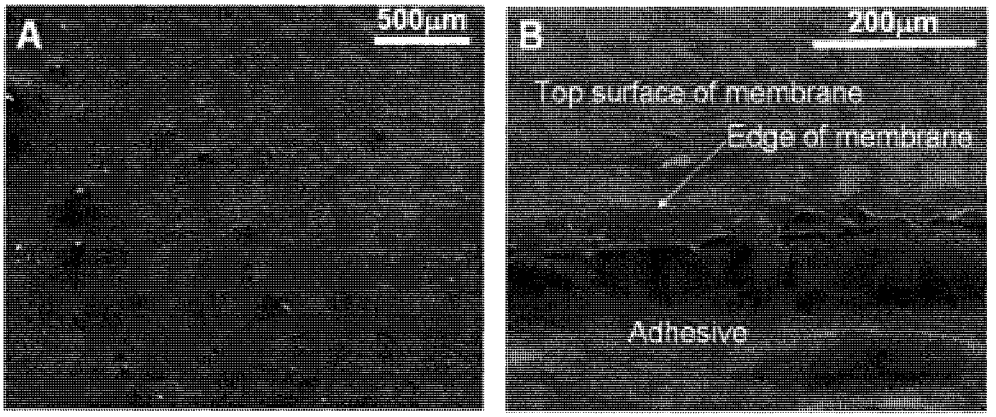

Figure 0-3. SEM scan of as-received film with no exposure to Fenton's reagent solution. Adhesive was used to attach the Nafion H^+ membrane to the SEM stage.

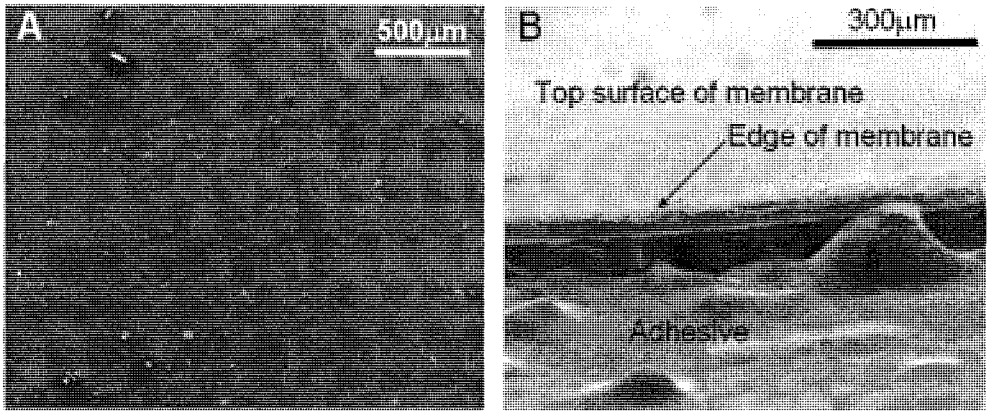

Figure 0-4. SEM scans of 45h film exposure to Fenton's reagent solution A) top, B) side views. Adhesive was used to attach the Nafion H^+ membrane to the SEM stage.

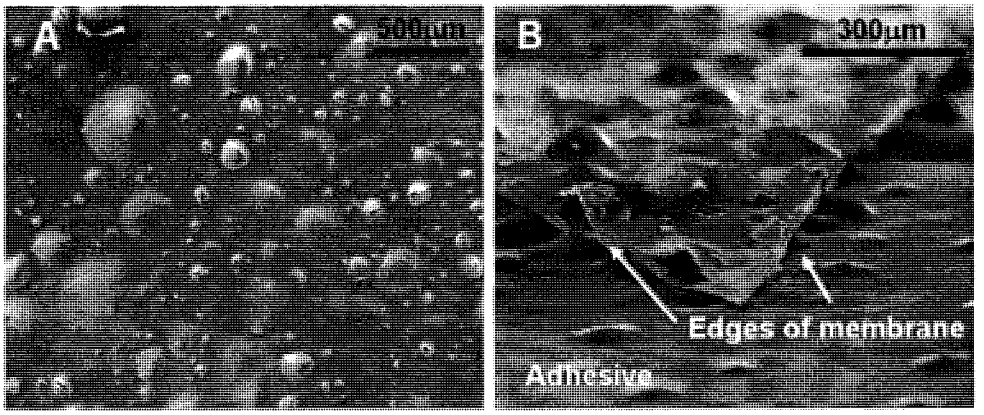

Figure 0-5. SEM scans of 60h film exposure to Fenton's reagent solution A) top, B) side views of two edges cut through the degraded membrane. Cuts made post-degradation.

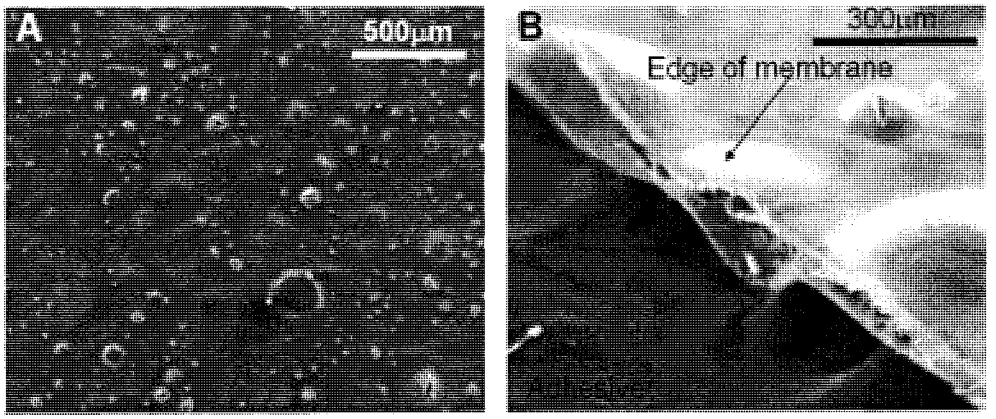

Figure 0-6. SEM scans of 75h film exposure to Fenton's reagent solution A) top, B) side views.

Interestingly, the film edges exposed to the Fenton's reagent solution do not have bubbles as illustrated in Figure 0-7. This may be because trapped gas can escape laterally out the edges of the membrane over short distances.

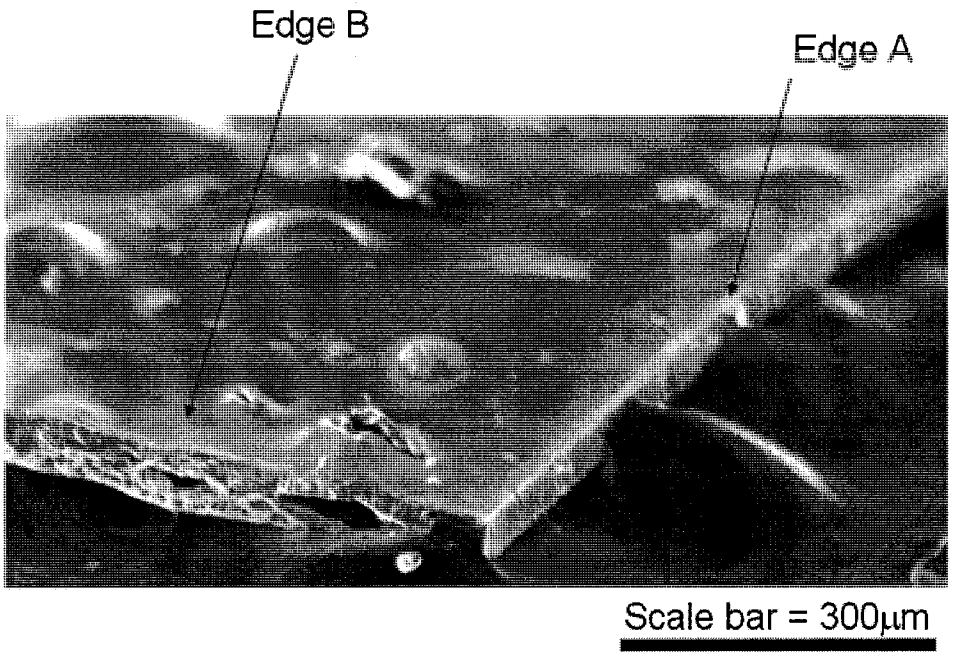

Figure 0-7. Corner of sample degraded for 75h. Edge A was exposed to Fenton's reagent solution. Edge B was created post-degradation by cutting the membrane with scissors.

Based on the enlarged image of a cracked bubble, generally speaking, bubble growth occurs in two ways: perpendicular to the film surface or parallel to the film surface. The difference between the two is related to the depth of bubble formation. Perpendicular bubble formation is more probable the closer the bubble is to the surface, and vice versa, parallel bubble formation is more probable the further the bubble is from the surface of the film, i.e. the deeper the bubble is embedded in the polymer membrane. Parallel bubble growth dominates bubbles that form in the middle of the film. Characteristically these bubbles have high aspect ratios of parallel to perpendicular growth. Most likely the balance of perpendicular vs. parallel growth is dependent on growth occurring along the path of least resistance. As the pressure of the trapped gas increases, the bubbles typically grow in spherical size before they rupture. For bubbles

that form in the middle of the film there is less resistance for the bubble to grow in size parallel with the surface of the film than for the bubble to grow outward, perpendicular. For bubbles that form at the center of the film, as it is suggested by the SEM side view images, the thickness of the bubbles wall to the surface is constant. This later point most likely suggests that the bubbles growth stays within a lamellar flow layer causing the polymer matrix to delaminate from itself. As the bubbles begin to grow perpendicular to the surface of the film pressure is exerted on the polymer matrix causing the molecules to stretch and the thickness of the bubble wall to thin. Eventually the stretching forces weaken the matrix and the bubble cracks. This argument is further purported by the notion that bubbles that are closer to surface have thinner walls allowing for those bubbles to crack sooner.

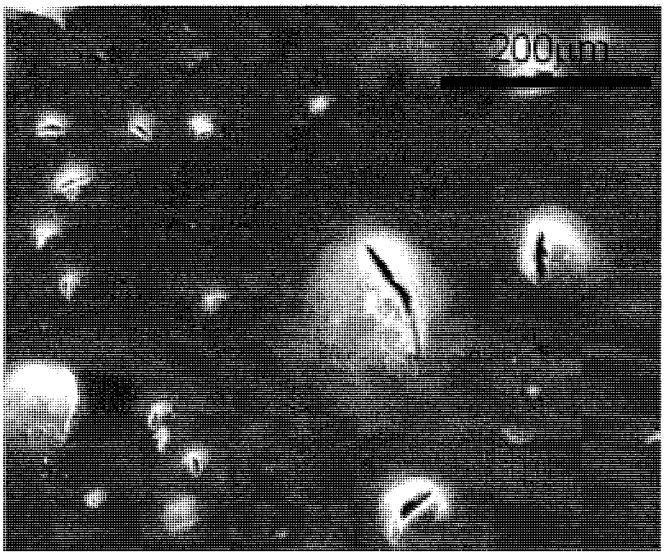

Figure 0-8. Top view, SEM scans of 75h film exposure to Fenton's reagent solution illustrating rupture crack.

As previously mentioned, the most widely accepted mechanism for Nafion® degradation is that of the main chain unzipping from radical attack on the –COOH end groups. Unzipping mechanisms occur rapidly and generate large amounts of small

volatile molecules, HF, H_2O_2, CO_2, SO, SO_2, H_2SO_2, and H_2SO_3.[3,17] Thus, if the Nafion® chains are unzipping, producing large localized amounts of gases, these immediately become trapped in the polymer matrix producing bubbles. A characteristic of the ruptured bubbles is that the rupture crack occurs over the entire surface of the bubble as seen in Figure 0-8. It was originally believed that bubble rupture could result from the high vacuum used in the SEM. However, the same ruptures are observed with optical microscopy at atmospheric pressure, figures are not shown. The fact that the ruptures have the appearance of tearing may be suggesting that the bubble growth is rapid. If the rupture was slower it is believed that the tear would result from thinning of the surface and possibly be more circular and not cover the entire distance of the bubble. The rapid production of gas gives little time for the material to relax to accommodate the stress resulting in either a growth in the parallel direction or a tear in the perpendicular direction.

Polymer Fragility.

In a previous study involving broadband dielectric spectroscopy on chemically degraded H^+Nafion, we reported on the effect of degradation on the segmental relaxation of Nafion®, namely the β relaxation. We determined that at a given temperature the β peak maximum shifted to lower frequencies with increasing degradation time resulting in higher Vögel temperatures. These two factors suggested that degradation results in more restricted segmental relaxations and the possibility that lower molecular weight components were leached out. More importantly, we now demonstrate that degradation not only shifts the β relaxation as previously reported, but also affects the dependence of the glass transition relaxation time on temperature, namely the fragility.

Glassy materials can be classified in terms of their 'fragility' which is a measure of the temperature dependence of τ_{max}. The more fragile a glass, the greater it deviates from linearity on a log τ_{max} vs. $1/T$ plot. The opposite of a fragile glass is a "strong" glass which has Arrhenius temperature behavior. SiO_2 is a classic example of a strong glass that has near linearity.[18] Fragility, relates to structure relaxation dynamics, segmental cooperativity along the chain, and short range order. For strong glasses, as temperature increases, short range order is maintained whereas fragile glasses lose their local structure. Fragile glasses have greater changes in relaxation time with respect to increasing T_g/T.

This phenomenon is quantified is by the fragility or steepness index defined by equation 6.

$$m = \left.\frac{d\log(\tau)}{d(T_x/T)}\right|_{T=T_x} \quad (5)$$

T_x is the dielectric relaxation-based glass transition temperature obtained by first fitting the relaxation vs. temperature data to the VFT equation and then extrapolating the VFT equation to τ_{max} = 100s, where at this long time the material is assumed to be frozen. An easy way to compare the fragility index of various glasses is by the following expression that results from substituting the VFT equation in equation 6, having determined E_a, T_g and T_V[19]:

$$m = \frac{E_a}{2.303R}\frac{T_g}{(T_g - T_V)^2} \quad (6)$$

Calculated m values, with their accompanying T_x values, are listed in Table 0-2. Generally speaking, for both cycle 1 and cycle 2, average m for degraded specimens are higher than the average m value for the as-received membrane, but not by much. Thus, it

appears that the Fenton's degradation process only slightly increases the fragility of the Nafion® membrane. This could be an indication that the molecular weight is altered or that the integrity of ionic network is altered. Comparing samples degraded for 75h with those for 60h appears contradictory. Samples degraded for 75h have an average *m* lower than for 60h. For instance, the 75h degraded sample (cycle 2) has an average *m* of 43 but the average *m*-value for the 60h degraded specimen is 46, which does not seem to be a significant difference. Interestingly, the standard deviation is much higher for the 60h and 75h samples compared with the as-received and 45h degraded samples. This latter point may indicate that membranes begin to chemically weaken 45 and 60h; however, this process is not reproducible as some individual specimens at 60 and 75h of degradation have *m* values similar to those degraded for 45h.

Table 0-2. *m* values with extrapolated T values at $\tau_{max}=10^2$.

		T_g at $\tau_{max}=10^2$s		*m*	
		Average	Stdev	Average	St dev
Cycle 1	AR-HCl	260	4.2	41	3
	Degraded 45h	258	6.7	42	3
	Degraded 60h	282	18.1	51	5
	Degraded 75h	252	10.0	46	14
Cycle 2	AR-HCl	265	7.5	38	3
	Degraded 45h	259	9.5	38	3
	Degraded 60h	289	18.8	46	9
	Degraded 75h	255	11.0	43	6

Figure 0-9 and Figure 0-10 are $\log_{10}\tau_{max}$ vs. 1/T plots for the 60 and 75h degraded specimens. It is evident that some of the curves are very similar to those of the as- received control, yet others show significant shifts to higher and lower temperatures. BDS tests the bulk properties of the films approximately 20mm in diameter. The fact that some samples show shifts and others do not suggests that on a bulk scale that the

Fenton's degradation process is heterogeneous— perhaps it does not homogenously degrade the films. It is not known why some samples from the same stock degraded faster than others. Originally it was thought that specimens closer to the top of the degraded film, as indicated in Figure 0-2, would be degraded more. However, this is not the case as observed by BDS as regions at the top do not consistently show more β relaxation shifts than those further from the top. It is believed that under the given reaction conditions the degradation process begins to affect the bulk properties of the membrane sometime between 45 and 60h of degradation. But, it must be remembered that this notion is not absolute as some of the 75h degraded specimens show no fragility or VFT changes.

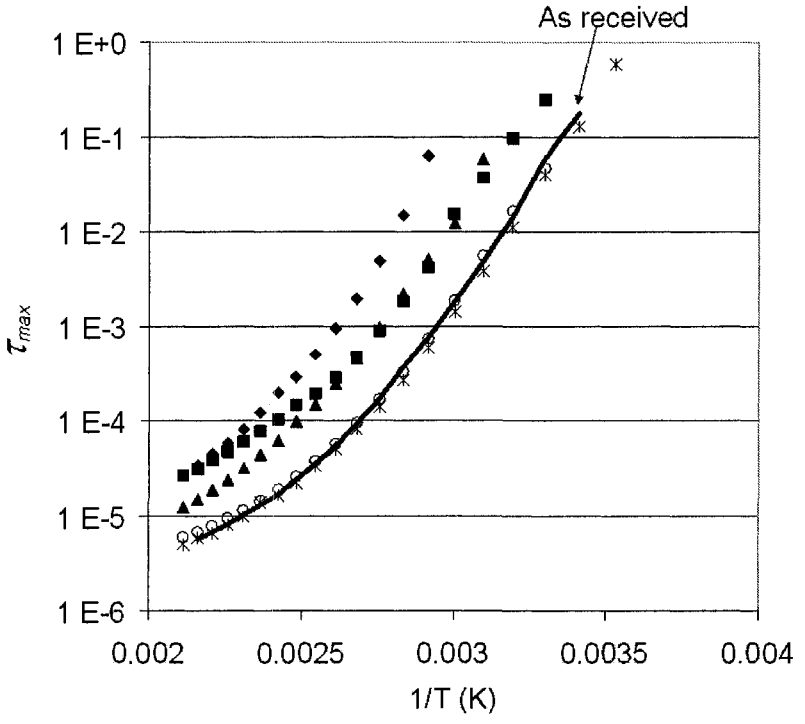

Figure 0-9. log τ_{max} vs. $1/T$ plots for five 60h degraded specimens (cycle 2 data) to compare with the as-received control (solid line with no symbol).

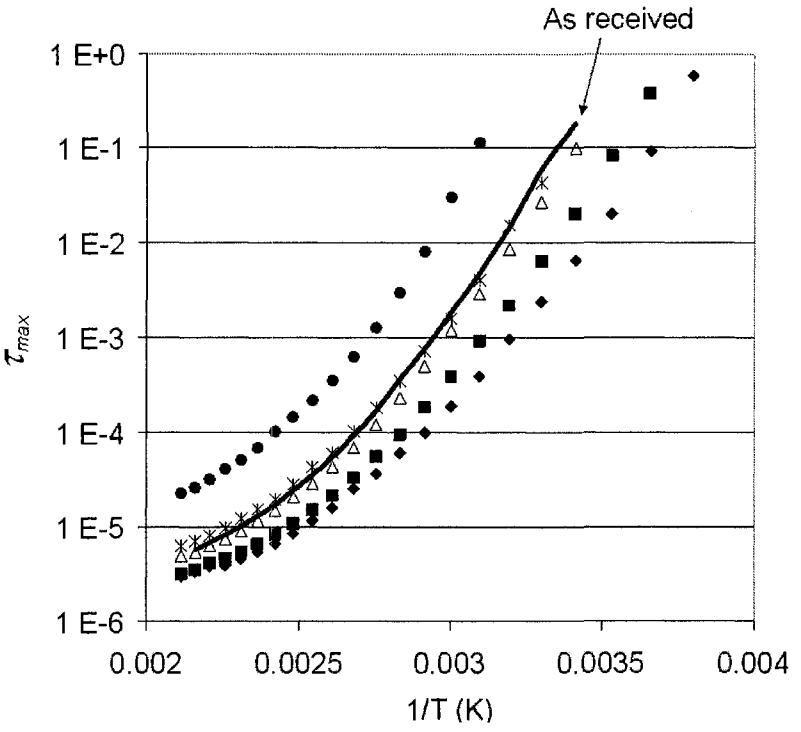

Figure 0-10. log τ_{max} vs. $1/T$ plots for five 75h degraded specimens (cycle 2 data) to compare with the as-received control (solid line with no symbol).

Many factors are known to cause changes in fragility: molecular weight, polymer chain flexibility, excess entropy and T_g.[20] However, many exceptions exist for trends in each property. For instance, for both polystyrene and poly(methyl methacrylate) fragility increases with increase in molecular weight. Yet, for poly(dimethyl siloxane), poly(propylene oxide), and polyisoprene, fragility is independent of molecular weight. Generally speaking two observations are made: 1) when T_g increases with molecular weight, fragility usually increases and 2) polymers with rigid backbones and high T_g are typically fragile.[20] For the Nafion® the calculated fragility values, in Table 0-2, are relatively low, meaning that the glass transition is rather strong and $\log_{10} \tau_{max}$ vs. 1/T curves are rather linear. Low m corresponds to strong glasses whereas high m corresponds to fragile glasses. Typical for polymer systems, fragility is usually greater

than 150. The Nafion® value of $m \approx 40$ which is indicative of a rather strong glass is more representative of a small molecule molecular system but with strong interactions. This low value is expected may be reasonable as polytetrafluorethylene, has a rather low glass transition of -73° C.[21]

FTIR-ATR spectroscopy.

Figure 0-11 is an FTIR-ATR spectrum of as-received Nafion® compared with those of several degraded samples. In analyzing these spectra, it should be remembered that ATR does not probe the bulk but the immediate subsurface region. Additionally, these IR spectra are on hydrated Nafion whereas the previous BDS discussion was on dehydrated Nafion. Three regions of the Nafion® IR spectrum show spectral differences believed to be due to degradation. No degradation effects are observed for the peaks at ~1200, 1100, 980 cm^{-1} which correspond, respectively, to CF_2 asymmetric stretching, CF_2 symmetric stretching and the C-O-C symmetric stretching.[22] For the three areas where degraded spectra are different than the control spectrum it must be pointed out that these differences are regional meaning that the entire surface of a degraded film does not show the exactly the same spectra. Some regions show similarities to the control and others show spectral differences. To illustrate this, in each of the following Figures two spectra for each degraded specimen are shown: one that is similar and one that is different than the control.

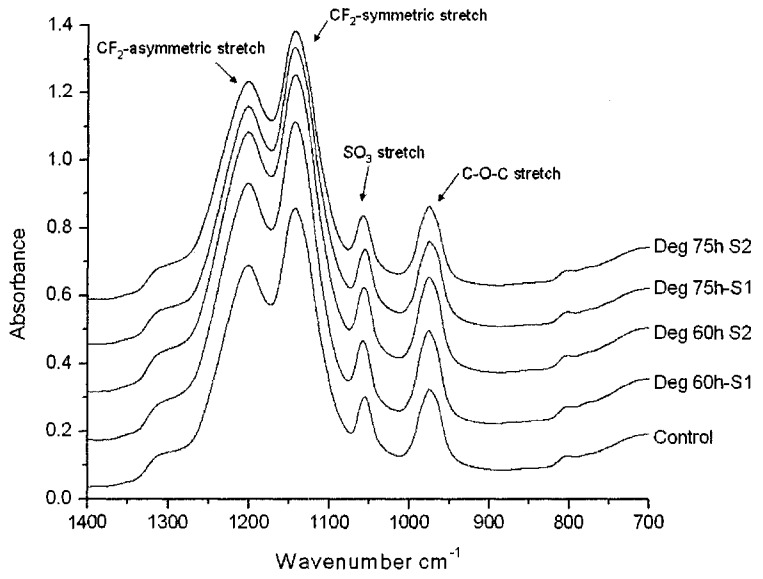

Figure 0-11. ATR-IR spectrum of as-received Nafion® and Nafion® degraded for 60 and 75h.

There is a spectral difference for the degraded specimens in the SO_3^- symmetric stretching vibration[22] as shown in Figure 0-12. The control sample has a peak at ~1055 cm^{-1} which shifts slightly to 1058 cm^{-1} with degradation although not all degraded samples show this shift.

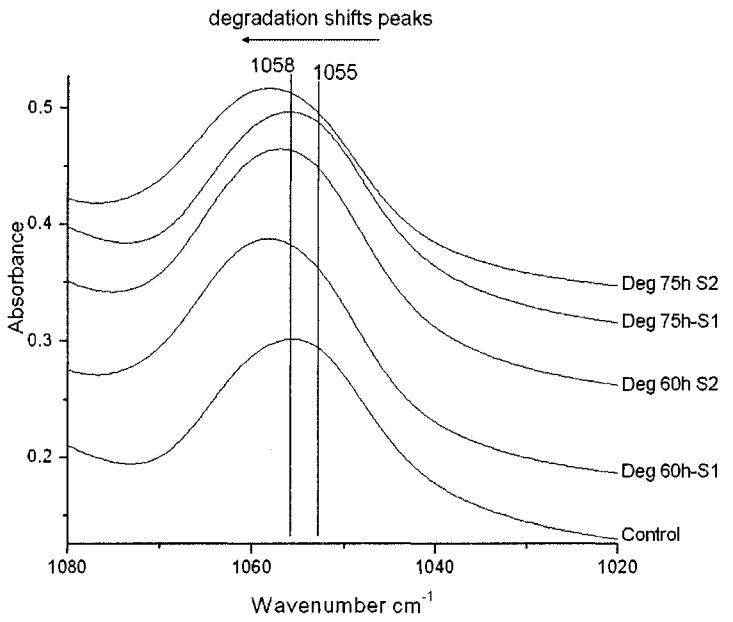

Figure 0-12. ATR-IR spectrum of the SO_3^- symmetric stretch as received Nafion® and Nafion® degraded for 60h and 75h highlighting the shift to higher wavenumber with degradation.

Figure 0-13 shows the portion of the spectrum from 1250 to 4000 cm^{-1} which includes the O-H stretching vibration[22] on the left. First, the O-H stretching peak of the control is at ~3441 cm^{-1}; some of the degraded specimens have this peak shifted to ~3468 cm^{-1} as is indicated in Figure 0-14. Second, the O-H deformation peaks, which occur at 1721 and 1637 cm^{-1} or the control specimen, change relative intensities for some of the degraded specimens, as better illustrated in Figure 0-15. For the as-received specimen the peak at 1721 cm^{-1} is greater in absorbance than the peak 1637 cm^{-1}. However, some of the surface regions of the films degraded for 60 and 75h show just the opposite trend where the 1637 cm^{-1} peak is of greater absorbance than the 1721 cm^{-1} peak. These peaks do not shift in wavenumber but their relative intensities change.

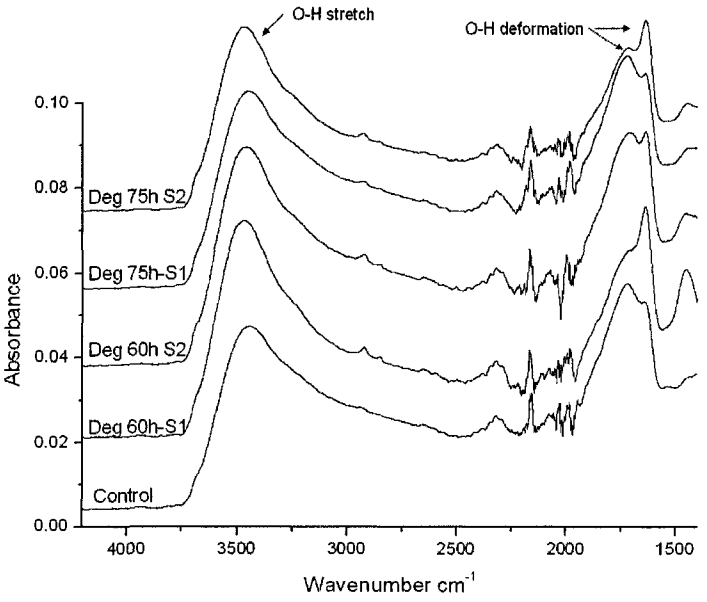

Figure 0-13. FTIR-ATR spectrum highlighting the O-H absorption of as received Nafion® and Nafion® degraded for 60 and 75h.

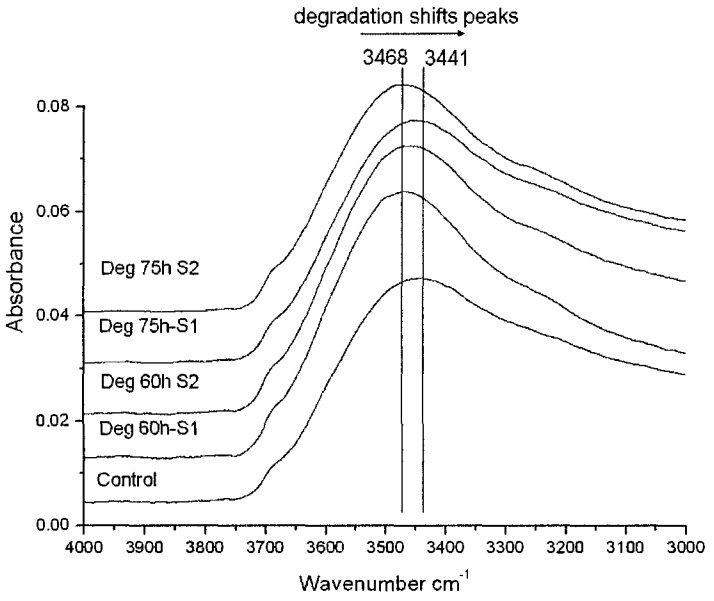

Figure 0-14. FTIR-ATR spectrum O-H stretch for as-received Nafion® and Nafion® degraded for 60 and 75h.

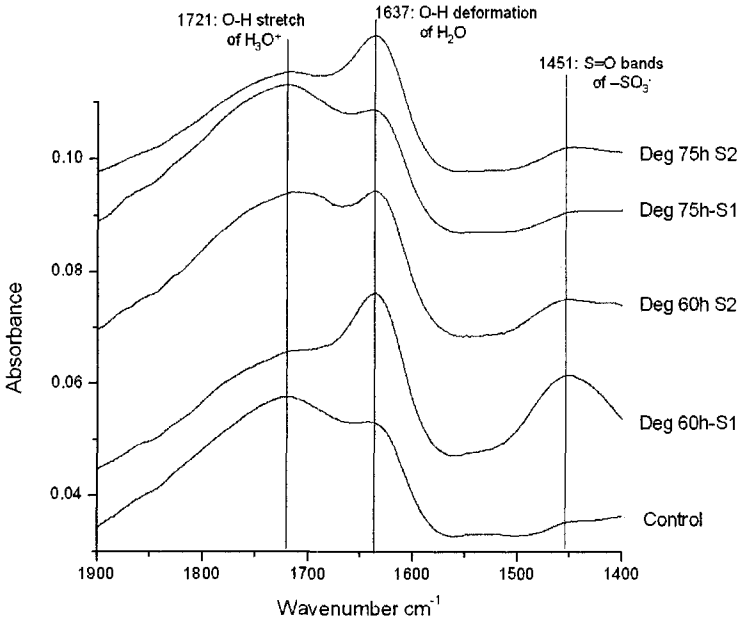

Figure 0-15. FTIR-ATR spectrum of as-received Nafion® and Nafion® degraded for 60 and 75h.

The third region that shows a spectral difference for degraded samples is associated with the S=O bands of the $-SO_3H$ functional group typically found around ~1410 cm^{-1}. As is further indicated in Figure 0-15 the control specimen shows only a very weak absorption peak in this region. However, some of the degraded specimens show a very distinct peak at ~1450 cm^{-1}. In particular, the same spectra that show an increase in the 1637 cm^{-1} peak relative to the 1721 cm^{-1} peak also show the distinct peak at ~1450 cm^{-1}, as is indicated in Figure 0-15.

Iwamoto *et al.* delineated the spectral differences of the O-H deformation that are attributed to H_2O from that of H_3O^+ by in situ dehydrating H^+Nafion.[22] In this experiment 1100EW H+Nafion was dehydrated in a closed ATR-IR cell over the course of approximately 2.5h. With increased drying time the peaks 3416 and 1729 cm^{-1} decreased in absorbance while peaks at 2741 and 2202 cm^{-1} simultaneously emerge and

increased in absorbance. The former two peaks are associated with the O-H motions of the H_3O^+; whereas, the later two peaks are associated with the O-H motions of the SO_3H functional group. Specifically, Iwamoto *et al.* associated the peak at 1721 cm^{-1} with the O-H deformation of H_3O^+ whereas the peak at 1637 cm^{-1} is associated with the O-H deformation of H_2O. This indicates that for the O-H absorbance of the SO_3H moiety cannot be directly studied for hydrated H^+Nafion. Although, the SO_3H moiety is not directly studied here (this will be reported in a subsequent publication) it appears that the water molecules that are relatively close to sulfonate end groups are altered by degradation. Specifically relative ratios of the O-H stretch of the H_3O^+ and that of the H_2O are altered with degradation, as indicated in Figure 0-14 and Figure 0-15.

As previously described for some of the degraded specimens the O-H stretch identified with the H_3O^+ (~1721 cm^{-1}) decreases in relationship to the O-H stretch of the H_2O. This may be further verified by the increase in absorbance of the O-H stretch in combination with the up field shift from 3468 to 3441 cm^{-1}. This seems to be indicating that the local environment of the water in relationship to the acidic counter ion is affected by degradation. More broadly it is possible that the hydration ability, the cluster network, or water absorbance, i.e. the state of water, is regionally altered with degradation This hypothesis is further supported by 1) the distinct peak increase at ~1450 cm^{-1} associated with the S=O bands of the $-SO_3H$ functional group, and 2) slight shift up field of the SO_3^- symmetric stretch at approximately ~1055 cm^{-1}. If it is true that the degradation process is chemically modifying the SO_3H end groups by changing them to a different functionality then this idea is supported by studies that detected SO, SO_2, H_2SO_2, and H_2SO_3 compounds in the solution post degradation.[3,17] It is highly probably that the

degradation process is not only altering the chemical composition of the end groups but it is also altering the ionic structural network. The net result of this is that the SO_3H end groups can no longer arrange themselves in the same capacity as they could before degradation. This possibility is supported by our previous work on unmodified H^+Nafion membranes which show that the ionic structures are very sensitive to thermal and hydration histories.[12]

Conclusions

In conclusion, it is not surprising that the IR spectrum do not show spectral differences for the CF_2 peaks and the C-O-C peaks, as illustrated in Figure 0-11, despite the fact that the SEM images show gross deformations of the interior and surface of the polymer membrane. After all, if the notion is true that the principal degradation mechanism is polymer chains unzipping then only complete undegraded polymer molecules would remain. The degraded polymer fragments are probably either evaporated out or washed away by the HCl boil and DI-H_2O reflux. The cracked bubbles in the SEM images further support the notion that the polymer degrades rapidly forming volatile gases.

In respect to the dielectric relaxation spectroscopic data the degradation process does not seem to become a factor below 45h. However, between 45 and 60h some specimens show significant degradation while others show resistance. It's not known why some regions of the film are more prone to degrade and others are not. Specifically, the average fragility begins to be affected sometime between 45 and 60h of exposure to Fenton's reagent. It is believe that the local order of the matrix is becoming more disrupted with degradation. This is supported by the fact that the average fragility

increases for the 60 and 75h degraded specimens. Furthermore, the IR results maintain the notion that the films are not degraded uniformly. Rather the IR suggest that some regions of the same film show effects of degradation but other regions show resistance to degradation. Specifically the sulfonate groups and the structure of water surrounding these groups show spectroscopic differences stemming from degradation. This may be suggesting that the degraded Nafion membranes are not able to hold the water the same post degradation as it was before the degradation or that the structuring of water around the sulfonate groups are changed. Thus, it is plausible that the change in hydration ability may affect the fragility of the polymer.

SEM images seem to support the notion that degradation is not substantial until after 45h of degradation. Just like the BDS data the SEM images indicate that between 45 and 60h of exposure to Fenton's reagent something occurs in the polymer matrix causing the membrane to rapidly degrade resulting in bubbles and ruptures. It's believed that these bubbles and ruptures are the result of the polymer molecules spontaneously unzipping and releasing localized large amounts gas. However, it is not known why these bubbles do not form earlier since F-ions are detected in the Fenton's reagent solution at both 15 and 30h of exposure to Fenton's reagent solution.

It is well accepted that the F-ion release rate is a good factor to monitor degradation. It was expected that the F-ion release rate would increase between 45 and 60h of degradation to support the SEM, BDS and FTIR data. However, the F-ion release rate does not suddenly jump up sometime between 45 and 60h of degradation. Just the contrary, the F-ion release rate is constant with respect to exposure time in the Fenton's reagent solution.

It recently has been suggested that the segmental β-relaxation is facilitated by ionic interactions of the side chains.[23,24] If this notion is true then the degraded specimens that show changes in fragility may possibly be correlated with the IR spectra of the degraded specimens. As a result it is suggested that the changes in fragility of the degraded specimens may be due to the changes in the ionic interactions of the sulfonate groups with the water that subsequently influence the segmental motions.

References

(1) Collier, A.; Wang, H.; Yuan, X.; Zhang, J.; Wilkinson, D. P. *International Journal of Hydrogen Engery* **2006**, *31*, 1838-1854.

(2) Schiraldi, D. A. *Journal of Macromolecular Science, Part C: Polymer Reviews* **2006**, *46*, 315-327.

(3) Borup, R.; Meyers, J.; Pivovar, B.; Kim, Y. S. *Chemical Reviews* **2007**.

(4) LaConti, A. B.; Fragala, A. R.; Royack, J. R. In *Proceeding of the Symposium on Electrode Materials and Process for Energy Conversion and Storage*; The Electrochemical Society, Inc.: Princeton, NJ, 1997.

(5) Curtin, D. E.; Lousenberg, R. D.; Henry, T. J.; Tangeman, P. C.; Tisack, M. E. *Journal of Power Sources* **2004**, *131*, 41-48.

(6) Zhou, C.; Guerra, M. A.; Qiu, Z.-M.; Zawodzinski, T. A.; Schiraldi, D. A. *Macromolecules* **2006**, *40*, 8695-8707.

(7) Rhoades, D. W.; Mauritz, K. A. *In Press.* **2007**.

(8) Kremer, F.; Schonhals, A. *Broadband Dielectric Spectroscopy*; Springer: Heidelberg, Germany, 2003.

(9) Havriliak, S.; Negami, S. *Journal of Polymer Science, Polymer Symposia* **1966**, *14*, 99-103.

(10) Havriliak, S.; Negami, S. *Polymer* **1967**, *8*, 161-205, appendix 206-110.

(11) Diaz-Calleja, R. *Macromolecules* **2000**, *33*, 8924.

(12) Rhoades, D. W.; Mauritz, K. A. **2008**.

(13) Vogel, H. *Physik. Z.* **1921**, *22*, 645-646.

(14) Fulcher, G. S. *Journal of the American Ceramic Society* **1925**, *8*, 339-355.

(15) Tamman, G.; Hesse, W. *Zeitschrift fuer Anorganische und Allgemeine Chemie* **1926**, *156*, 245-257.

(16) Schonhals, A.; Kremer, F. *Broadband Dielectric Spectroscopy*, 1 ed.; Springer, 2002.

(17) Teranishi, K.; Kawata, K.; Tsushima, S.; Hirai, S. *Electrochemical and Solid-State Letters* **2006**, *9*, A967.

(18) Angell, C. A. *Journal of Physics and Chemistry of Solids* **1988**, *49*, 863-871.

(19) Vilgis, T. A. *Physical Review B* **1993**, *47*, 2882-2885.

(20) Sokolov, A. P.; Novikov, V. N.; Ding, Y. *Journal of Physics: Condensed Matter* **2007**, *19*, 205116-205124.

(21) Lau, S.-F.; Wesson, J. P.; Wunderlich, B. *Macromolecules* **1984**, *17*, 1102-1104.

(22) Iwamoto, R.; Oguro, K.; Sato, M.; Iseki, Y. *The Journal of Physical Chemistry B* **2002**, *106*, 6973-6979.

(23) Page, K. A.; Cable, K. M.; Moore, R. B. *Macromolecules* **2005**, *38*, 6472-6484.

(24) Osborn, S. J.; Hassan, M. K.; Divoux, G. M.; Rhoades, D. W.; Mauritz, K. A.; Moore, R. B. *Macromolecules* **2007**, *40*, 3886-3890.

CHAPTER VI

CONCLUSIONS

This dissertation presents a fundamental exploration of the relaxations in Nafion® materials using modern broadband dielectric spectroscopy. Owing to the ambiguity in previous results of dielectric spectral studies, mainly because of the lack of precise knowledge of water contents, a main goal of this research was to identify and quantify the dependence of the α and β relaxations on frequency in the range 10^2-10^6 Hz and temperature over the range -130 to 200° C. Four particular systems were analyzed: (1) the non-ionic precursor form of Nafion® (sulfonyl fluoride), (2) a chemically crosslinked precursor form, (3) the acid form of Nafion® with particular attention to hydration and (4) chemically degraded acid form Nafion®. For all for systems, the glass transition (β relaxation) was primarily analyzed although two other relaxations above and below the glass transition were also identified and are discussed herein. For each system, the β relaxation was quantified by fitting the Vögel-Fulcher-Tammann (VFT) equation to data for which there is non-linear (non-Arrhenius) log τ_{max} vs. $1/T$ dependence.

The VFT equation and a fragility index, m, were used to quantify the degree to which log τ_{max} vs. $1/T$ behavior deviates from linearity. An anomaly exists when examining the front factor (hypothetical relaxation time at infinite temperature) τ_0 of the VFT equation for all the above forms of Nafion®, namely, $\tau_0 >> 10^{-14}$ s despite the fact that τ_0 equals 10^{-14} s for most simple polymers. The extent to which τ_0 deviates from 10^{-14}s also tracks with the m values. τ_0 and m values correlate with the degree of restricted motion imposed on the ether side chains from the crosslink or counterion. This is clearly

illustrated by examining the A1R relaxation of the chemically crosslinked amine modified sulfonyl fluoride films (12h cured) samples, of Chapter 2. A1R is the lower of the two new relaxations that appear with amine modification. It is believed that the A1R relaxation is from a chemical crosslink whereas the A2R value is of an ionic physical crosslink. For the amine modified systems, τ_0 values of A1R increase with decreasing molecular weight between linear amine crosslinks. Shorter amine crosslinks have greater restricted motions. This suggests that the greater the restriction on the side chains the greater is the impact on the τ_0 values. As molecular weight increases τ_0 becomes closer to that of the unmodified sulfonyl fluoride precursor, which further supports the notion that restriction of the side chain from either a chemical or physical crosslink influences τ_0. Furthermore, this reinforces the idea that these are all similar polymer segmental relaxation motions which only differ by the influence of restriction imposed on the end group of the side chain. Higher τ_0 values are also observed for the β-relaxation of the H^+ Nafion® system. The current state of understanding of the relaxation of H^+ Nafion® is that the β relaxation is the glass transition of the fluorocarbon matrix. τ_0 values of H^+ Nafion® are similar to τ_0 values of the EDA modified sulfonyl fluoride films. Not only does this suggests this motion is relatively strongly restricted but it also reinforces the notion that this is the glass transition of the polymer. This seems to be another common link between the glass transition of the precursor relaxation (i.e. the precursor's α-relaxation), the A1R relaxation of the amine modified sulfonyl films and the β relaxation for H^+Nafion®. If this is true, then as water is introduced into the dehydrated H^+Nafion® system τ_0 should increase in value with the addition of water.

In addition to quantifying the dependence of the molecular relaxations on temperature and frequency baseline testing procedures were established for the H^+form of Nafion®. BDS requires very low moisture contents to reduce d.c. conductivity, which when present overwhelms the molecular relaxations response. The condition of dehydration is difficult to attain and maintain during sample preparation and testing and the literature, to date, offers no advice on reliable and repeatable testing H^+Nafion® using the BDS technique. To improve on this situation, we have established reliable baselines that that can be used to standardize subsequent research for future investigation. In particular, H^+ Nafion® is sensitive to hydration in terms of thermal history and the acid reflux precondition step. Without proper control of these factors, the dielectric spectra changes with testing as a result of preconditioning and this is believed to be due to structural rearrangement from an expanded to a shrunken state.

These baseline studies were used to track accelerated chemical degradation of H^+Nafion® with BDS. Specifically, this impact was quantified using the VFT equation and fragility values of the β relaxation which indicated that the H^+Nafion® does not degraded uniformly or repeatable. Some specimens show significant differences after 45h of exposure to the chemical reagents whereas others showed no affects after 75h. It is believed that an unknown variable may be causing this non-uniform degradation which may be an artifact of sample conditioning.